University of Stavanger

Faculty of Science and Technology

MASTER'S THESIS

Study program/ Specialization: MSc. Subsea and Marine Technology	Autumn semester, 2016 Open / ~~Restricted~~ access
Writer: Rami Zughayar	…… (Writer's signature)
Faculty supervisor: Ove Tobias Gudmestad and Sverre Kristian Haver	
Thesis title: Eastern-Mediterranean Metocean Design Basis	
Credits (ECTS): 30	
Key words: Wave height, wave period, hindcast, measurements, extremes, design, operations, return period, contour, 100-year wave, swells, directional, seasonal, distribution fitting,	Pages: …… + enclosure: …… Stavanger, …….. Date/year

Acknowledgement

“The future belongs to those who believe in the beauty of their dreams.”
– Eleanor Roosevelt

To my father Ghaleb, mother Suad, wife Razan and son Yamen, thank you for your love, support and patience, I would never have done it without you.

To Prof. Ove Tobias Gudmestad and Prof. Sverre Kristian Haver from the University of Stavanger, thank you for believing in me and for spending your time in teaching me. You opened my eyes to industry challenges that I would like to continue to research.

To Prof. Giovanni Besio and PhD student Francesco DeLeo from the University of Genova, thank you for welcoming me to Genova and providing me with the data. It is my pleasure to continue scientific collaboration with you.

To Dr. Eli Biton from the Israel Oceanographic & Limnological Research Ltd (IOLR), thank you for providing me with the data, looking forward to meeting you and it is my pleasure to continue scientific collaboration with you.

To PhD student Adekunle Orimolade from the University of Stavanger, thank you for giving me your time and helping me whenever I needed it.

To my friends.

Abstract

Energy is one of the basic requirements of sustainable development of civilizations. Mankind is moving further to harsher environments, e.g. marine and arctic environments, to sustain energy production. Technology evolution is continuously opening new frontiers, potentials and of course more challenges to overcome. Alike onshore operations, offshore developments require a certain safety level to be maintained. A safety level that limits the risks related to health, environment and assets. One basic requirement for achieving that safety level may be simplified as: understanding the environment actions caused by waves, winds and currents, and building marine structures that can handle the worst conditions. Commonly used safety levels according to Norwegian Standard NORSOK N-003 are pre-defined by annual exceedance probabilities of 10^{-2} (return period of 10^{2} years) and 10^{-4} (return period of 10^{4} years). International Standard ISO 19902 refers to them as the return periods of the ultimate limit state design (ULS) and the accidental limit state design (ALS) respectively. Starting from the defined safety levels, extreme environmental states (e.g. wave height) and loads corresponding to these levels can be calculated.

Ocean waves (or sea waves in this case) are irregular and random by nature, wave data or wave model are essential for predicting the ocean state. In this thesis two kinds of wave data from the Eastern-Mediterranean are used, hindcast data and measurement data. First of all the hindcast validity is checked versus the measurements. The hindcast data, then, is used for two main things, general description of the sea-state and description of the design sea-state (i.e. the 100-year and 10000-year extreme sea-states). Sea-state is described; directions, seasons, locations and swell waves are analyzed.

NORSOK standard defines the "*design storm concept*" which states that instead of performing a full long-term response analysis, the extreme actions and actions effects can be estimated directly corresponding to annual exceedance probabilities, e.g. 10^{-2} or 10^{-4}. There are a number of different techniques but there is no theoretical best method for estimating the extreme sea-state. *DNV recommended practices* refer to few statistical methods. Among the different recommended extreme estimation methods, an interest in the uncertainties and their significance was developed that lead to a focus on extremes uncertainty assessment. Extremes are estimated, uncertainties are evaluated, and environment contours are presented.

Table of Contents

Nomenclature

Acronyms & Abbreviations:

ALS	Accidental Limit State
AM	Annual Maxima
CDF / cdf	Cumulative distribution function
DICCA	the Department of Civil, Chemical and Environmental Engineering at the University of Genova
DOF	degree of freedom
DNV	Det Norske Veritas is an international certification body and classification society with main expertise in technical assessment, advisory, and risk management. It is a merger between two leading organizations in the field - Det Norske Veritas (Norway) and Germanischer Lloyd (Germany).
ecdf	Empirical cumulative distribution function
EIA	Environmental Impact Assessment
FLNG	Floating liquefied natural gas
FPSO	A floating production, storage and offloading vessel

ID	Initial Distribution / All Sea-states
IOLR	Israel Oceanographic & Limnological Research Ltd
MLE	Maximum likelihood estimation
MME	Method of moments
MOM	Method of moments
MSL	Mean sea level
NORSOK	The NORSOK standards are developed by the Norwegian petroleum industry to ensure adequate safety, value adding and cost effectiveness for petroleum industry developments and operations. Furthermore, NORSOK standards are as far as possible intended to replace oil company specifications and serve as references in the authorities regulations.
PDF / *pdf*	Probability density function
POT	Peak-Over-Threshold
SD	Standard deviation
SPAR	a type of an offshore floating platform
SWOT	a study undertaken by an organization to identify its internal strengths and weaknesses, as well as its external opportunities and threats.
TLP	a tension-leg platform
ULS	Ultimate Limit State
USGS	the United States Geological Survey

Symbols:

Hs	Significant wave height
Tm	Mean period
Tp	Spectral peak period
Tr	Return Period
Na	Average annual number of observations

List of Tables

List of Figures

List of Equations

1 Introduction

1.1 Motive

The Eastern Mediterranean has an enormous potential, it is estimated that there are 122 trillion cubic feet (tcf) of undiscovered, technically recoverable natural gas volumes, as assessed by the USGS (2010). The region has lately been experiencing a natural gas “revolution”, since 2009, four huge fields were discovered with estimated combined recoverable reserves of up to 70 tcf (Ratner, 2016; NBL, 2016). Tamar field, offshore Israel, is producing since 2013, currently around 1 Bcf/d. Leviathan field, offshore Israel, and Zohr field, offshore Egypt, are currently undergoing development and they are planned to start production in 2017. This is a vibrant period of time for drilling and pipe laying activities, and it will continue as an active area for marine operations in the long run.

Due to this potential, there was a mutual interest, between the professor and I, in undertaking a thesis that is related to the Eastern Mediterranean developments. The metocean design basis topic was selected because it is a basic topic that touches on both design and operations concepts of the offshore industry. It requires special bundle of skills such as programming and application of statistical methods. And it is a widely applicable topic, relevant knowledge and skills are required in the shipping industry, offshore wind turbine projects, coastal engineering and structural reliability studies. The joint interest in the location and the subject made this topic a passion I follow.

Therefore I decided to grab this chance and learn from the 45 years of Norwegian offshore experience and apply some of it to the Eastern Mediterranean.

1.2 Location Overview

The main newly discovered natural gas fields in the Eastern Mediterranean are Tamar, Leviathan, Zohr and Aphrodite fields. The map in Figure 1 shows their locations and the area of interest for this thesis.

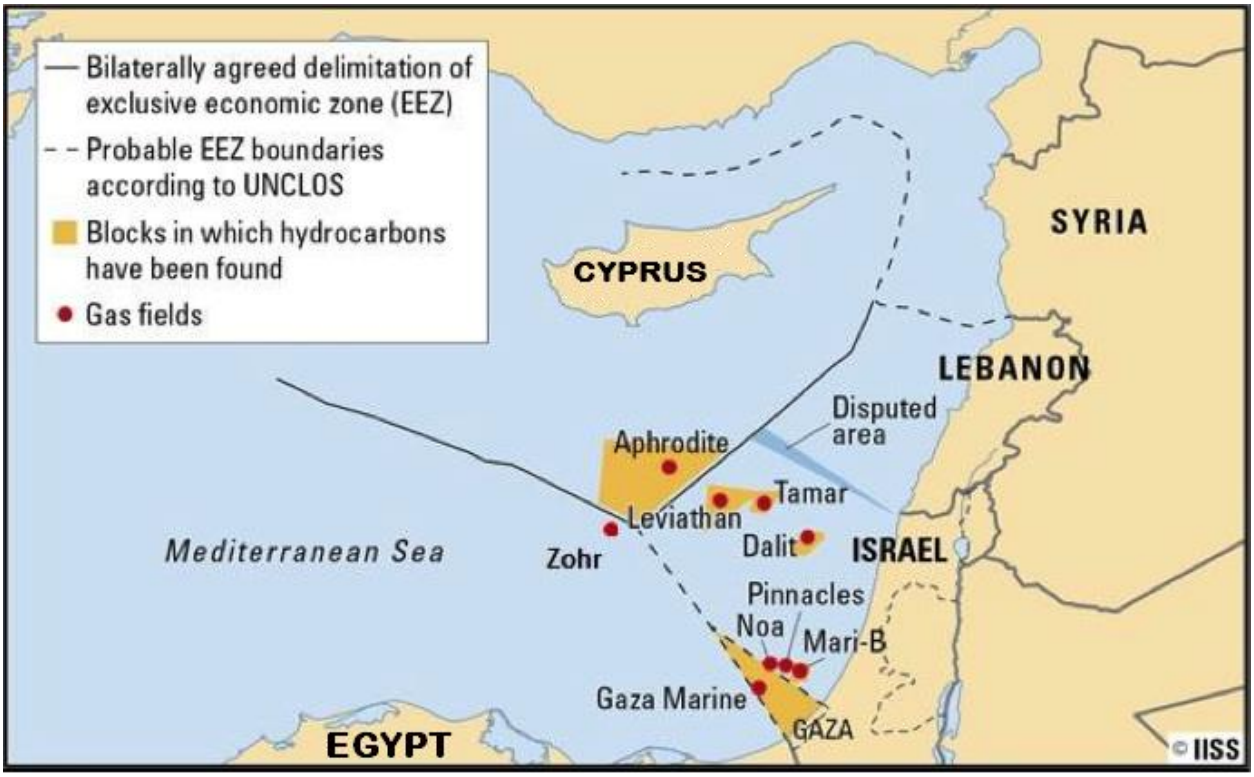

Figure 1: Eastern Mediterranean major discoveries (IISS)

According to *Nobel Energy* (NBL, 2016, p.16), the operator of both Tamar and Leviathan fields, said that the fields are: "*world-class resources in a high-demand region, exceptional assets, margins and growth*". Tamar is documented to have 10 tcf and Leviathan 22 tcf of natural gas as gross recoverable resources. Tamar has been producing from March 2013 and is currently supplying 60% of Israel's power generation. Leviathan is under development, expected to start production in early 2017 according to *Nobel Energy's Outlook* report dated November 2016. Aphrodite is said to hold 7 tcf (Ratner, 2016, p.6), but is not under development yet, however, there is an agreement between the Cypriot government and Nobel Energy regarding the field's commercial development. Zohr field is described by Eni, the operator, as a world class supergiant discovery, with estimated potential of 30 tcf of gas in place. Zohr was just recently discovered, August 2015. It is currently under development and expected to start production soon. The natural gas discovery boom is probably attractive for other exploration and production companies to join the future investment efforts in this region. For the sake of comparison, the Norwegian giant gas field Troll originally had 50 tcf of recoverable gas (NPD, 2015).

A zoomed out map of the Mediterranean Sea is shown in Figure 2. It is indeed a closed sea, with a maximum width of 3700 km (in the east west direction, from Gibraltar to Lebanon) and

max height of 1500 km (in the north south directions, from Trieste in Italy to Tripoli in Libya). The max height of the Eastern Mediterranean is 550 km (from Antalya to Alexandria). The Mediterranean covers the area 2.5 million km^2 with average water depth of 1500 meters approximately. Water depth at Tamar field wells is about 1700 meters (Healy et al., 2013).

Figure 2: Map of the Mediterranean Sea (Google Maps, 2016)

Several countries are involved in the recent discoveries in this region, both the ownerships of the resources and the geopolitics of the area may play important roles in decision making, even in technical decision-making of development scheme such as, platform concept, locations and technologies. A huge discussion was held in Israel for the decision of domestic use only, versus tandem solution of export and domestic use, and the tandem solution was adopted (Mackenzie, 2011), but this brings the next challenging discussion of installing a pipeline selling CNG, building an onshore liquefied natural gas (LNG) plant, or an offshore floating LNG (FLNG) plant. Regardless of the decisions, the offshore activity is boosting, and the near future will involve increased drilling, exploration, new bidding rounds and production activities. Hence this thesis is rather less concerned about the geopolitics of the region and will focus on technical matters.

1.3 Scope and Objectives

The scope of this thesis is describing and understanding the metocean conditions (especially waves) of the Eastern Medirranean and investigating the implications of such conditions on both

the design of marine structures and the offshore operations. The thesis can be broken down into three main parts:

A. **Data:** the first challenge is to knock the doors of data providers and achieve access to data of sufficient length and quality. Data can be either measurements or synthetic data. Plus to evaluate the validity of the data. Eventually the student achieved to get both synthetic data and measurement data, and performed a validity check by comparing them together.

B. **Description of the Sea-state:** Describing the theory behind wave modelling and extreme analysis, and presenting the condition of the sea, in terms of seasons and directions, based on data analysis. Plus describing swells and their presence in the location of interest.

C. **Design Sea-state:** this part is the main part; it includes a considerable focus on extreme estimations and the linked uncertainties. Following a statistical approach for estimating the extremes by using long term history of wave observations. Working with a variety of industry-recommended statistical models and then assessing the sensitivities of model-to-outcome. Next, selecting a shortlist of the “best” statistical models and presenting their uncertainties. Wave extremes and their uncertainties are used to represent the long term sea-state by extreme contours, to determine the design waves, to check the applicability of wave theory to the design wave, and include a discussion of such design sea-state (NORSOK-N003, 2007; ISO 19902, 2007).

The fourth part will be researched separately soon after the thesis:

D. **Operation Sea-state:** this part shows that long term wave data is not only useful for design, but also for operations. Wave data is used to assess the operability of a given operation. The operability is defined as the ability to perform the operation safely according to pre-set criteria. Operability is considered as the chance of having a sea-state that is calmer than what the criteria specify. Operability is assessed by predicting the behavior of the future using data from the past. This section will also include introduction about vessel response theory and a link between vessel response and operability.

1.4 Input Data and Tools

Data availability was an important factor for the flow of this thesis. The student achieved to get access to two data files from two different providers. One is synthetic (hindcast) data from the Department of Civil, Chemical and Environmental Engineering (DICCA) at the University of Genova, and the other is measurement data from the Israel Oceanographic & Limnological Research (IOLR). Description of both hindcast and measurement data follows.

Hindcast data:

According to the webpage of the data provider, the hindcast data is described as follows: "The MeteOcean group at DICCA has performed a re-analysis of atmospheric and wave conditions, producing a hindcast database spanning from January 1979 till the end of December 2015 over the domain employed for the atmospherical and wave condition simulations. The hindcast dataset for wave characteristics can be employed for Coastal and Ocean Engineering studies and researches. Meteorological re-analyses have been developed employing NCEP Climate Forecast System Reanalysis, CFSR for the period from January 1979 to December 2010 and CFSv2 for the period January 2011 to December 2015." The re-analysis of wave conditions relies on the wave model *WavewatchIII*. (http://www.dicca.unige.it/meteocean/index.php).

The hindcast file includes general, wind, wave, and swell parameters for every observation. General parameters are the date and time. Wind parameters are west-east wind velocity and south-north wind velocity. Wave parameters are significant wave height (Hs), mean and spectral peak period (Tm & Tp respectively), mean and peak directions of waves, directional spreading, mean and peak wavelengths. Wave component parameters are grouped into three groups named "wind waves; first swell; and second swell" and for every group wave height, mean period and mean direction are given.

Hindcast file includes 23 columns. Descriptions of the columns' names and units are listed as follows:

1. YYYY - Year
2. mm - month
3. dd - day
4. HH – hour; MM – minutes; SS – seconds;

5. Hs - Significant Wave Height [m]
6. Tm - Mean Period [s]
7. Tp - Peak Period [s]
8. Dirm - Mean Direction [°N]
9. Dirp - Peak Direction [°N]
10. Spread - Directional Spreading [°]
11. Lm - Mean Wavelength [m]
12. Lp - Peak Wavelength [m]
13. uw - West-East Wind Velocity [m/s]
14. vw - South-North Wind Velocity [m/s]
15. Hsws - Wind Waves Significant Height [m]
16. Tmws - Wind Waves Mean Period [s]
17. Dirws - Wind Waves Mean Direction [°N]
18. s1Hs - First Swell Wave Height [m]
19. s1Tm - First Swell Mean Period [s]
20. s1Dir - First Swell Mean Direction [°N]
21. s2Hs - Second Swell Wave Height [m]
22. s2Tm - Second Swell Mean Period [s]
23. s2Dir - Second Swell Mean Direction [°N]

Hs and Tp were the most extensively used columns in this thesis; however all of columns of the hindcast were used except the directional spreading and wavelengths. It is a solid advantage that this data is organized and stable, that is, it does not have missing entries, empty cells, or repeated rows. This caused a smooth workflow while working with this data.

Upon request, the compressed file that was received from DICCA includes hindcast information for 5 different locations in the Eastern Mediterranean and these locations are shown in the map in Figure 3.

Location 1 was selected as the point representative for the marine activity offshore Israel, with longitudinal and latitudinal coordinates of 33.4 and 32.9 respectively (coordinates of next points will be given in same order, longitudinal first). Location 2 was selected for representing marine activity offshore Egypt, with coordinates of 32.3 and 31.8. Location 3 was selected for activity offshore Lebanon, with coordinates of 35.1 and 34.5. Location 4 was selection for marine activity offshore Cyprus, a pipeline may be constructed there that links Israel to Cyprus to Greece (Pre-FEED Studies, European Commission, 2016). Coordinates of Location 4 are 32.3 and 34.5. And Location 5 is selected on the exact location of the measurement data (buoy location) provided by IOLR, with coordinates of 32.469720 and 34.862820.

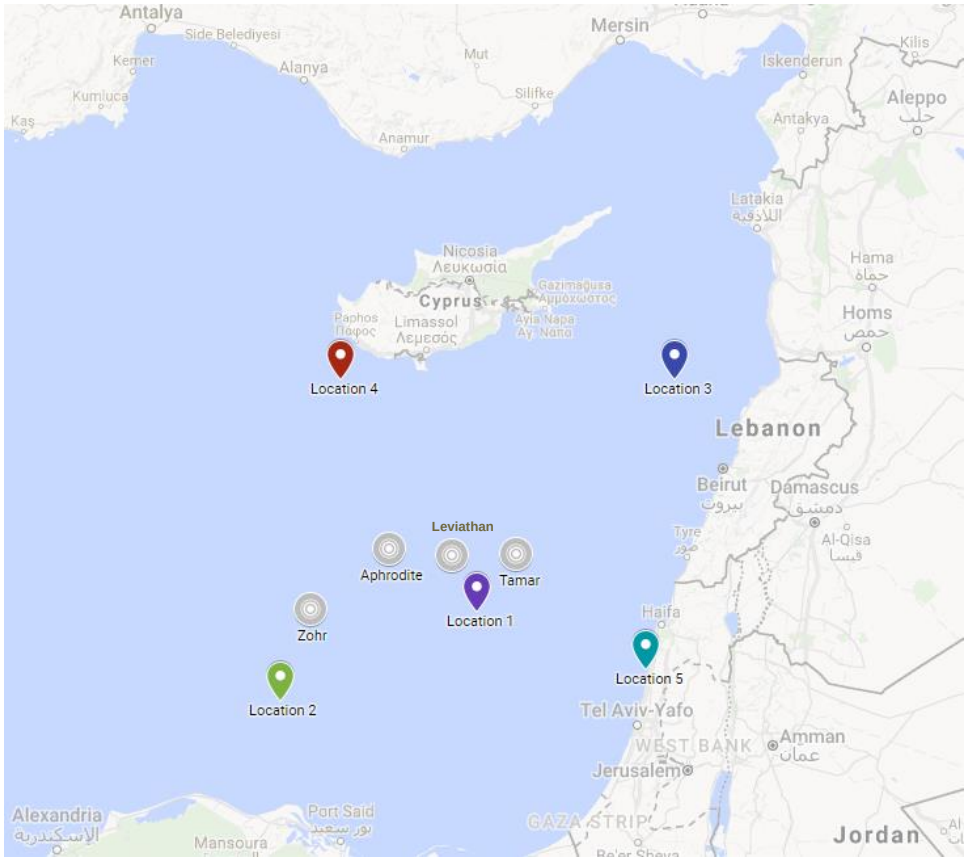

Figure 3: Map showing the 5 locations of available hindcast data

For every location the number of observations (data point) is in the magnitude of 3×10^5. Hence every hindcast location has a matrix in the size of 3×10^5 by 23 where the former number is the (approximate) number of rows and the latter is the number of columns.

The approximate number of rows is given instead of the exact because there are two different versions of hindcast file, each with a different number of rows. One includes swell information and covers the duration until end of year 2014; therefore it has the exact number of rows of 315572. The other does not include swell information and covers the duration until end of year 2015; therefore it has the exact number of rows of 324332. The latter has been used in all the parts of this thesis except the swell analysis part.

Measurement data:

The IOLR provided a data file that consists of buoy time-series measurement recordings from the Hadera Station, located exactly at Location 5. The Time Series database contains observational data from fixed or permanent oceanographic, according to the

IOLR, the data is described as follows: “The data quality assurance consist of two stages: data are collected in near real time from stations and an automated preliminary quality control procedure is implemented. At this stage, gaps in the observations are possible due to connection problems and problems with observation equipment. This stage is represented in the data by a zero (0) quality flag. Every several months some observational instruments are replaced for recalibration and the data collected by them is reprocessed with full quality control procedure (which includes filling communication gaps, and correcting biases due to “instrument drift”).” (http://isramar.ocean.org.il/isramar_data/AboutTimeSeriesDB.aspx)

Measurement data consists of one-hourly recordings, that starts with the beginning of the year 2006 and ends on the 1st of January 2016 at 22:30.

This data file is matrix of the size 78887×7, descriptions of the columns’ names and units are listed as follows:

1. Date&Time [dd-mmm-yyyy hh:ss]
2. Hs – Significant Wave Height [m]
3. Tp – Spectral Peak Period [s]
4. Dpeak – Peak Direction [deg]
5. Depth – Water depth [mm]
6. Hmax – Maximum Wave Height [m]
7. Tm - Mean Period [s]

Significant wave height Hs, is the focus from this dataset. Other perimeters such as peak period Tp, date, time and peak direction were also used. This dataset was not completely organized, that means that there were very few empty cells, repeated rows, missing entries, and readings that were recorded at the middle of the hour (e.g. 22:30) instead of consistently staying at the beginning of the hour (e.g. 22:00), which resulted in fixing challenges. However, the availability of this data was important in the validation part of the hindcast data.

Software:

Tools used for processing the data and for generating plots are Matlab, Excel, R Workspace and Gnuplot. Script writing skills and validating own results by hand calculation (or Excel calculation) were vital for this thesis.

Others:

The Norwegian standards NORSOK, the international standard ISO, the recommended practices of DNV, Haver 2013 book and Gudmestad 2015 book were the backbone references for this thesis.

1.5 Preface

This student planned to finish the degree in three semesters instead of four. Therefore, he had to work on the thesis together with courses. One of the courses was Marine Operations course, and the student selected the project topic for this course to be relevant to the thesis, the course project title was “Wave Extremes Analysis”. An updated revision of that project will be presented in this thesis in chapter 6 “Wave Extreme Estimations”. The project was used as a draft version in this thesis. Noting that section 6.4 “Threshold Selection” is new and was not part of the course project.

After the hindcast data was received, a collaboration initiative was setup with the University of Genova. The student travelled to Genova for a week to work together with Prof. Giovanni Besio and PhD student Francesco DeLeo on extreme sea-state estimations. The collaboration was a step forward in terms of exposure and sharing multidisciplinary perspectives, and it revealed mutual interests that may lead to continuation of joint research.

2 General Guidelines

2.1 Units

International SI convention is the unit system used in this thesis, except the units for natural gas volumes (in section 1.2) were given in trillion cubic feet (tcf) and billion cubic feet (Bcf). Useful conversion factors are found in Table 1.

Table 1: Useful gas volume conversion factors

$BTU = British\ Thermal\ Unit$	$1\ TCF = 28\ BCM$
$1\ MCF = 10^3 ft^3$	$1\ MMBTU = 10^6\ BTU = 1\ MCF$
$1\ BCM = 10^9 m^3$	$10^6\ MMBTU = 1\ BCF$
$1\ BCM = 35\ BCF$	$1\ BCM = 36 \times 10^6 MMBTU$

2.2 Locations

The locations where data is provided are defined according to Figure 4 (presented for the second time), and the locations will be called in the thesis with their defined names as shown on the map, e.g. the hindcast validation was performed on Location 5 only whereas Location 1 was the main point for the whole thesis.

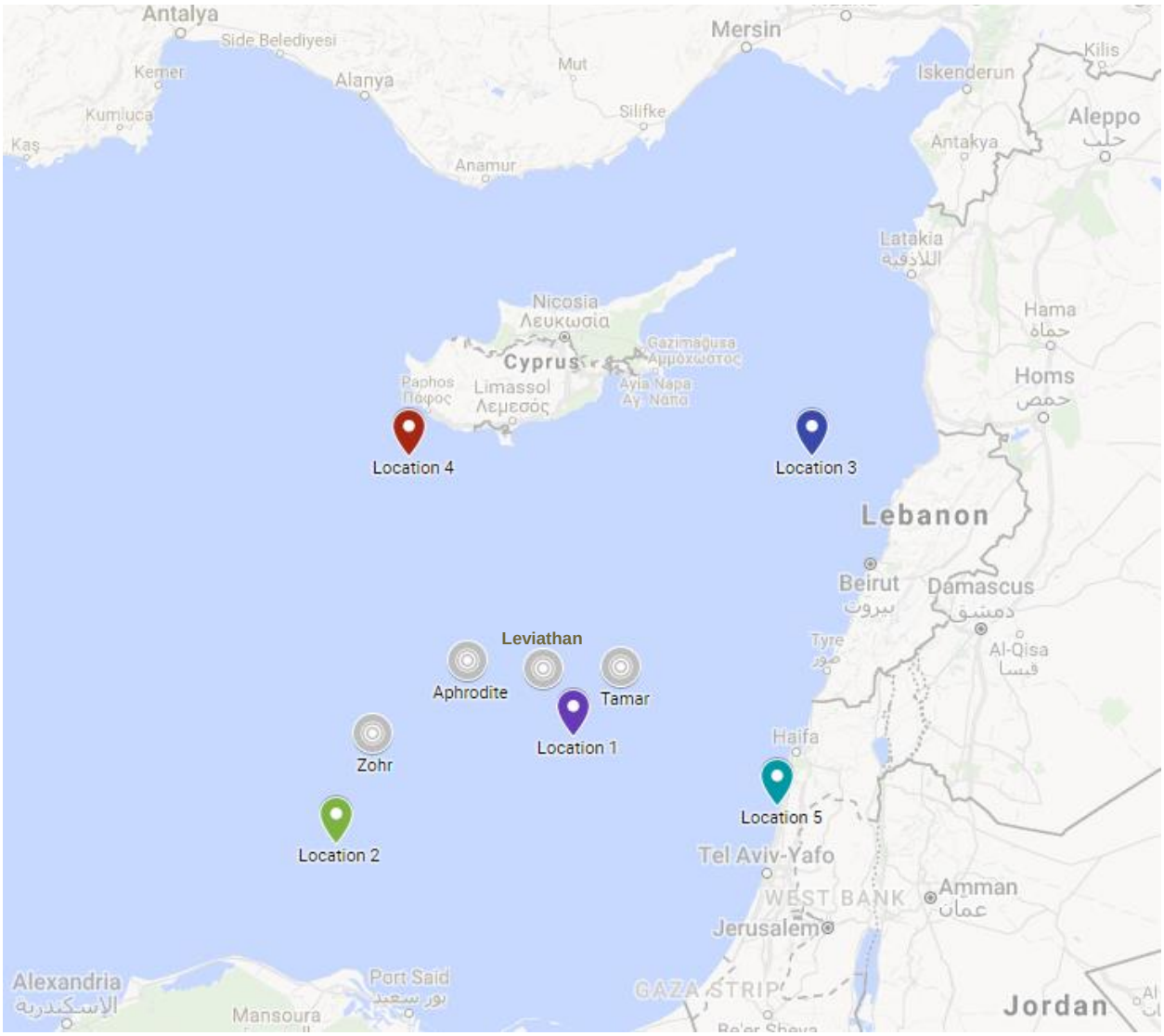

Figure 4: Map showing the 5 locations of available hindcast data

Location 1 is the primary location in this thesis for the analysis, most of the figures and diagrams found in the body of the report belong to Location 1. Other locations are used minimally, only when it was required by the task of the section.

2.3 Directions

The direction convention in this thesis may be the opposite of what the reader is used to, please note that directions are only presented in rose diagrams, and that wind has a different convention than wave, and the conventions are as follows:

Wind

Wind directions refer to the direction towards which the wind is blowing. For example if the wind direction in the rose diagram was pointing north, that means that the wind is blowing towards north.

Wave

Wave directions refer to the direction from which the waves are coming. For example if the wave direction in the rose diagram was pointing north, that means that the wave is coming from north.

Symbols

Capital letters N, S, E, and W are used as short-words for north, south, east and west. And combinations are also used, e.g. NE for north-east (angle 45 degrees clockwise from north) and NEE for north-east-to-east (angle 67.5 degrees clockwise from north).

Definitions

Metocean	in offshore and coastal engineering metocean refers to the combined effect of meteorology (the study of the atmosphere) and oceanography (the study of the ocean). Example of the factors that can be considered in metocean study: wind, wind waves, swells waves, storms, water depth, currents, and tides (Chakrabarti, 2005).
Omnidirectional	an omnidirectional sea-state is the sea with waves coming from one direction
Wind wave	the waves created by local winds, also referred to as wind-sea or wind-sea waves

Directional Analysis

The industry practices suggest that directional analyses are performed in 15 degrees segments, resulting in a distribution of 24 segments. However In this thesis 6 direction segments (60 degrees each) are adopted for the directional analysis, numbered from segment 1 to segment 6, oriented as shown in Figure 5. This simplification has been done for time saving consideration.

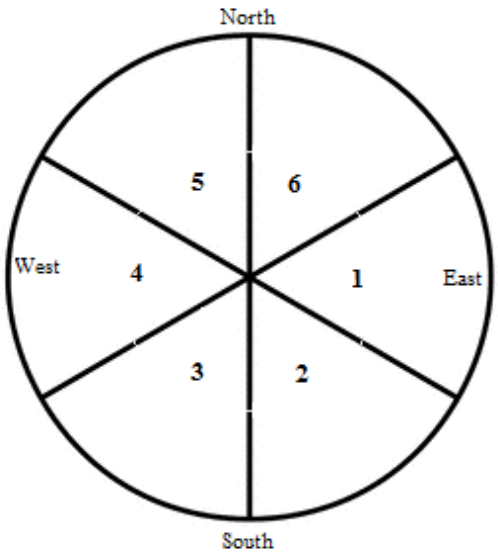

Figure 5: Definition of direction segments

2.4 Seasons

The industry practices suggest that a monthly basis analysis is performed, however in this thesis a seasonal analysis is rather performed. The year is split into 4 seasons, spring, summer autumn and winter. The periods of the seasons are considered as defined in Table 2. Note that seasons consist of three full months each.

Table 2: Definition of seasonal distribution

Season #	Season Name	Months
1	Spring	April, May, June
2	Summer	July, August, September
3	Autumn	October, November, December
4	Winter	January, February, March

3 Hindcast Validation with Measurements

Measurement data in the open seas is scarce. A replacement of measurement data is synthetic data (hindcast). A metocean study normally uses either measurements or hindcast. In case hindcast data is used, a proper validation should be performed, to assure the reliability of such data. Reliability evaluations are mainly done by the hindcast providers. Nevertheless, a validation study is done on the hindcast data from Location 5 against the measurement data from that same location. This chapter provides a set of comparisons between the hindcast and measurement datasets. The comparisons include time series plots, scatter diagrams, quantile plots, cumulative distribution function plots, probability paper plots, and directional rose diagrams. The purpose of this investigation is to visually illustrate the differences between the datasets in terms of amplitude, direction and probability. This difference, if found sufficiently small, can be considered acceptable, thus proving the validity of using the hindcast data, of this location (Location 5) and all other locations as well.

Location 5 is used because it is the location where the two kinds of data are available. A highlight of the differences between the datasets is shown in Table 3.

Table 3: Highlight of main differences between the hindcast and the measurements datasets

	Hindcast	**Measurements**
Starts	01/01/1979 at 05:00	01/01/2006 at 00:00
Ends	31/12/2015 at 23:00	01/01/2016 at 22:30
Sampling rate	1 hourly	1 hourly
Uniform sampling?	Yes	No
Number of data points	324,331	78,887
Continuous?	Yes	No
Repeated samples?	No	Yes
Data provider	DICCA	IOLR

Matching the two datasets in simultaneous pairs is the first step. The changes in the two datasets make the matching very challenging. A Matlab script is created that performs the matching task by filtering out the data that does not have a simultaneous pair in the other dataset. (02_Validation.m, Appendix C).

The matching algorithm is summarized as follows:

i. Setting the range:
   a. Excluding data before the beginning of 2006 from hindcast dataset
   b. Excluding data after the end of 2015 from measurement dataset
ii. The two datasets at this point do not match, i.e. they have different lengths:
iii. Matching pairs of Hs from both datasets to a common time series
   a. Creating a common dataset that runs from first hour in year 2006 and ends in last hour in year 2015
      - Matching hindcast data to the common time series
      - Matching the measurement data the common time series
      - Length of common time series: 87,648 data points (10 full years of 1 hourly values)
   b. Filtering missing data points:
      - For values that are equal to zero or simply missing data points, then the pair is considered as incomplete
      - Filtering out all incomplete pairs

The number of rows for the matched dataset is 78,493 data points. This corresponds to 9 years of data in a time period of 10 years of measurements. There is 1 year-worth of unmatched or missing data. In fact, the size of the matched data is large enough and makes a good basis for a thorough validation.

3.1 Time Series Comparisons

Synchronization evaluation of hindcast (relevant to buoy measurements) is done, by simply generating time-series plots that compares hindcast with measurements and give indications of the integrity of the hindcast. Different scale synchronization plots are presented, starting from a plot the includes the whole range of the matched data, then zoomed-in plots that include single winter seasons, and then further zoomed-in plots showing the synchronization in the resolution of couple of storms.

First, a time series plot, presented in Figure 6, that includes both datasets, is showing a comparison between hindcast and measurement data for the whole matched period of time.

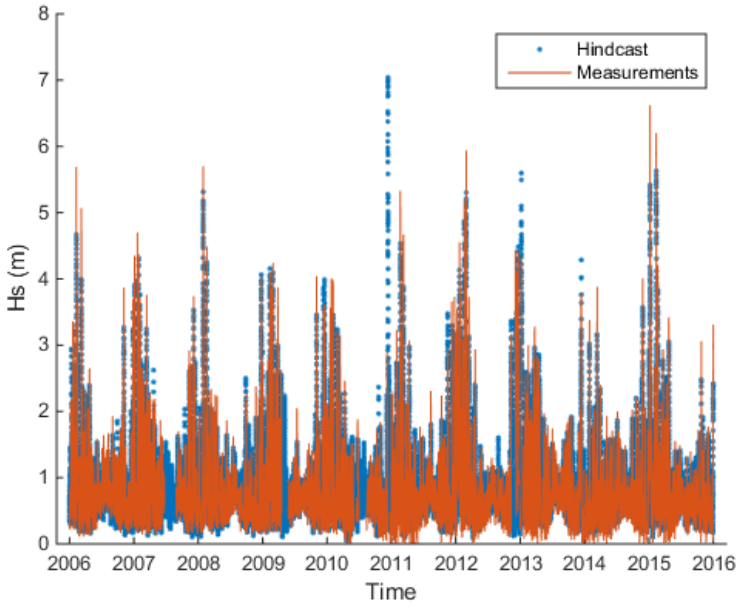

Figure 6: Hs (Hindcast vs. Measurements) Time Series from location 5

Figure 6 is an overview of the whole period, the resolution is coarse but it shows that there is a general agreement between the hindcast and measurements. Figure 7 to Figure 10 show a closer look at the time series, zoomed in at winters of the years 2007/08, 2009/10, 2011/12 and 2013/14 to present the comparison of hindcast versus measurement data in a higher resolution.

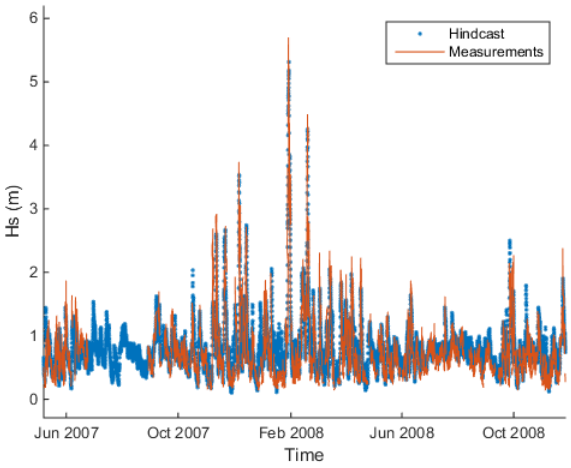

Figure 7: Hindcast vs. Measurements 2007/08

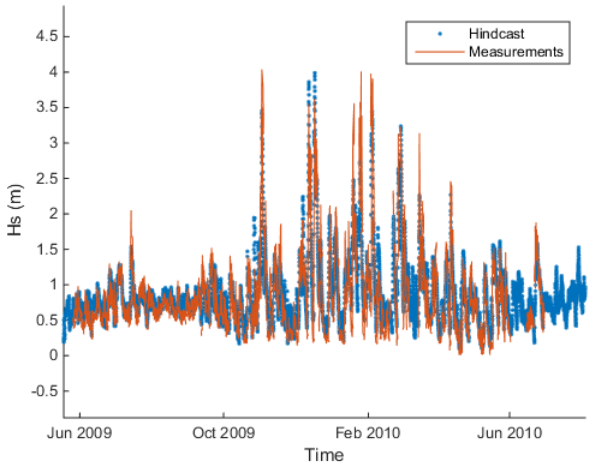

Figure 8: Hindcast vs. Measurements 2009/10

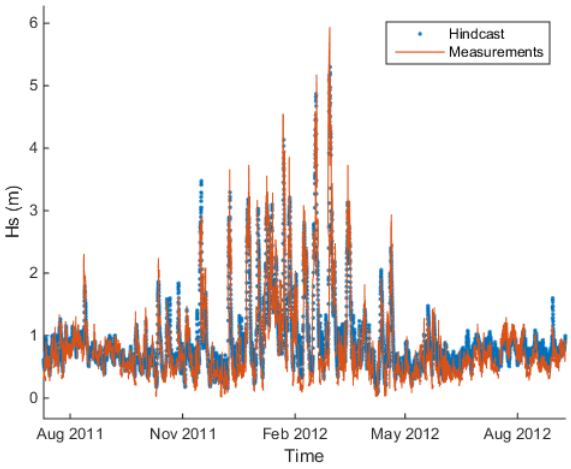

Figure 9: Hindcast vs. Measurements 2011/12

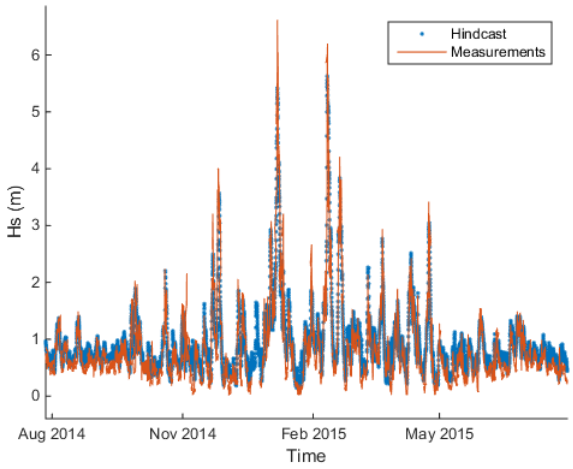

Figure 10: Hindcast vs. Measurements 2014/15

Figure 7 to Figure 10 show that the hindcast and measurements do not match perfectly; however, there is an excellent conformity. Further zoomed-in comparisons, down to the scale of couple-of-storms are presented in Figure 11 to Figure 22. A group of storms is selected, this group is believed to be representative for the whole dataset because in some of them it shows the strengths of the hindcast (when it is synchronized and matched with measurements) and in others it shows the weaknesses of the hindcast (when there are missing measurements or differences in amplitude).

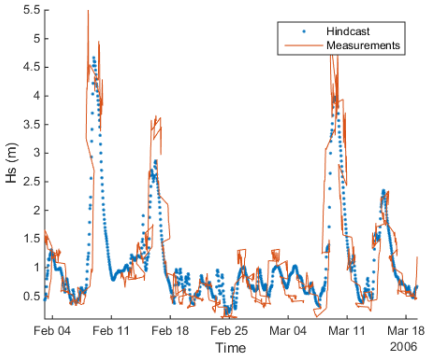

Figure 11: Hindcast Synchronization 1

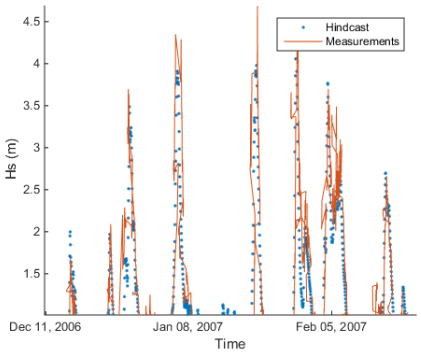

Figure 12: Hindcast Synchronization 2

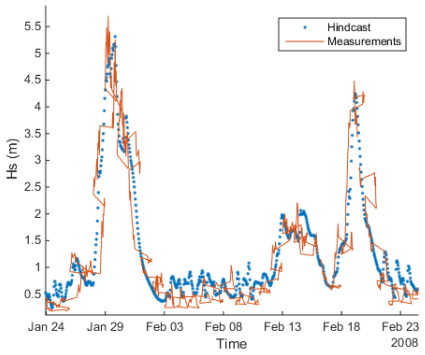

Figure 13: Hindcast Synchronization 3

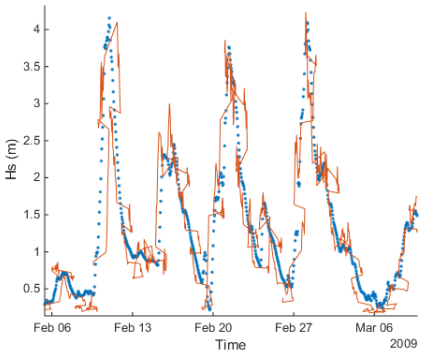

Figure 14: Hindcast Synchronization 4

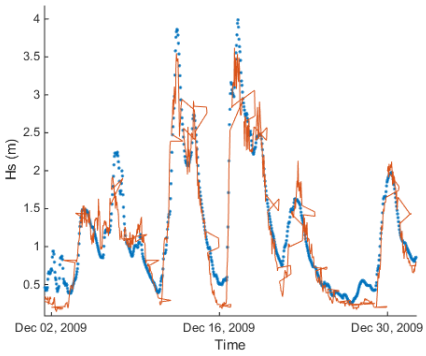

Figure 15: Hindcast Synchronization 5

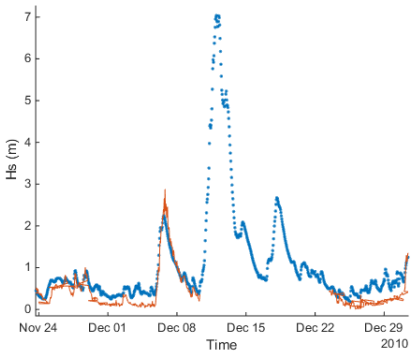

Figure 16: Hindcast Synchronization 6

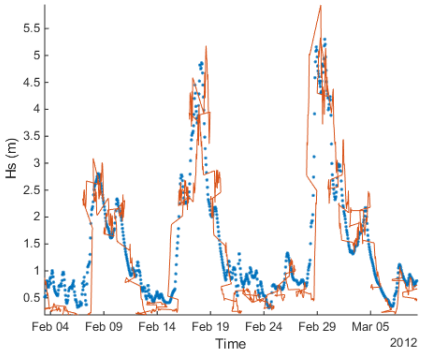

Figure 17: Hindcast Synchronization 7

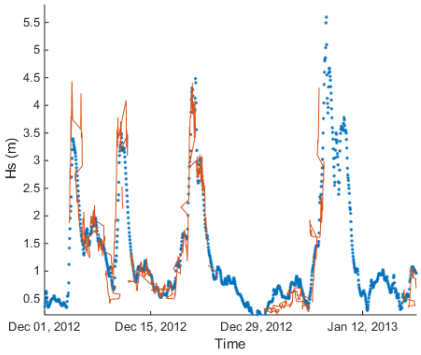

Figure 18: Hindcast Synchronization 8

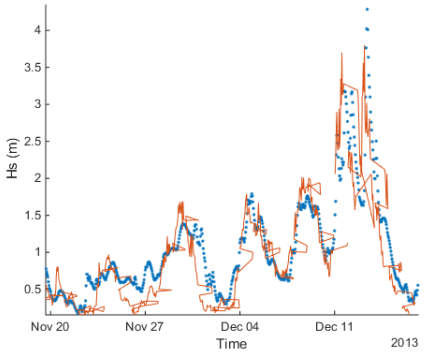

Figure 19: Hindcast Synchronization 9

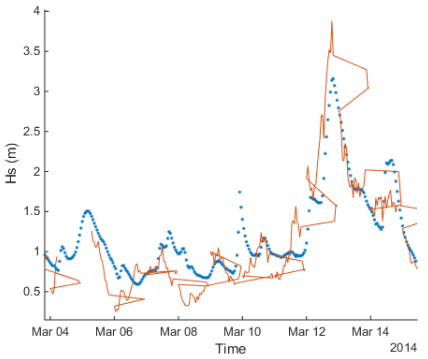

Figure 20: Hindcast Synchronization 10

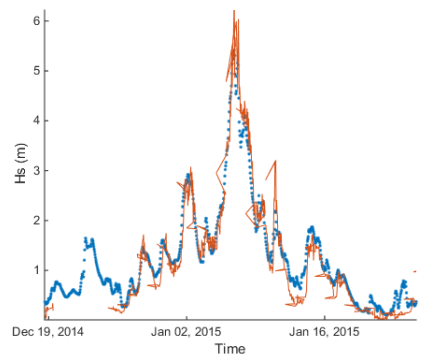

Figure 21: Hindcast Synchronization 11

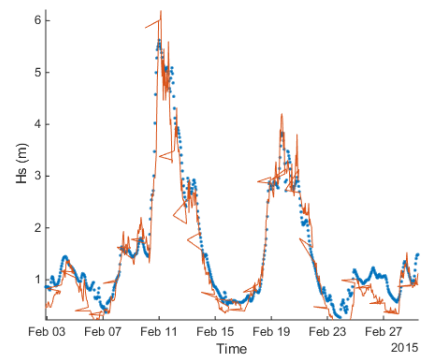

Figure 22: Hindcast Synchronization 12

Most of the figures (Figure 11 to Figure 22) show a good match and synchronization between the hindcast and the measurements. First three of them (Figure 11 to Figure 13) show that hindcast storm peaks are a little bit higher than measurement peaks; whereas the next three (Figure 14 to Figure 16) show that measurement peaks are a little bit higher. Next two figures, Figure 16 & Figure 18, show times where measurement data is missing during a storm. Figure 20 shows highest disconformity. Overall quality of hindcast is considered to be positive in terms of time and amplitude synchronization. Further comparisons using different types of plots are presented below.

3.2 Comparison of Hs Simultaneous Pairs (Scatter)

A comparison of the hindcast Hs dataset against buoy measurements over the period 01 January 2006 to 31 December 2015 is given in a scatter diagram in Figure 23.

The dots in Figure 23 represent simultaneous pairs of Hs values. Each pair has one value from the hindcast data, and the other from the measurement data at the exact same time. The line in the middle represents the function:

$$H_{s\ (measurements)} = H_{s\ (hindcast)}$$

Points located on this line are the representing data where hindcast is representing the measurements in the best possible way. The two lines aside, one to the right and one to the left, are the lines that represent the 90% interval of confidence, which implies that 90% of the data points are within the two lines. The percentage of the number of pairs of absolute difference larger than a certain margin of error is 10%, defined as follows:

$$\frac{N_{out\ of\ range}}{78493} * 100\% = 10\%$$

Therefore, the number of points out of 10% range is about 7850 points out of 78493 points. The margin of error is found. The condition to satisfy the margin of error is defined as follows:

$$N_{out\ of\ range}\ (condition): |\ H_{s\ (measurements)}(i) - H_{s\ (hindcast)}(i)\ | >\ Hs_{error}$$

Where an index (i) is defined and it runs from 1 to 78,493. The margin of error associated with the 90% confidence interval is 0.46 meters. And Figure 23 shows this margin visually (the distance between the outer lines is double the 0.46 m interval). The performance of the hindcast is judged to be very reliable because the figure shows that 90% of the pairs fall within the margin of error, which is a narrow margin as shown in the figure, a deviation of less than 0.5 meters. It is worth to note that as Hs increases, the hindcast reliability decreases, values above

3.5 meters show a significant reduction in the quality of fit between the hindcast and the measurement data, and that may be a point of concern in the extreme estimations.

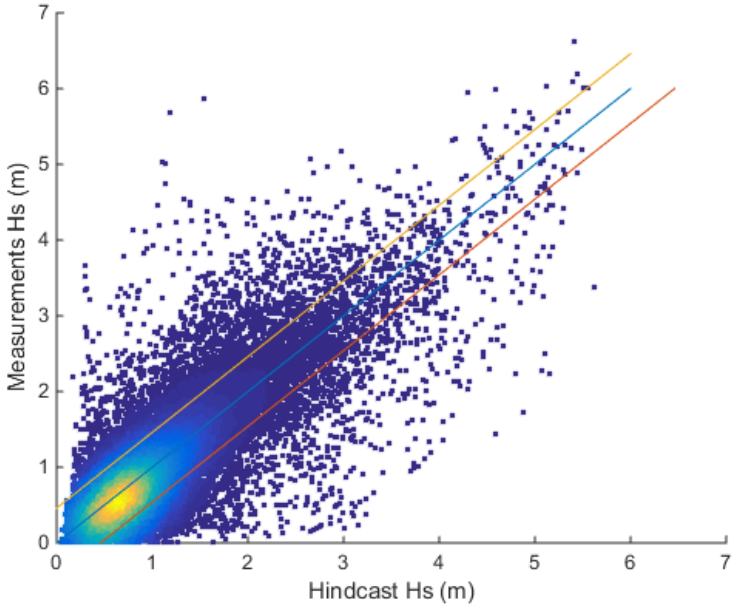

Figure 23: Hindcast against Measurements Hs Scatter Comparison

3.3 Probabilistic Plots

A plot of the quantiles, known as the q-q plot is shown in Figure 24. The q-q plot as the name suggests plots quantiles. Usually it plots the quantiles of the hypothesized cumulative distribution plot (*cdf*) against the empirical cumulative distribution plot (*ecdf)*. The hypothesized quantiles are the quantiles that follow the distribution that is believed to represent the data (Stanford and Vardeman, 1994). However q-q plot in this case is not used to assess the how the data follows a certain distribution, rather it is used to assess whether the two sets of data (hindcast and measurements) come from the same distribution by comparing their *ecdf* quantiles together. If the resulting plot is linear, then the two sets of data likely come from the same distribution. The distribution itself is not under question in this section, but the agreement between the two data sets is.

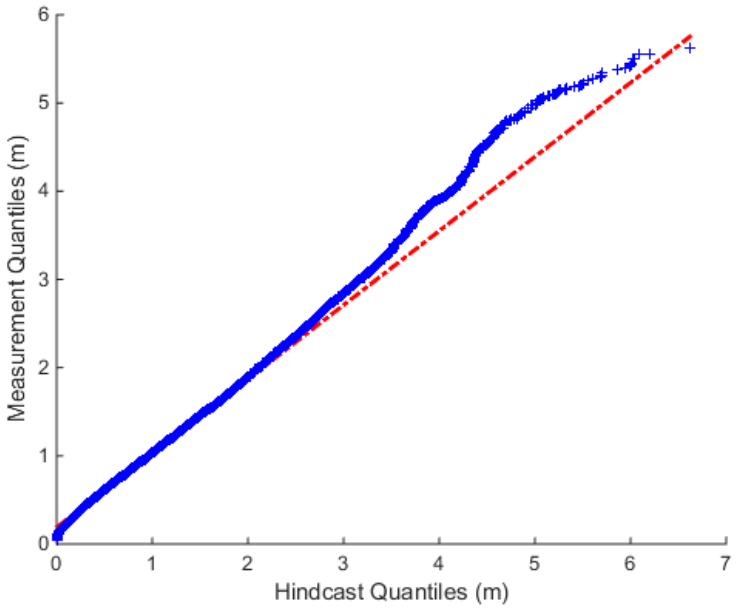

Figure 24: q-q plot for measurements against hindcast data

The q-q plot in Figure 24 shows a blue line and a red line, the blue line is made from pairs of hindcast and measurements; every point on this line is a pair of quantiles that correspond to the same ecdf. The red line is the straight reference line, it joins the first and third quartiles of each dataset and extrapolates out to the minimum and maximum values in to help evaluate the linearity of the data, it is there for comparison only, if the blue line is over the red line that means, for a certain *ecdf,* the measurement quantile is higher than the hindcast quantile and vice versa. The plot shows agreement of both datasets for waves heights lower than 3.5 m (as concluded from scatter comparison in Figure 23). And it shows that the hindcast has the tendency to underestimate the measurement in waves higher than 3.5 meters.

There is a need to compare the dataset's *ecdf* behavior in an *ecdf* plot and in probability paper plots to investigate whether hindcast, if fitted with a distribution, and that distribution is used for extreme estimations, would overrate or underrate the extremes. Figure 25 to Figure 28 show e*cdf* and paper plots for comparing hindcast with measurements data. The *ecdf* plot normally does not show much, it is a general comparison, and it shows that for lower waves, below 1 meter, the hindcast over-estimates Hs for a given cumulative probability, F. And for larger wave heights, above 1 meter, hindcast estimates are quite accurate. The probability paper plots (Figure 26 Figure 27) show the quality of the Weibull-III distribution fits to represent the data. It is clear that the hindcast fitted distribution is a very good fit until wave height of 5 meters, the tale is not well honored, and the measurements it also a very good fit until wave height of 6

meters, with better tail fitting. Weibull-III parameters for both fitted distributions are given in Table 4:

Table 4: Weibull-III parameters for both hindcast and measurement fitting

	Shape	Scale	Location
Hindcast	0.9168014	0.5680092	0.9518889
Measurements	1.1743161	0.9601789	0.5559491

A 3-parameter Weibull is chosen according to the recommendation of *DNV-RP-C205*, however an extreme assessment comparing five distributions is found in chapter 6 of this thesis. Hindcast and measurements datasets are fitted with Weibull-III, and probability papers are plotted in the Gumbel scale with H_s in the x-axis and $-\log[-\log(F_{Hs}(h)]$ in the y-axis, i.e. a Gumbel scale distribution will form a straight line with this axis scales. A Gumbel scale is used because it keeps Hs in the horizontal axis; this is preferred by engineers to deal with practical wave values straight away, instead of having the need to convert. Logarithmic scale for Hs will compress the behavior of the tail deterring the visual evaluation. The Weibull, if plotted on Gumbel scale, would form a line that is almost straight; it begins with a bend (due to the third parameter of Weibull), and continues straight until the maximum values.

The Weibull and Gumbel distributions are defined as follows:

Weibull-III distribution cumulative density function (CDF) is represented by the following equation:

W-III CDF (1)

$$F_{H_s}(h_s) = 1 - e^{-\left(\frac{h_s-\lambda}{\rho}\right)^{\beta}}$$

Where ß > 0 is the shape parameter, ρ > 0 is the scale parameter, and λ is the location parameter.

Gumbel distribution CDF is represented by:

Gumbel CDF (2)

$$F_{H_s}(h_s) = \mathrm{e}^{-\,e^{-\frac{x-\mu}{\beta}}}$$

Where μ: is the location parameter, and β > 0 is the scale parameter.

The parameters are calculated by the methods of moments (MME) and their values are presented in Table 4. MME parameter estimation method is explained in chapter 4.

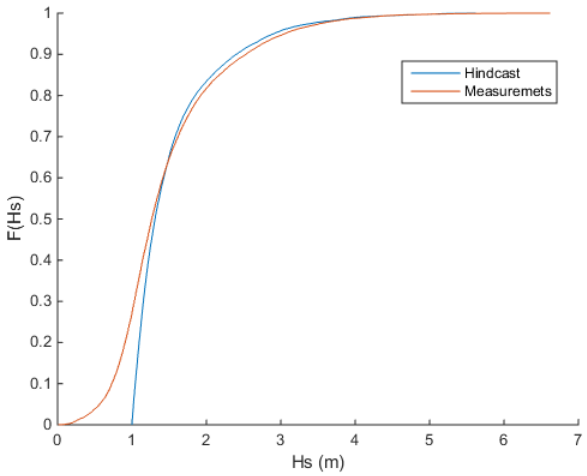

Figure 25: CDF comparison of Hindcast and Measurements

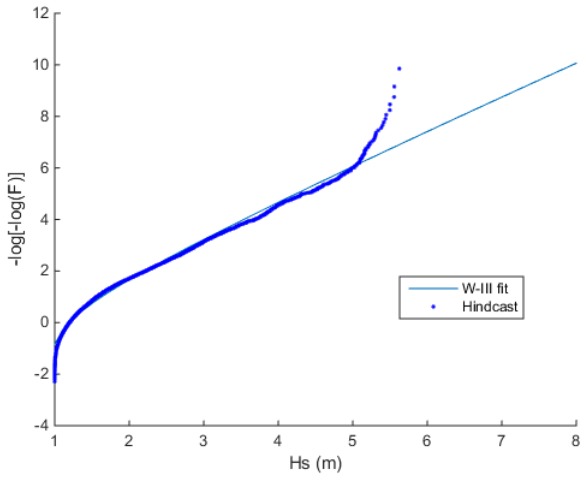

Figure 26: Hindcast fit to W-III distribution

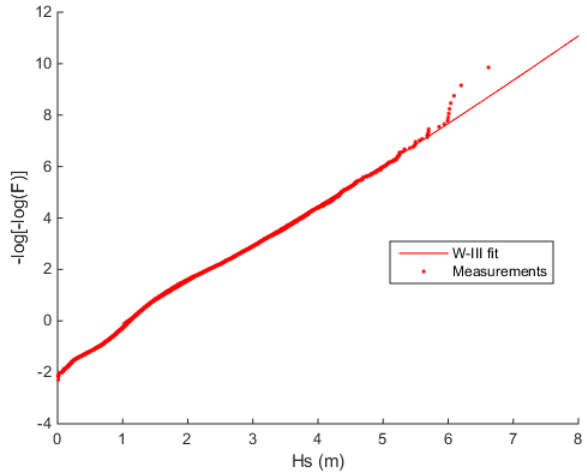

Figure 27: Measurements fit to W-III distribution

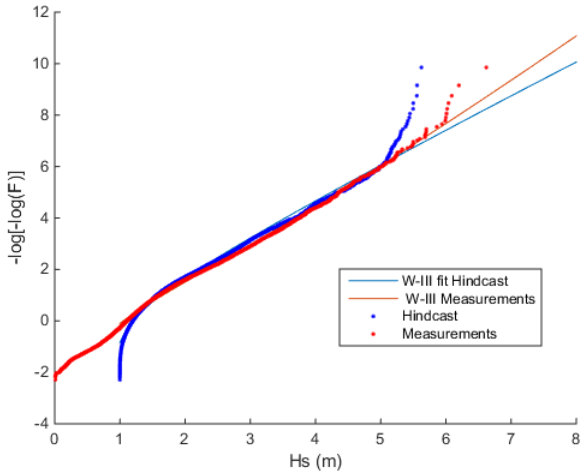

Figure 28: Comparison of fitted distributions

The probability plots provide a clearer picture of hindcast performance in estimating wave heights, Hs, for a given cumulative probability, F. It was found from Figure 23 and Figure 24 that hindcast data underestimates the measurement data. Figure 28 is used to test this finding, where it shows dots and lines. The dots are the data points and the lines are the fitted distributions. First, looking at the data (dots), at the tails, the blue dots are to the left of the red ones, that means for a certain probability, the hindcast will in fact underestimate the measured

wave. This agrees with findings from Figure 23 and Figure 24, however, looking at the fitted distributions (lines), at the tails, the situation here is the opposite, the red line is to the left of the blue life, that is, the hindcast fitted distribution is not underestimating the extremes, in the contrary, it is fairly conservative.

Looking at Figure 28, the dots at the low sea-states behave differently, and that is a result of the filtering done to the matched datasets. The data is filtered according to the following criteria: The data pairs are sorted according to hindcast value in ascending order, and all pairs with hindcast value of less than 1 meter are filtered out. This caused a clear drop in the blue dotted line, whereas the red one continued to zero meters, because there are matched pairs with hindcast values of above 1 meter and measurement values below 1 meter. The filtering of the low sea-states is performed to increase the quality of the fitting for the high sea-states. For extreme estimations, the interest is getting a distribution that fits the data and most importantly honors the tail, to produce realistic and meaningful estimates.

3.4 Directional Comparison

A final comparison to evaluate the validation of hindcast is checking the direction of waves in comparison to measurements. Direction rose diagrams are shown in Figure 29 to Figure 32, that compare bivariate data, i.e. rose diagrams that show the relation between two variables, that are the direction density with either Hs or Tp. Rose diagrams of significant wave heights, Hs, and of peak periods, Tp, are presented in Figure 29 to Figure 32. The main reason for this comparison is to check that the hindcast data directions are good estimates of those of the measurement data, and to link the amplitudes of Hs or Tp accompanied with directions.

Figure 29 to Figure 32 show that the hindcast in general represents the measurement data in terms of directions, the main direction of waves (where waves are coming from) is the West. However, if a detailed look is given, there is less spreading in the hindcast data than spreading in the measurements.

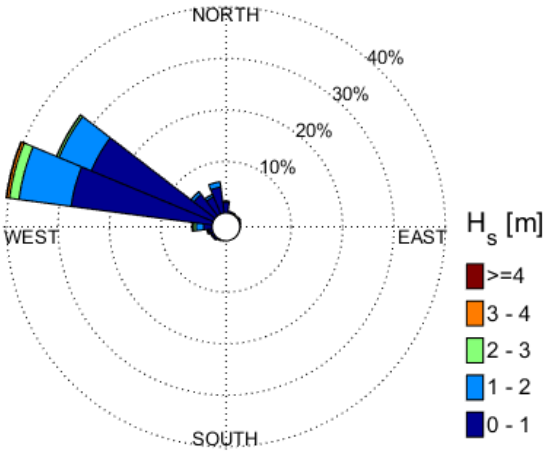

Figure 29: Rose diagram for Hindcast Hs (Direction of where the waves are coming from)

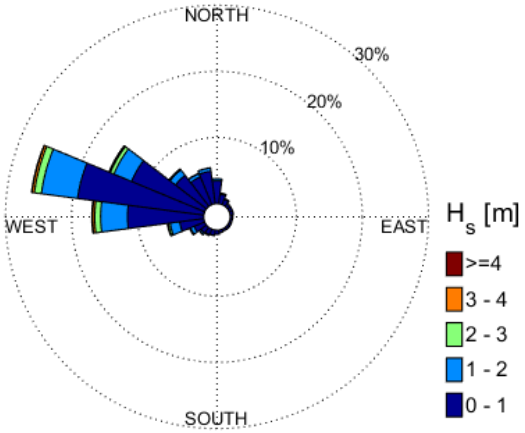

Figure 30: Rose diagram for Measurements Hs (Direction of where the waves are coming from)

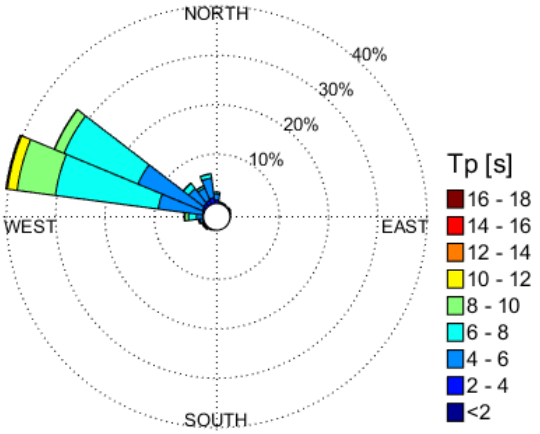

Figure 31: Rose diagram for Hindcast Tp (Direction of where the waves are coming from)

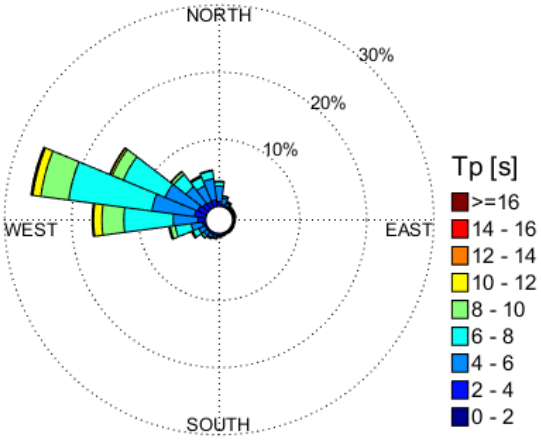

Figure 32: Rose diagram for Measurements Tp (Direction of where the waves are coming from)

3.5 Conclusion of Hindcast Validation

The time series comparisons show that the hindcast is capable of representing the sea to some degree. A more detailed look at the scatter of simultaneous pairs, and qq-plot showed that for the high sea-states, the hindcast tends to give lower wave heights that the measurement wave heights. Probability paper plots with 3-parameter Weibull fitting of both hindcast and measurement data showed that the hindcast will not underestimate the extremes; it will rather be slightly conservative. And the direction roses show good alignment.

As a result of hindcast validation comparisons, the level of agreement between the hindcast the measurement data shown in this section is good enough to consider the hindcast a valid representative of the sea. This conclusion, of the hindcast validity of Location 5, assumes that the hindcast data is a good replacement of measurement data and will represent the sea-state, both low and high, in an appreciable way. Hindcast data of the other locations, locations 1 – 4, where no buoy measurements are available, will be considered also as valid data and will be used in further study of extremes in the Eastern Mediterranean. Nevertheless, uncertainties increase with higher sea-states.

4 Literature Review

4.1 Introduction

Environmental loading is a major concern for offshore structures. According to NORSOK standard, combination of environmental actions can be calculated based pre-defined probabilities of exceedance (safety levels) as shown in the following table, Table 5. Among the different factors contributing to environmental action, such as wind, wave, current, ice, snow and earthquake, the waves are normally the governing environmental load factor for floating structures. For subsea structures such as pipelines, where the effect of wave demolishes with water depth and the effect of current is still there, current may become the governing factor. However, a system of pipes is connected from a source to a sink, is seriously affected by movements, therefore, failure moods due to movements are most likely to be the governing factor in design, i.e. heave motion of a platform or VIV motions in riser. This thesis provides estimates of the 10^{-2} and 10^{-4} waves.

A wave model is essential for predicting the ocean state. Ocean waves are irregular and random by nature. Both linear and non-linear random wave models are available. A linear random wave model constructs the wave as a summation of many small linear waves with different sizes and frequencies, and random phases to each other. A non-linear random wave model constructs the wave from small waves with components that interact non-linearly with each other.

Table 5: Combination of environmental actions with expected mean values and annual probability of exceedance 10-2 and 10-4 (NORSOK N-003, 2007, p.30)

Limit state	Wind	Waves	Current	Ice	Snow	Earthquake	Sea level [a]
Ultimate Limit State	10^{-2} 10^{-1} 10^{-1} - -	10^{-2} 10^{-1} 10^{-1} - -	10^{-1} 10^{-2} 10^{-1} - -	- - 10^{-2} - -	- - - 10^{-2} -	- - - - 10^{-2}	10^{-2} 10^{-2} m m m
Accidental Limit State	10^{-4} 10^{-2} 10^{-1} - -	10^{-2} 10^{-4} 10^{-1} - -	10^{-1} 10^{-1} 10^{-4} - -	- - - 10^{-4} -	- - - - -	- - - - 10^{-4}	m* m* m* m m

[a] m - mean water level
m* - mean water level, including the effect of possible storm surge
Seismic response analysis should be carried out for the most critical water level.

Wave conditions are required for build the wave model, then to be used for structural design. Wave conditions can be represented by both deterministic and stochastic methods (DNV-RP-C205, 2007; ISO 19902, 2007).

Deterministic equations are used to describe the wave particle motion based on hydrodynamics, boundary conditions and applicable wave theory for a given wave condition. For quasi-static structural responses it is recommended to use the deterministic methods to describe a wave. Deterministic methods are simpler than the other methods and they are based on static structure design. Define a variable β as follows:

Relative frequency relation, Beta (3)

$$\beta = \frac{\omega}{\omega_o} = \frac{Excitation\ Frequency\ (of\ the\ load)}{Eigen\ Frequency\ (of\ the\ structure)}$$

For $\beta \ll 1$, the excitation frequency is much lower than the natural frequency of the structure, the dynamic behavior of the structure is described as quasi-static, where the dynamics are govern by stiffness. Offshore jacket platforms and tension-leg platforms are examples of quasi-static structures.

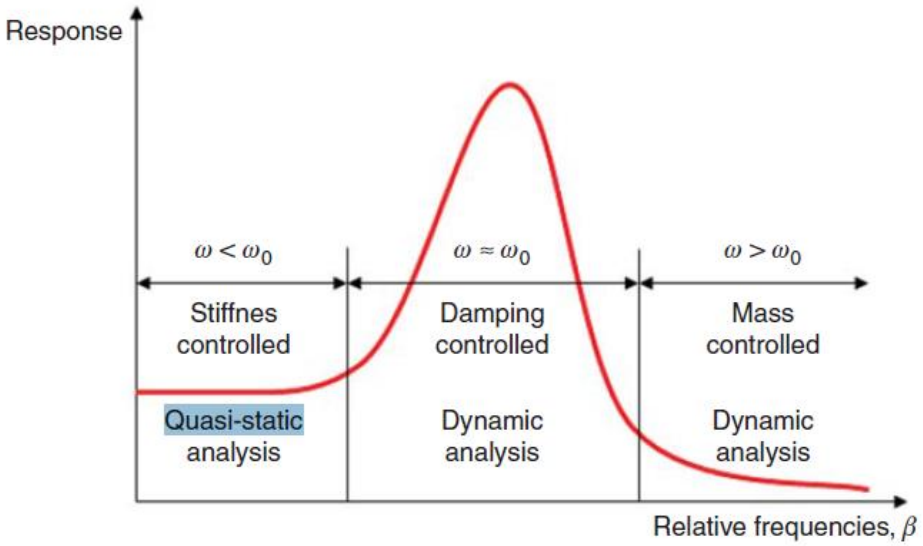

Figure 33: Different dynamic cases for harmonic loading (Gudmestad, 2015)

Structures with $\beta \approx 1$ are subject to resonance, with dynamics response behavior governed by damping. And structures with $\beta \gg 1$ have a dynamic response behavior governed by mass.

Probabilistic methods are used to estimate wave parameters. Stochastic methods are used for structures that have considerable dynamic responses. Time series stochastic modeling of the sea-state and the structure kinematics is required in such cases (Gudmestad, 2015).

The sea-state is assumed to be stationary process, i.e. the mean and standard deviation of elevation at a given point are constant, for a period of three hours is set as a standard. However the period of stationarity can range from 30 minutes to 10 hours (DNV-RP-C205, 2007).

Wave conditions have two components, wind waves and swell waves. Wind waves are the waves created locally, and swell waves are the waves created remotely and traveled considerable distance (fetch) to arrive at the location being studied. The two components of waves do not merge into one wave system and they may flow in different directions; therefore we have to study them separately. (Wang and Hwang, 2001).

4.2 Wave Theory

After using statistical methods for finding the wave parameters of the desired safety level, a valid wave theory is to be selected. Some of the commonly used wave theories are the Linear and the Stokes (2nd to 5th order) wave theories.

For a given wave height H, wave period T (normally obtained by statistical methods), and water depth d, the selection of a valid wave theory is done using the ranges of validity graph, shown in Figure 34. The horizontal axis $\left(\frac{d}{T^2}\right)$ is a measure of water shallowness, and the vertical axis $\left(\frac{H}{T^2}\right)$ is a measure of wave steepness. The point is to be plotted for the wave condition being considered, and the graph will indicate the applicable theory for such a wave condition.

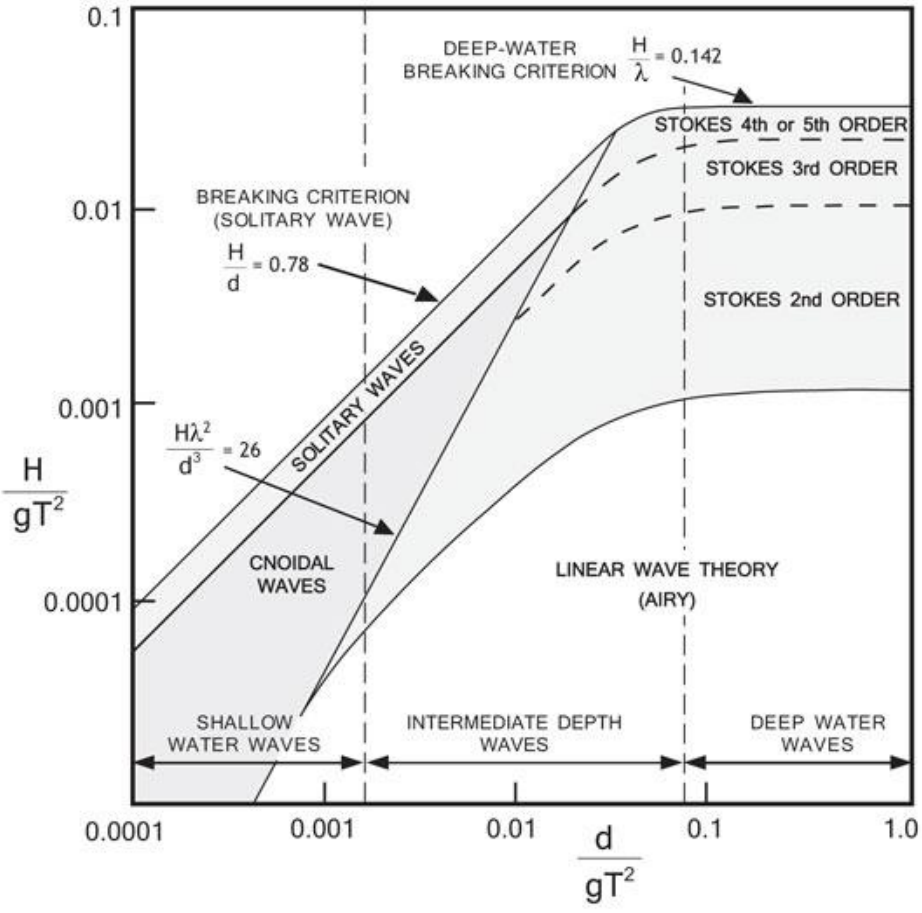

Figure 34: Ranges of validity for various wave theories

For a particular sea-state (H and Tp), relevant valid wave theory gives equations that solve the kinematics, horizontal fluid velocity and acceleration, of a 2D regular wave. The linear wave

theory solves for a uniform sinusoidal wave. Those velocity and acceleration are used as input information for calculating wave loads on structures. Kinematic equations are relevant for the seabed (z= - d) up to the mean sea level (MSL, at z=0). Stretching or extrapolation techniques are used to account for the points higher the MSL up to the wave crest. Figure 35 shows the difference between a linear and a non-linear wave.

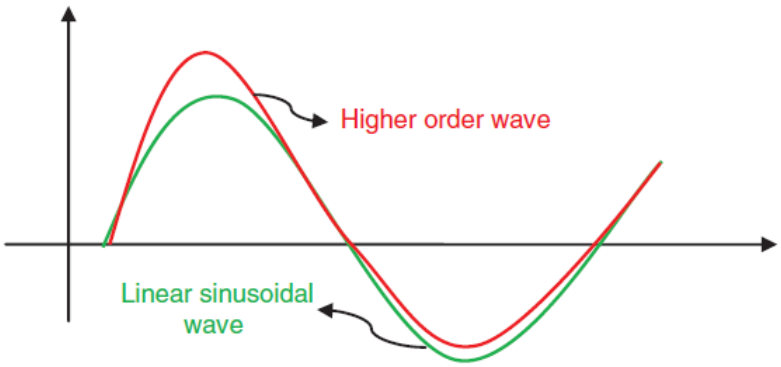

Figure 35: Nonlinear versus linear wave (Gudmestad, 2015)

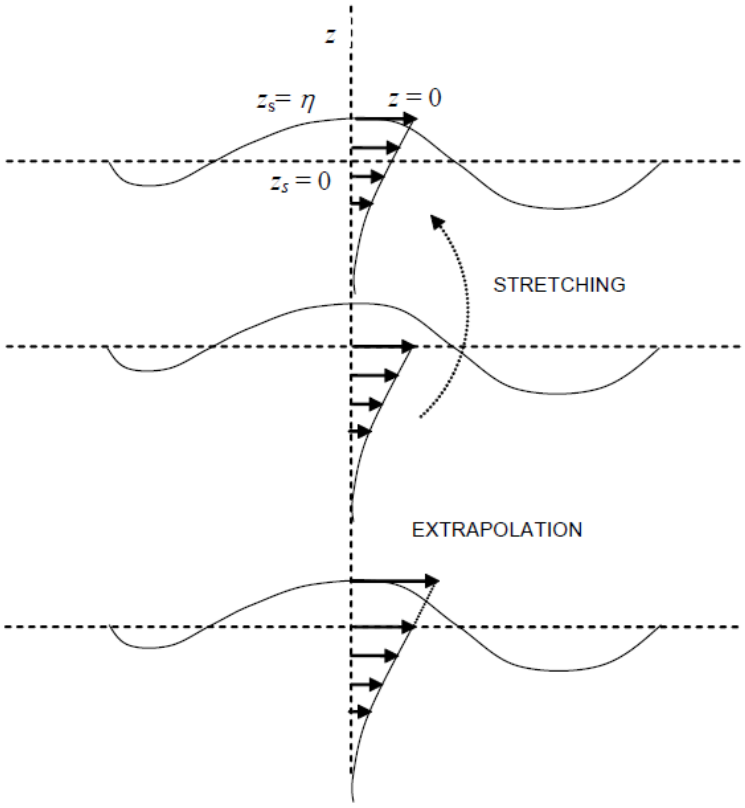

Figure 36: Stretching and extrapolation of velocity profile

Figure 35 shows the difference between a linear wave and a non-linear wave. Non-linear waves have higher crests and smaller troughs. Figure 36 shows the difference between extrapolation and stretching techniques. Where z is the particle elevation (reference is MSL at $z = 0$) z_s is the stretched elevation, and η is the crest height. Extrapolation is a continuation of the velocity profile from MSL to crest height, resulting in a crest height velocity that is considerably larger than velocity at MSL; it overrates the wave induced forces. Whereas stretching, as the name suggests, is stretches the velocity profile from MSL to wave crest, resulting in a crest height velocity that is equal to the "pre-stretching MSL velocity"; it slightly underrates the wave induced forces on marine structures.

4.3 Short term wave conditions

For a stationary sea-state, that is described by Hs and Tp, where Hs is the significant wave height (average height of wave crest to trough), defined as (Gudmestad, 2015, p.41):

"Average of the third of the highest waves in irregular sea-state from a given wave group, or the wave height a trained observer would estimate by looking at the sea surface." Nowadays it is usually defined as (Holthuijsen, 2007, p.70):

"*Four times the standard deviation of the surface elevation, or equivalently as four times the square root of the zeroth-order moment of the variance density spectrum*."

Real sea-state waver are irregular and random, and they can be modelled as a summation of sinusoidal wave components. Short term stationary irregular sea-states are described by wave spectra, i.e. the power spectral density function of the vertical sea surface displacement (DNV-RP-C205). Tp is the spectral peak period, the period that corresponds to the maximum energy density of the wave spectrum. The wave spectrum is the energy density of a wave as a function of frequency, in terms of vertical sea surface displacement. The most commonly used wave spectra for wind-seas are the Pierson-Moskowitz (PM) spectrum and the JONSWAP spectrum. Both spectra very well represent the most severe cases of wind-sea, PM is better for fully-developed sea and JONSWAP is better for developing sea-states (fetch limited) (Hasselmann et al. 1976; Pierson and Moskowitz, 1964).

Whereas, in open seas, waves consists of wind waves and swell waves. Two-peaked spectrum is available for such open sea locations and could account for both wind and swell wave components. A commonly used example is the Torsethaugen spectrum (Torsethaugen, 1996). Equations for PM and JONSWAP spectra are found below.

The spectral moments m_n of general order n are defined as

Spectral moments (4)

$$m_n = \int_0^\infty f^n S(f)\, df$$

Where f is the wave frequency, and $n = 0, 1, 2, \ldots$

The power spectral density $S(\omega)$ is a function of the angular frequency ω, and it is defined as:

Spectral power density (5)

$$S(\omega) = S(f)/2\pi$$

The corresponding spectral moment M_n, is defined as a function of frequency, spectral power density and spectral moments.

Corresponding spectral moments (6)

$$M_n = \int_0^\infty \omega^n \; S(\omega)\, d\omega = (2\pi)^n \, m_n$$

The following sea-state parameters can be defined in terms of spectral moments:

Table 6: Sea-state parameters definitions in terms of spectral moments

The significant wave height Hs:	$H_{m0} = 4\sqrt{m_0} = 4\sqrt{M_0}$	**Wave height Hs (7)**
The zero-up-crossing period T_z:	$T_{m02} = \sqrt{\frac{m_0}{m_2}} = 2\pi\sqrt{\frac{M_0}{M_2}}$	**Zero-up-crossing Tz (8)**
The mean wave period T_1:	$T_{m01} = \frac{m_0}{m_1} = 2\pi\frac{M_0}{M_1}$	**Mean period T1 (9)**
The mean crest period T_c:	$T_{m24} = \sqrt{\frac{m_2}{m_4}} = 2\pi\sqrt{\frac{M_2}{M_4}}$	**Mean crest period (10)**

The significant wave steepness S_c: $S_{m02} = \frac{2\pi}{g}\frac{H_{m0}}{T_{m02}^2} = \frac{2}{\pi g}\frac{M_2}{\sqrt{M_0}}$ **Wave steepness (11)**

The Pierson-Moskowitz (PM) Spectrum $S_{PM}(\omega)$ is given by:

The Pierson-Moskowitz Spectrum (12)

$$S_{PM}(\omega) = \frac{5}{16} H_s^2 \omega_p^4 \, \omega^{-5} \exp\left(-\frac{5}{4}\left(\frac{\omega}{\omega_p}\right)^{-4}\right)$$

Where $\omega_p = 2\pi/T_p$ is the angular peak spectral peak frequency.

The JONSWAP Spectrum $S_J(\omega)$ is given by:

The JONSWAP Spectrum (13)

$$S_J(\omega) = (1 - 0.287 \ln\gamma)\, S_{PM}(\omega)\, \gamma^{\exp\left(-0.5\left(\frac{\omega-\omega_p}{\sigma\,\omega_p}\right)^2\right)}$$

Where γ is a non-dimensional peak shape parameter, σ is a spectral width parameter.

$\sigma = 0.07\ for\ \omega \le \omega_p$, and $\sigma = 0.09\ for\ \omega > \omega_p$.

According to DNV, for the JONSWAP experiment data, the average value for the peak shape parameter is $\gamma = 3.3$. The effect of the peak shape parameter is shown in Figure 37.

For $\gamma = 1$, the JONSWAP spectrum reduces to the PM spectrum.

The JONSWAP spectrum is considered valid for the following criterion:

Validity criterion for using JONSWAP (14)

$$3.6 < \frac{T_p}{\sqrt{H_s}} < 5$$

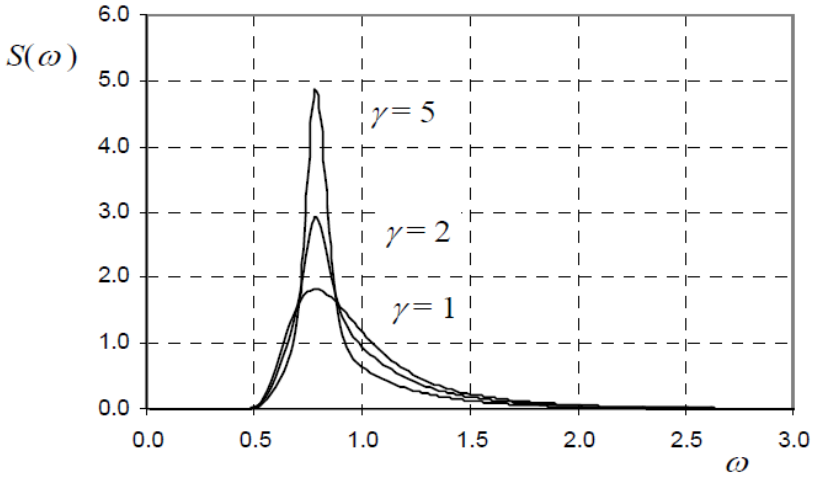

Figure 37: The effect of peak shape parameter on JONSWAP spectrum

The use of wave spectra is helpful in response analysis of marine structures and vessels. Directional effects are of critical importance to response. The spectrum itself does not give information about direction; therefore attention is required, due to the fact that swell sea and wind-sea may be acting on the structure from different directions, causing an undesired loading state that may cause losses. Therefore, directional sea-state analysis is required for marine structures response analysis.

4.4 Long term wave statistics

The long-term variation of a sea-state can be described by a generic probabilistic distribution (model) or a scatter diagram. Governing parameters of a sea-state are the significant wave height Hs, spectral peak period Tp, and direction. Generic models are established by fitting probabilistic distributions to wave data. Both marginal distributions (1-variable distribution, say, for Hs) and joint environmental models (2-variable distribution, say, for Hs and Tp) can be applied for describing a given location's wave conditions. Scatter diagrams show the frequency of occurrence of a given wave height and period pair (Hs, Tp). Wave heights and periods are split into classes (bins), the width for Hs classes is 0.5 meters, and for Tp classes is 1 second.

According to DNV recommended practices, two different analysis strategies are normally applied: *the global model* (referred to in this project as All Sea-states approach or abbreviated as ID: initial distribution). And the *event model* (referred to as Peak-over-threshold (POT) approach or Annual Maxima (AM) approach). The two analysis strategies are applied in this thesis in the form of three approaches, ID, POT and AM.

The global model is typically applied for the whole dataset of one of sea-state parameter, say Hs. The event model can be applied to a defined event dataset (a subset of the whole dataset), say monthly or yearly maxima. There is a trade-off in the selection of approach, for the ID approach the whole dataset is used, the number of points is large (in hundreds of thousands for a hindcast covering around 40 years of 3-hourly data) but the data is highly correlated and this may cause the distribution fitting unable to discriminate the tail behavior properly. For AM and POT approaches, where a subset of the whole dataset is used (i.e. for AM the number of points is equal to the number of years covered by hindcast), the data is highly independent, but their scarceness increase statistical uncertainty. This makes the POT as the preferred approach

because it has the advantages of AM and the number of points in a POT dataset is higher than that of AM, leading to a smaller statistical uncertainty. However the selection of the threshold is critical, therefore, for selecting a suitable threshold, it is required to perform a sensitivity analysis of extreme estimation with respect to threshold level.

Commonly used fitting techniques are the Method of Moments (MOM or MME) and the Maximum Likelihood Estimation (MLE). In MME the dataset's moments (mean, variance and skewness) are calculated and applied to those of the selected distribution. In MLE the function representing the likelihood for obtaining the values of the dataset is maximized. In the fitting procedure, it is crucial that the fitted distribution represents the tail of the dataset, especially if the purpose of the fitting was extreme sea-state estimation.

Probabilistic distributions

This section lists the distributions being considered in this study and the section below covers the parameter estimation methods. These five distributions are considered based on industry best practices in relevant offshore engineering applications (Haver, 2013; DNV, 2007). Followed by the *ecdf* definition of the dataset, which is always plotted on the same figure with one (or more) of the distributions for evaluating the quality of the fit.

Weibull (3-pararameters) distribution cumulative density function (CDF) is represented by the following equation:

W-III CDF (15)

$$F_{H_s}(h_s) = 1 - e^{-\left(\frac{h_s-\lambda}{\rho}\right)^{\beta}}$$

Where β > 0 is the shape parameter, ρ > 0 is the scale parameter, and λ is the location parameter. 2-parameter Weibull is not used in this document, and the name Weibull refers only to 3-parameter Weibull unless else specified.

Gamma distribution CDF is represented by:

Gamma CDF (16)

$$F_{H_s}(h_s) = 1 - \frac{1}{\Gamma(\alpha)}\Gamma(\alpha, \beta.h_s)$$

Where α > 0 is the shape parameter, and β > 0 is the rate parameter.

GEV distribution CDF is represented by:

GEV CDF (17)

$$F_{H_s}(h_s) = \mathrm{e}^{-\left(1+s.\frac{(h_s-a)}{b}\right)^{-\frac{1}{s}}}$$

Where a: is the location parameter, b: is the scale parameter, and s: is the shape parameter.

Lognormal distribution probability density function (PDF) is represented by the following equation:

Lognormal CDF (18)

$$F_{H_s}(h_s) = \Phi\left[\frac{\ln(h_s) - \mu_{\ln h_s}}{\sigma_{\ln h_s}}\right]$$

Lognormal CDF (19)

$$F_{H_s}(h_s) = \frac{1}{\sigma_{h_s}\sqrt{2\pi}} \cdot \int_{-\infty}^{h_s} \frac{\exp\left(\frac{-\left(\ln(h_s) - \mu_{h_s}\right)^2}{2\sigma_{h_s}^2}\right)}{h_s} dh_s$$

Where σ is the standard deviation and μ is the mean of significant wave height dataset. Two equations for CDF of lognormal are presented above; the first is the function in terms of the standard normal function. And the second is the full function for lognormal CDF.

Gumbel distribution CDF is represented by:

Gumbel CDF (20)

$$F_{H_s}(h_s) = \mathrm{e}^{-\,e^{-\frac{x-\mu}{\beta}}}$$

Where μ: is the location parameter, and β > 0 is the scale parameter.

Data *ecdf*, the empirical CDF of the dataset is represented by:

$$F_{Hs}(i) = \frac{i}{N+1}$$

For instance, if *Hs* is a dataset with N values, and *i* is the index of *Hs* that runs from 1 to N, then the empirical cumulative density function of *Hs(i)* is $F_{Hs}(i)$, that is only valid if the dataset *Hs* is sorted in an ascending manner. The dataset is always plotted using the *ecdf* against the distributions to evaluate their fitting performance.

4.5 Parameter estimation methods

The parameters of the above distributions were either estimated by the “Maximum Likelihood Estimator” (MLE) method or by the “Method of Moments” (MME). Both are widely used methods in statistics, in applications where a sample set of data is given, say of height measurements that are assumed to follow a certain statistical model, these methods are tools to find the model’s parameters that fits sample data set.

MLE method estimates the parameters by maximizing the likelihood function, a function that maximizes the probability agreement of the selected model with the sample dataset. MLE is the best possible estimator method if the sample being modelled is of a very large size (given that the data is independent).

MME method estimates the parameters by setting the moments of the selected model equal to those of the sample dataset. Model moments are the mean, variance, skewness and kurtosis. MOM approach gives more weight to tail observations than MLE, it fits the moments of the population to those of the distribution.

The moments for a given dataset X are found as follows:

First moment: Mean (21)

$$m_X = \frac{1}{n}\sum_{i=1}^{n} x_i$$

Second moment: Variance (22)

$$s_X^2 = \frac{1}{n-1}\sum_{i=1}^{n}(x_i - m_X)^2$$

Third moment: Skewness (23)

$$\gamma_X = \frac{\frac{1}{i}\sum_{i=1}^{i}(x_i - m_X)^3}{[s_X^2]^{3/2}}$$

For example, MME for a Gumbel distribution (where μ is the location parameter, and β is the scale parameter) is defined as follows for a dataset with mean m_X, and standard deviation s_X. Two equations with two unknowns, the Gumbel parameters can be solved (Haver, 2013)

MME mean equation for Gumbel (24)

$$m_X = Mean_{\,of\ distribution} = \mu + 0.57722\beta$$

MME SD equation for Gumbel (25)

$$s_X = SD_{\,of\ distribution} = 1.28255\beta$$

For 3-parameter Weibull (where β is the shape parameter, ρ is the scale parameter, and λ is the location parameter), use of the third moment is needed, which is the skewness. The parameters can be solved using the following (three) equations (Bury, 1975).

MME mean equation for Weibull (26)

$$m_X = Mean_{\,of\ distribution} = \lambda + \rho\Gamma\left(1 + \frac{1}{\beta}\right)$$

MME SD equation for Weibull (27)

$$s_X^2 = \left[SD_{\,of\ distribution}\right]^2 = \rho^2\left[\Gamma\left(1 + \frac{2}{\beta}\right) - \Gamma^2\left(1 + \frac{1}{\beta}\right)\right]$$

MME skewness equation for Weibull (28)

$$\gamma_X = Skewness_{\,of\ distribution} = \frac{\Gamma\left(1 + \frac{3}{\beta}\right) - 3\Gamma\left(1 + \frac{1}{\beta}\right)\Gamma\left(1 + \frac{2}{\beta}\right) + 2\Gamma^3\left(1 + \frac{1}{\beta}\right)}{\left[\Gamma\left(1 + \frac{2}{\beta}\right) - \Gamma^2\left(1 + \frac{1}{\beta}\right)\right]^{\frac{3}{2}}}$$

In this project the MME and MLE calculations are computed with R Workspace *fitdistrplus* package, except for the MME Weibull distribution. MME Weibull distribution parameters are manually calculated using the equations given above.

4.6 Distribution selection recommendations

For ID approach, 3-parameter Weibull distribution can be assumed for the marginal distribution of Hs (Nordenstrøm, 1973). For POT approach, a 2-parameter Weibull distribution or exponential distribution is recommended, and the General Pareto distribution is not recommended (DNV-RP-C205, 2007). And for AM approach, the recommendations are as follows: a Gumbel distribution is a best estimate for a distribution of maxima, a record of at least 20 years of data points, and considering the year to be from June to June (instead of January to January) to represent the whole winter in one year period.

4.7 Extreme estimations

Extreme events are rare, their chance of occurrence is often rated with return periods; say the 100-year wave, defined as the wave that is expected to occur once in a period of 100 years. However this can also be defined as the wave that has the annual probability of exceedance of 0.01, i.e. there is 1% percent chance that the 100 year wave happens every year.

In order to find extremes that correspond to certain return period, a relation between the annual probability of exceedance (P_a) and cumulative probability (F_{Hs}) is required. And this relation is set as follows,

Annual Probability of Exceedance (29)

$$Annual\ probability\ of\ exceedance\ (P_a) = \frac{1}{return\ period\ (T_r)}$$

Converting the annual probability of exceedance to a probability of exceedance that agrees with the number of observations available in the dataset being considered,

Probability of Exceedance (30)

$$Probability\ of\ exceedance\ (P) = \frac{Annual\ probability\ of\ exceedance\ (P_a)}{Annual\ average\ number\ of\ data\ points\ (N_a)}$$

Finding cumulative probability (F_{Hs})

Cumulative Probability (31)

$$Cumulative\ probability, F_{Hs} = 1 - Probability\ of\ exceedance\ (P)$$

Hence, the cumulative probability (F_{Hs}) is related to the return period (Tr) by the following equation:

Cumulative Probability Calculated from Return Period (32)

$$Cumulative\ probability\ (F_{Hs}) = 1 - \frac{\frac{1}{return\ period\ (T_r)}}{Annual\ average\ number\ of\ data\ points\ (Na)}$$

Cumulative probability (F_{Hs}) is used in the statistical models (fitted to data) to find wave height Hs corresponding to certain return period.

Where *Na* is the average annual observations of Hs values in the created (method specific) Hs dataset. For example, for annual maxima approach the annual average number of observations, Na = 1, since only the max annual value is being considered. For all sea-states approach, associated with 3-hourly sampling, the annual average number of observations, Na = 2920. And for POT approach, the average annual number of observations for the selected threshold of 3 meters is, Na = 9.1, however, in POT approach the *Na* number is a function of threshold, a higher threshold will lead to less annual observations in average.

5 Sea-State Analysis

Hindcast data provided by DICCA is used for this section. This section provides a sea-state analysis that includes seasonal, directional, swell and location analysis. This analysis answers important questions for marine design and operations, such as: how harsh is the ocean in winter? Where do the wind waves come from? Where do the swell waves come from? Where the winds are blowing from? What is the difference in waves between locations?

The analyses include scatter diagrams, quantile plots, probability papers, and directional rose diagrams. The purpose of this investigation is to illustrate the differences between the seasons, direction segments, and locations. This analysis is a main input for decision-making for the following issues: the omnidirectional assumption validity, the spectrum selection, start of operation (for long and “intellectual” operations), and others.

5.1 Seasonal Analysis

The main goal of this section is to visualize the natural variation of significant wave height, Hs, and spectral peak period, Tp, in terms of seasons. Hindcast data are split into four seasons: Spring, summer, autumn and winter. The separated data is analyzed separately (season by season). The Hs-Tp scatter diagram of the original data is shown in Figure 38, and the seasonal scatters are shown as well, from Figure 39 to Figure 42. The four seasons are presented. It is interesting to see the contrast between the scatters. If attention is given to wave heights between 8 – 8.5 meters, in the original hindcast shows that the total is 2 wave occurrences, but winter scatter does not show any of them. Looking at waves between 7.5 – 8 meters, the original scatter shows 9 wave occurrences, however winter scatter shows only 3 of them. Concluding that the highest 11 waves that occurred in the 37 years being provided by hindcast,

only 3 of them occurred in winter seasons, the rest occurred in other seasons, that means other seasons could be worth attention while planning marine operations, especially operations that take relatively long time periods to be accomplished.

It is also notes that spring and summer are very calm. Highest waves in summers (for the 37 years of hindcast) are between 2.5 – 3 meters high with corresponding spectral-peak periods of 7 – 10 seconds. Highest waves in springs are between 3.5 – 4.5 meters high with corresponding spectral-peak periods of 9 – 11 seconds.

However autumns and winters are enormously different. Highest waves in autumns are between 6.5 – 8.5 meters high with corresponding spectral-peak periods of 12 – 14 seconds. Highest waves in winters are between 7 – 8 meters high with corresponding spectral-peak periods of 11 – 14 seconds. Noting that in those two seasons, rarely occurred, very long waves with spectral-peak periods of 14 – 18 seconds with corresponding heights from 0.5 – 2 meters.

The scatters presented from Figure 38 to Figure 42 belong to Location 1. The full set of scatters for all the points is available in the APPENDIX B.

Tp(s) / Hs(m)	0 - 1	1 - 2	2 - 3	3 - 4	4 - 5	5 - 6	6 - 7	7 - 8	8 - 9	9 - 10	10 - 11	11 - 12	12 - 13	13 - 14	14 - 15	15 - 16	16 - 17	17 - 18	18 - 19	Total
0 - 0.5	2	5	1,241	7,235	11,929	8,716	2,523	1,471	556	315	238	104	42	27	3	-	-	-	-	34,407
0.5 - 1	1	-	132	9,195	33,916	55,533	44,432	9,422	3,120	1,568	427	155	86	44	3	-	1	-	-	158,035
1 - 1.5	-	-	-	79	5,011	16,445	27,973	23,814	4,369	2,235	1,093	371	121	36	5	1	-	-	-	81,553
1.5 - 2	-	-	-	-	75	2,192	6,214	10,576	6,205	1,660	556	287	97	27	2	-	-	1	-	27,892
2 - 2.5	-	-	-	-	-	95	1,311	3,227	3,580	1,763	457	171	57	12	-	-	-	-	-	10,673
2.5 - 3	-	-	-	-	-	1	128	1,120	1,874	1,627	452	132	60	5	-	-	-	-	-	5,399
3 - 3.5	-	-	-	-	-	-	-	254	804	1,134	559	109	65	8	-	-	-	-	-	2,933
3.5 - 4	-	-	-	-	-	-	-	24	255	765	426	133	46	-	-	-	-	-	-	1,649
4 - 4.5	-	-	-	-	-	-	-	-	52	257	330	155	29	1	-	-	-	-	-	824
4.5 - 5	-	-	-	-	-	-	-	-	2	94	237	144	32	1	-	-	-	-	-	510
5 - 5.5	-	-	-	-	-	-	-	-	-	22	92	85	30	-	-	-	-	-	-	229
5.5 - 6	-	-	-	-	-	-	-	-	-	3	36	45	37	3	-	-	-	-	-	124
6 - 6.5	-	-	-	-	-	-	-	-	-	-	5	6	28	1	-	-	-	-	-	40
6.5 - 7	-	-	-	-	-	-	-	-	-	-	2	11	22	3	-	-	-	-	-	38
7 - 7.5	-	-	-	-	-	-	-	-	-	-	-	4	4	6	-	-	-	-	-	14
7.5 - 8	-	-	-	-	-	-	-	-	-	-	-	1	5	3	-	-	-	-	-	9
8 - 8.5	-	-	-	-	-	-	-	-	-	-	-	-	2	-	-	-	-	-	-	2
8.5 - 9	-	-	-	-	-	-	-	-	-	-	-	-	-	-	-	-	-	-	-	-
Total	3	5	1,373	16,509	50,931	82,982	82,581	49,908	20,817	11,443	4,910	1,913	763	177	13	1	1	1	-	324,331

Figure 38: Hs-Tp Scatter Diagram: All year round, hindcast Location 1

Hs(m) \ Tp(s)	0 - 1	1 - 2	2 - 3	3 - 4	4 - 5	5 - 6	6 - 7	7 - 8	8 - 9	9 - 10	10 - 11	11 - 12	12 - 13	13 - 14	14 - 15	15 - 16	16 - 17	17 - 18	18 - 19	Total
0 - 0.5	2	2	558	2,764	4,726	3,162	636	334	139	112	80	34	16	5	-	-	-	-	-	12,570
0.5 - 1	-	-	59	3,158	9,845	15,701	10,841	1,564	419	163	40	15	8	7	-	-	-	-	-	41,820
1 - 1.5	-	-	-	19	1,205	3,375	6,938	6,102	756	223	68	19	6	1	-	-	-	-	-	18,712
1.5 - 2	-	-	-	-	14	259	925	2,712	1,227	180	45	17	11	4	-	-	-	-	-	5,394
2 - 2.5	-	-	-	-	-	12	110	535	633	206	56	13	3	-	-	-	-	-	-	1,568
2.5 - 3	-	-	-	-	-	-	8	80	232	157	45	-	-	-	-	-	-	-	-	522
3 - 3.5	-	-	-	-	-	-	-	5	53	105	21	-	-	-	-	-	-	-	-	184
3.5 - 4	-	-	-	-	-	-	-	-	-	13	22	-	-	-	-	-	-	-	-	35
4 - 4.5	-	-	-	-	-	-	-	-	-	-	3	-	-	-	-	-	-	-	-	3
4.5 - 5	-	-	-	-	-	-	-	-	-	-	-	-	-	-	-	-	-	-	-	-
5 - 5.5	-	-	-	-	-	-	-	-	-	-	-	-	-	-	-	-	-	-	-	-
5.5 - 6	-	-	-	-	-	-	-	-	-	-	-	-	-	-	-	-	-	-	-	-
6 - 6.5	-	-	-	-	-	-	-	-	-	-	-	-	-	-	-	-	-	-	-	-
6.5 - 7	-	-	-	-	-	-	-	-	-	-	-	-	-	-	-	-	-	-	-	-
7 - 7.5	-	-	-	-	-	-	-	-	-	-	-	-	-	-	-	-	-	-	-	-
7.5 - 8	-	-	-	-	-	-	-	-	-	-	-	-	-	-	-	-	-	-	-	-
8 - 8.5	-	-	-	-	-	-	-	-	-	-	-	-	-	-	-	-	-	-	-	-
8.5 - 9	-	-	-	-	-	-	-	-	-	-	-	-	-	-	-	-	-	-	-	-
Total	2	2	617	5,941	15,790	22,509	19,458	11,332	3,459	1,159	380	98	44	17	-	-	-	-	-	80,808

Figure 39: Hs-Tp Scatter Diagram for Season 1 (spring)

Hs(m) \ Tp(s)	0 - 1	1 - 2	2 - 3	3 - 4	4 - 5	5 - 6	6 - 7	7 - 8	8 - 9	9 - 10	10 - 11	11 - 12	12 - 13	13 - 14	14 - 15	15 - 16	16 - 17	17 - 18	18 - 19	Total
0 - 0.5	-	-	84	450	1,429	1,500	307	118	69	20	9	-	-	1	1	-	-	-	-	3,988
0.5 - 1	-	-	4	742	5,104	20,843	20,275	3,219	398	49	8	4	8	2	-	-	-	-	-	50,656
1 - 1.5	-	-	-	-	125	2,290	10,267	9,031	1,235	115	14	5	1	-	-	-	-	-	-	23,083
1.5 - 2	-	-	-	-	-	26	417	1,801	1,088	153	7	-	-	-	-	-	-	-	-	3,492
2 - 2.5	-	-	-	-	-	-	16	111	211	88	21	-	-	-	-	-	-	-	-	447
2.5 - 3	-	-	-	-	-	-	-	9	17	4	-	-	-	-	-	-	-	-	-	30
3 - 3.5	-	-	-	-	-	-	-	-	-	-	-	-	-	-	-	-	-	-	-	-
3.5 - 4	-	-	-	-	-	-	-	-	-	-	-	-	-	-	-	-	-	-	-	-
4 - 4.5	-	-	-	-	-	-	-	-	-	-	-	-	-	-	-	-	-	-	-	-
4.5 - 5	-	-	-	-	-	-	-	-	-	-	-	-	-	-	-	-	-	-	-	-
5 - 5.5	-	-	-	-	-	-	-	-	-	-	-	-	-	-	-	-	-	-	-	-
5.5 - 6	-	-	-	-	-	-	-	-	-	-	-	-	-	-	-	-	-	-	-	-
6 - 6.5	-	-	-	-	-	-	-	-	-	-	-	-	-	-	-	-	-	-	-	-
6.5 - 7	-	-	-	-	-	-	-	-	-	-	-	-	-	-	-	-	-	-	-	-
7 - 7.5	-	-	-	-	-	-	-	-	-	-	-	-	-	-	-	-	-	-	-	-
7.5 - 8	-	-	-	-	-	-	-	-	-	-	-	-	-	-	-	-	-	-	-	-
8 - 8.5	-	-	-	-	-	-	-	-	-	-	-	-	-	-	-	-	-	-	-	-
8.5 - 9	-	-	-	-	-	-	-	-	-	-	-	-	-	-	-	-	-	-	-	-
Total	-	-	88	1,192	6,658	24,659	31,282	14,289	3,018	429	59	9	9	3	1	-	-	-	-	81,696

Figure 40: Hs-Tp Scatter Diagram for Season 2 (summer)

Hs(m) \ Tp(s)	0 - 1	1 - 2	2 - 3	3 - 4	4 - 5	5 - 6	6 - 7	7 - 8	8 - 9	9 - 10	10 - 11	11 - 12	12 - 13	13 - 14	14 - 15	15 - 16	16 - 17	17 - 18	18 - 19	Total
0 - 0.5	-	1	350	2,509	3,729	2,138	820	617	253	100	96	49	16	15	1	-	-	-	-	10,694
0.5 - 1	1	-	38	3,136	11,715	10,842	7,505	2,494	1,195	798	224	84	33	16	2	-	-	-	-	38,083
1 - 1.5	-	-	-	25	1,673	5,145	4,950	3,832	1,135	877	390	139	40	14	3	1	-	-	-	18,224
1.5 - 2	-	-	-	-	12	825	2,127	2,387	1,581	588	179	116	39	13	-	-	-	-	-	7,867
2 - 2.5	-	-	-	-	-	26	441	944	982	547	148	42	5	3	-	-	-	-	-	3,138
2.5 - 3	-	-	-	-	-	1	47	366	492	448	133	29	19	5	-	-	-	-	-	1,540
3 - 3.5	-	-	-	-	-	-	-	91	236	359	193	35	6	2	-	-	-	-	-	922
3.5 - 4	-	-	-	-	-	-	-	9	96	305	120	50	8	-	-	-	-	-	-	588
4 - 4.5	-	-	-	-	-	-	-	-	23	113	137	56	2	-	-	-	-	-	-	331
4.5 - 5	-	-	-	-	-	-	-	-	1	35	72	44	6	-	-	-	-	-	-	158
5 - 5.5	-	-	-	-	-	-	-	-	-	10	28	30	12	-	-	-	-	-	-	80
5.5 - 6	-	-	-	-	-	-	-	-	-	-	8	19	19	-	-	-	-	-	-	46
6 - 6.5	-	-	-	-	-	-	-	-	-	-	-	1	8	-	-	-	-	-	-	9
6.5 - 7	-	-	-	-	-	-	-	-	-	-	-	2	-	1	-	-	-	-	-	3
7 - 7.5	-	-	-	-	-	-	-	-	-	-	-	-	1	4	-	-	-	-	-	5
7.5 - 8	-	-	-	-	-	-	-	-	-	-	-	-	3	3	-	-	-	-	-	6
8 - 8.5	-	-	-	-	-	-	-	-	-	-	-	-	2	-	-	-	-	-	-	2
8.5 - 9	-	-	-	-	-	-	-	-	-	-	-	-	-	-	-	-	-	-	-	-
Total	1	1	388	5,670	17,129	18,977	15,890	10,740	5,994	4,180	1,728	696	219	76	6	1	-	-	-	81,696

Figure 41: Hs-Tp Scatter Diagram for Season 3 (autumn)

Hs(m) \ Tp(s)	0 - 1	1 - 2	2 - 3	3 - 4	4 - 5	5 - 6	6 - 7	7 - 8	8 - 9	9 - 10	10 - 11	11 - 12	12 - 13	13 - 14	14 - 15	15 - 16	16 - 17	17 - 18	18 - 19	Total
0 - 0.5	-	2	249	1,512	2,045	1,916	760	402	95	83	53	21	10	6	1	-	-	-	-	7,155
0.5 - 1	-	-	31	2,159	7,252	8,147	5,811	2,145	1,108	558	155	52	37	19	1	-	1	-	-	27,476
1 - 1.5	-	-	-	35	2,008	5,635	5,818	4,849	1,243	1,020	621	208	74	21	2	-	-	-	-	21,534
1.5 - 2	-	-	-	-	49	1,082	2,745	3,676	2,309	739	325	154	47	10	2	-	-	1	-	11,139
2 - 2.5	-	-	-	-	-	57	744	1,637	1,754	922	232	116	49	9	-	-	-	-	-	5,520
2.5 - 3	-	-	-	-	-	-	73	665	1,133	1,018	274	103	41	-	-	-	-	-	-	3,307
3 - 3.5	-	-	-	-	-	-	-	158	515	670	345	74	59	6	-	-	-	-	-	1,827
3.5 - 4	-	-	-	-	-	-	-	15	159	447	284	83	38	-	-	-	-	-	-	1,026
4 - 4.5	-	-	-	-	-	-	-	-	29	144	190	99	27	1	-	-	-	-	-	490
4.5 - 5	-	-	-	-	-	-	-	-	1	59	165	100	26	1	-	-	-	-	-	352
5 - 5.5	-	-	-	-	-	-	-	-	-	12	64	55	18	-	-	-	-	-	-	149
5.5 - 6	-	-	-	-	-	-	-	-	-	3	28	26	18	3	-	-	-	-	-	78
6 - 6.5	-	-	-	-	-	-	-	-	-	-	5	5	20	1	-	-	-	-	-	31
6.5 - 7	-	-	-	-	-	-	-	-	-	-	2	9	22	2	-	-	-	-	-	35
7 - 7.5	-	-	-	-	-	-	-	-	-	-	-	4	3	2	-	-	-	-	-	9
7.5 - 8	-	-	-	-	-	-	-	-	-	-	-	1	2	-	-	-	-	-	-	3
8 - 8.5	-	-	-	-	-	-	-	-	-	-	-	-	-	-	-	-	-	-	-	-
8.5 - 9	-	-	-	-	-	-	-	-	-	-	-	-	-	-	-	-	-	-	-	-
Total	-	2	280	3,706	11,354	16,837	15,951	13,547	8,346	5,675	2,743	1,110	491	81	6	-	1	1	-	80,131

Figure 42: Hs-Tp Scatter Diagram for Season 4 (winters)

Summer and spring are much calmer seasons than winter and autumn. Winter and autumn are almost alike in the severity of waves.

Ranges of wave heights and periods change from a season to another, and the direction where the waves are coming from also change. Four rose diagrams are plotted from Figure 43 to Figure 46, one for each season, showing the direction densities. The direction information used in the following roses is the mean direction, part of the hindcast dataset. Other direction information available are the peak direction and spread angles. A relation is made between

direction densities and range of significant wave height, therefore the rose diagrams, in addition to density, also show the corresponding Hs range (density) for every direction range (bivariate directional roses).

It is clear from rose diagrams that spring and summer waves are coming from same direction, between west and north-west. There is almost no spreading in the mean directions of waves and it is convenient to assume that the sea is omnidirectional, in spring and summer. Autumn and winter show more variation in the directions where waves are coming from. The main direction is still the same as spring and summer seasons. Moreover, the variation increase is mainly coming in the range from north to north-east. It is interesting to check wind speed directions and check correlation between wind and wave directions.

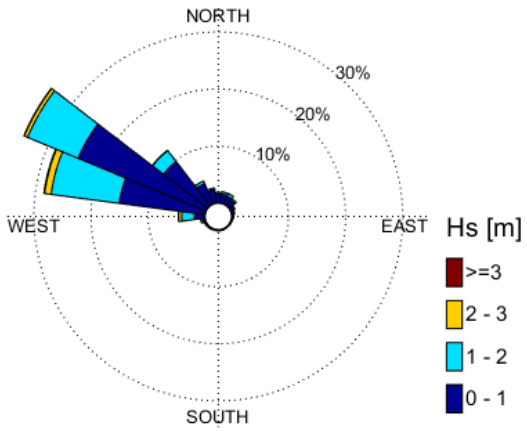

Figure 43: Rose diagram of Hs for Season 1 (spring)

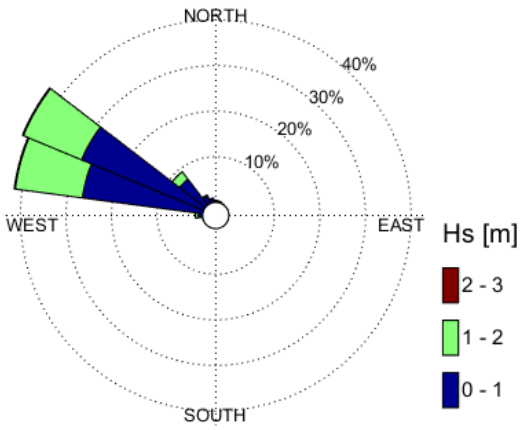

Figure 44: Rose diagram of Hs for Season 2 (summer)

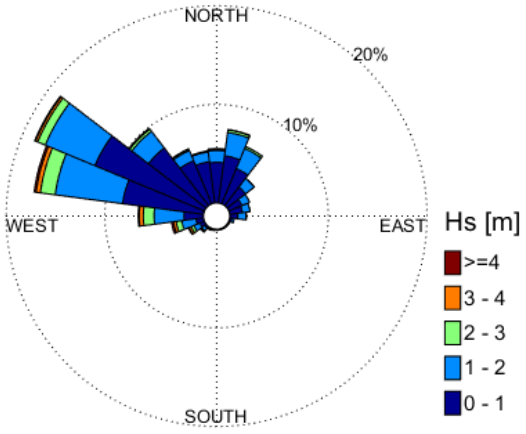

Figure 45: Rose diagram of Hs for Season 3 (autumn)

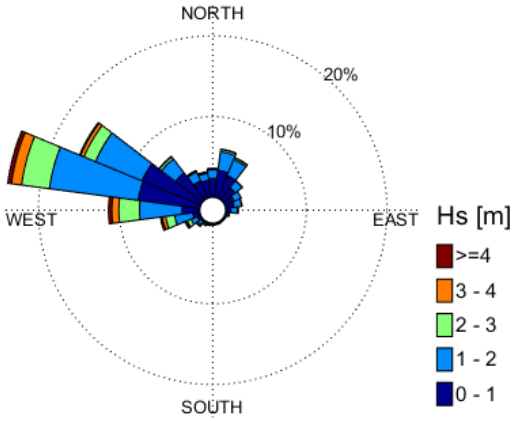

Figure 46: Rose diagram of Hs for Season 4 (winter)

The used hindcast file includes information about wind speed and direction, but is not given straight forward such as wave information. Wind information is given in two data columns, as shown in the Figure 47; the first column is wind speed component in the longitude direction, V_U, and the second column is the wind speed component in the latitude direction, V_v.

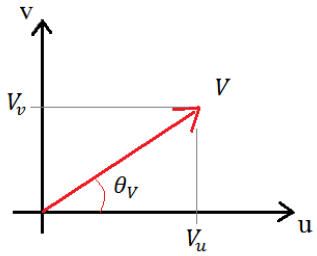

Figure 47: Wind velocity components

Therefore, the resultant wind speed and its direction shall be computed in order to generate wind speed rose diagrams. The resultant wind speed, V, and its direction, θ_V, are calculated as follows:

Resultant wind speed (33)

$$V = \sqrt{V_u^2 + V_v^2}$$

Wind direction (34)

$$\theta_V = \tan^{-} \frac{V_v}{V_u}$$

In regards to the definition of direction, the case of winds is different than that of waves in this study. The definitions are clarified as follows: A wave direction is the direction where the wave is coming from. However a wind direction is the direction where the wind is blowing towards.

Rose diagrams for wind direction in relation to wind speed are shown in Figure 48 to Figure 51. A contrast is found here if the wave and wind direction are compared. In spring and summer the wave is mainly coming from same direction as wind, but wind looks more distributed. Wind can be considered omnidirectional for spring and summer semesters, however, in autumn and winter this assumption is not valid for wind, because, as the figures show, wind blowing direction in those semesters is almost equally distributed in the range of north to south (coming from west and blowing east). Winter semester still has the same Omni-direction as the direction with the highest density, however, autumn is showing an interesting change, wind directions in autumn, in spite of the almost equal distribution, peak at a different direction, which is blowing to range

north to north-east. This direction is not indicated in the wave rose diagrams in Figure 45 and Figure 46, this finding deserves more investigation.

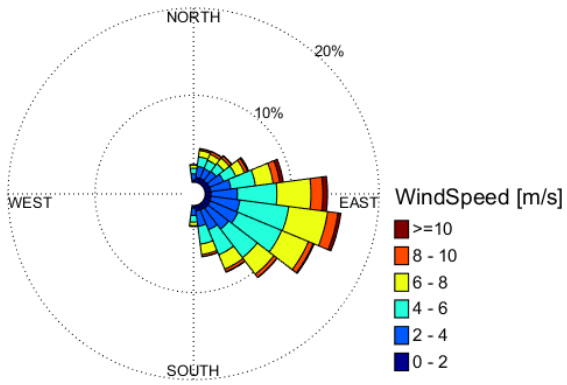

Figure 48: Rose diagram of wind speed for spring

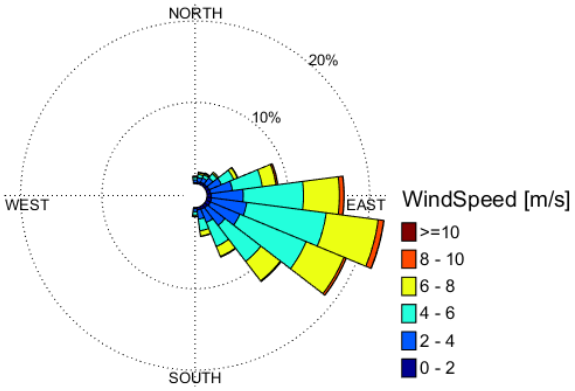

Figure 49: Rose diagram of wind speed for summer

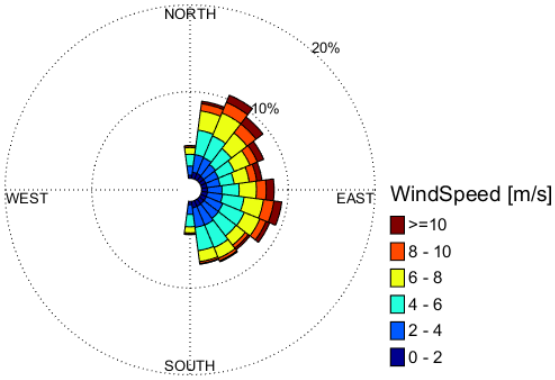

Figure 50: Rose diagram of wind speed for autumn

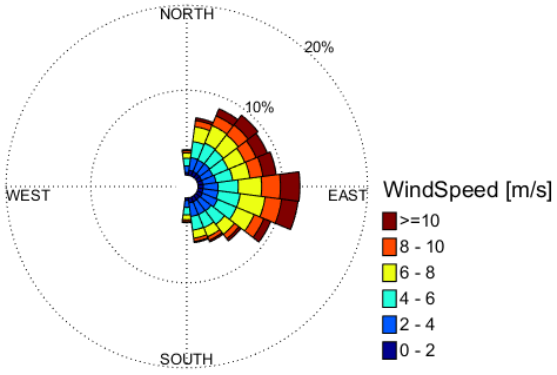

Figure 51: Rose diagram of wind speed for winter

Wind is more spread out than wave. But still it is also limited for specific direction. Looking at Figure 51, winds are going east (with deviations to the north and south) but no winds are going west. Half of the rose range is occupied. Waves can obviously be assumed omnidirectional because in the four semesters they are coming from the same direction. But winds, only for cases where it is not a governing parameter, wind can be assumed omnidirectional.

In this location, autumn is as rough as winter, attention to be given to both seasons equally, regarding marine operations. Whereas the summer and spring seasons are calm.

5.2 Directional Analysis

The main goal of this section is to visualize the natural variation of significant wave height, Hs, and spectral peak period, Tp, in terms of directions.

The 37 years of available data, at Location 1, are split in terms of direction. The data is split into 6 equal segments as defined in Figure 5, from Segment 1 to Segment 6. Scatter diagrams are shown in Figure 52 to Figure 57. The scatter diagrams show the difference between direction segments in terms of frequency of occurrence of different classes of waves, and together with directional analysis, these two tools are used to better understand the nature of sea in the Mediterranean and to pick the most critical direction.

Tp(s) / Hs(m)	0 - 1	1 - 2	2 - 3	3 - 4	4 - 5	5 - 6	6 - 7	7 - 8	8 - 9	9 - 10	10 - 11	11 - 12	12 - 13	13 - 14	14 - 15	15 - 16	16 - 17	17 - 18	18 - 19	Total
0 - 0.5	-	-	125	624	243	23	10	12	5	-	8	6	-	1	-	-	-	-	-	1,057
0.5 - 1	-	-	17	1,071	2,644	868	53	32	15	15	11	6	8	10	-	-	-	-	-	4,750
1 - 1.5	-	-	-	11	721	1,710	638	5	2	10	7	1	7	3	1	-	-	-	-	3,116
1.5 - 2	-	-	-	-	8	374	549	107	-	1	2	-	-	2	-	-	-	-	-	1,043
2 - 2.5	-	-	-	-	-	11	94	83	2	-	-	-	-	-	-	-	-	-	-	190
2.5 - 3	-	-	-	-	-	-	5	20	8	-	-	-	-	-	-	-	-	-	-	33
3 - 3.5	-	-	-	-	-	-	-	5	4	-	-	-	-	-	-	-	-	-	-	9
3.5 - 4	-	-	-	-	-	-	-	-	1	-	-	-	-	-	-	-	-	-	-	1
4 - 4.5	-	-	-	-	-	-	-	-	-	-	-	-	-	-	-	-	-	-	-	-
4.5 - 5	-	-	-	-	-	-	-	-	-	-	-	-	-	-	-	-	-	-	-	-
5 - 5.5	-	-	-	-	-	-	-	-	-	-	-	-	-	-	-	-	-	-	-	-
5.5 - 6	-	-	-	-	-	-	-	-	-	-	-	-	-	-	-	-	-	-	-	-
6 - 6.5	-	-	-	-	-	-	-	-	-	-	-	-	-	-	-	-	-	-	-	-
6.5 - 7	-	-	-	-	-	-	-	-	-	-	-	-	-	-	-	-	-	-	-	-
7 - 7.5	-	-	-	-	-	-	-	-	-	-	-	-	-	-	-	-	-	-	-	-
7.5 - 8	-	-	-	-	-	-	-	-	-	-	-	-	-	-	-	-	-	-	-	-
8 - 8.5	-	-	-	-	-	-	-	-	-	-	-	-	-	-	-	-	-	-	-	-
8.5 - 9	-	-	-	-	-	-	-	-	-	-	-	-	-	-	-	-	-	-	-	-
Total	-	-	142	1,706	3,616	2,986	1,349	264	37	26	28	13	15	16	1	-	-	-	-	10,199

Figure 52: Scatter diagram for direction segment 1

Tp(s) / Hs(m)	0 - 1	1 - 2	2 - 3	3 - 4	4 - 5	5 - 6	6 - 7	7 - 8	8 - 9	9 - 10	10 - 11	11 - 12	12 - 13	13 - 14	14 - 15	15 - 16	16 - 17	17 - 18	18 - 19	Total
0 - 0.5	-	-	68	164	30	11	5	5	6	-	1	3	3	-	-	-	-	-	-	296
0.5 - 1	-	-	14	450	510	48	7	9	9	12	3	1	1	-	-	-	-	-	-	1,064
1 - 1.5	-	-	-	11	239	168	11	-	1	5	6	3	3	-	-	-	-	-	-	447
1.5 - 2	-	-	-	-	6	28	19	1	-	-	-	-	-	-	-	-	-	-	-	54
2 - 2.5	-	-	-	-	-	5	6	-	-	-	-	-	-	-	-	-	-	-	-	11
2.5 - 3	-	-	-	-	-	-	1	1	-	-	-	-	-	-	-	-	-	-	-	2
3 - 3.5	-	-	-	-	-	-	-	-	-	-	-	-	-	-	-	-	-	-	-	-
3.5 - 4	-	-	-	-	-	-	-	-	-	-	-	-	-	-	-	-	-	-	-	-
4 - 4.5	-	-	-	-	-	-	-	-	-	-	-	-	-	-	-	-	-	-	-	-
4.5 - 5	-	-	-	-	-	-	-	-	-	-	-	-	-	-	-	-	-	-	-	-
5 - 5.5	-	-	-	-	-	-	-	-	-	-	-	-	-	-	-	-	-	-	-	-
5.5 - 6	-	-	-	-	-	-	-	-	-	-	-	-	-	-	-	-	-	-	-	-
6 - 6.5	-	-	-	-	-	-	-	-	-	-	-	-	-	-	-	-	-	-	-	-
6.5 - 7	-	-	-	-	-	-	-	-	-	-	-	-	-	-	-	-	-	-	-	-
7 - 7.5	-	-	-	-	-	-	-	-	-	-	-	-	-	-	-	-	-	-	-	-
7.5 - 8	-	-	-	-	-	-	-	-	-	-	-	-	-	-	-	-	-	-	-	-
8 - 8.5	-	-	-	-	-	-	-	-	-	-	-	-	-	-	-	-	-	-	-	-
8.5 - 9	-	-	-	-	-	-	-	-	-	-	-	-	-	-	-	-	-	-	-	-
Total	-	-	82	625	785	260	49	16	16	17	10	7	7	-	-	-	-	-	-	1,874

Figure 53: Scatter diagram for direction segment 2

Hs(m) \ Tp(s)	0 - 1	1 - 2	2 - 3	3 - 4	4 - 5	5 - 6	6 - 7	7 - 8	8 - 9	9 - 10	10 - 11	11 - 12	12 - 13	13 - 14	14 - 15	15 - 16	16 - 17	17 - 18	18 - 19	Total
0 - 0.5	-	-	48	214	117	29	46	25	5	7	4	2	1	-	-	-	-	-	-	498
0.5 - 1	-	-	7	386	599	270	98	67	45	12	4	2	-	-	-	-	-	-	-	1,490
1 - 1.5	-	-	-	14	469	511	95	32	17	15	9	6	4	-	-	-	-	-	-	1,172
1.5 - 2	-	-	-	-	21	317	235	51	13	4	-	-	-	-	-	-	-	-	-	641
2 - 2.5	-	-	-	-	-	32	203	84	9	4	-	-	-	-	-	-	-	-	-	332
2.5 - 3	-	-	-	-	-	1	50	127	22	12	-	-	-	-	-	-	-	-	-	212
3 - 3.5	-	-	-	-	-	-	-	79	46	14	-	-	-	-	-	-	-	-	-	139
3.5 - 4	-	-	-	-	-	-	-	15	48	30	-	-	1	-	-	-	-	-	-	94
4 - 4.5	-	-	-	-	-	-	-	-	25	15	5	-	-	-	-	-	-	-	-	45
4.5 - 5	-	-	-	-	-	-	-	-	1	12	1	-	-	-	-	-	-	-	-	14
5 - 5.5	-	-	-	-	-	-	-	-	-	8	1	-	-	-	-	-	-	-	-	9
5.5 - 6	-	-	-	-	-	-	-	-	-	2	1	-	-	-	-	-	-	-	-	3
6 - 6.5	-	-	-	-	-	-	-	-	-	-	-	-	-	-	-	-	-	-	-	-
6.5 - 7	-	-	-	-	-	-	-	-	-	-	2	2	-	-	-	-	-	-	-	4
7 - 7.5	-	-	-	-	-	-	-	-	-	-	-	-	-	-	-	-	-	-	-	-
7.5 - 8	-	-	-	-	-	-	-	-	-	-	-	-	-	-	-	-	-	-	-	-
8 - 8.5	-	-	-	-	-	-	-	-	-	-	-	-	-	-	-	-	-	-	-	-
8.5 - 9	-	-	-	-	-	-	-	-	-	-	-	-	-	-	-	-	-	-	-	-
Total	-	-	55	614	1,206	1,160	727	480	231	135	27	12	6	-	-	-	-	-	-	4,653

Figure 54: Scatter diagram for direction segment 3

Hs(m) \ Tp(s)	0 - 1	1 - 2	2 - 3	3 - 4	4 - 5	5 - 6	6 - 7	7 - 8	8 - 9	9 - 10	10 - 11	11 - 12	12 - 13	13 - 14	14 - 15	15 - 16	16 - 17	17 - 18	18 - 19	Total
0 - 0.5	-	-	135	560	3,141	4,620	1,304	721	256	127	65	25	6	8	1	-	-	-	-	10,969
0.5 - 1	-	-	21	1,144	5,931	29,621	31,833	6,798	1,921	995	250	71	46	15	3	-	1	-	-	78,650
1 - 1.5	-	-	-	19	929	5,367	18,026	18,152	3,506	1,896	835	281	81	21	4	-	-	-	-	49,117
1.5 - 2	-	-	-	-	21	802	3,285	7,561	4,734	1,539	532	279	83	24	1	-	-	-	-	18,861
2 - 2.5	-	-	-	-	-	35	719	2,164	2,761	1,536	456	171	57	12	-	-	-	-	-	7,911
2.5 - 3	-	-	-	-	-	-	50	758	1,472	1,330	422	130	60	5	-	-	-	-	-	4,227
3 - 3.5	-	-	-	-	-	-	-	148	610	902	518	109	65	8	-	-	-	-	-	2,360
3.5 - 4	-	-	-	-	-	-	-	9	190	599	404	118	45	-	-	-	-	-	-	1,365
4 - 4.5	-	-	-	-	-	-	-	-	20	196	296	149	29	1	-	-	-	-	-	691
4.5 - 5	-	-	-	-	-	-	-	-	1	65	207	137	32	1	-	-	-	-	-	443
5 - 5.5	-	-	-	-	-	-	-	-	-	10	85	77	30	-	-	-	-	-	-	202
5.5 - 6	-	-	-	-	-	-	-	-	-	1	25	43	37	3	-	-	-	-	-	109
6 - 6.5	-	-	-	-	-	-	-	-	-	-	4	6	28	1	-	-	-	-	-	39
6.5 - 7	-	-	-	-	-	-	-	-	-	-	-	9	22	3	-	-	-	-	-	34
7 - 7.5	-	-	-	-	-	-	-	-	-	-	-	4	4	6	-	-	-	-	-	14
7.5 - 8	-	-	-	-	-	-	-	-	-	-	-	1	5	3	-	-	-	-	-	9
8 - 8.5	-	-	-	-	-	-	-	-	-	-	-	-	2	-	-	-	-	-	-	2
8.5 - 9	-	-	-	-	-	-	-	-	-	-	-	-	-	-	-	-	-	-	-	-
Total	-	-	156	1,723	10,022	40,445	55,217	36,311	15,471	9,196	4,099	1,610	632	111	9	-	1	-	-	175,003

Figure 55: Scatter diagram for direction segment 4

Hs(m) \ Tp(s)	0 - 1	1 - 2	2 - 3	3 - 4	4 - 5	5 - 6	6 - 7	7 - 8	8 - 9	9 - 10	10 - 11	11 - 12	12 - 13	13 - 14	14 - 15	15 - 16	16 - 17	17 - 18	18 - 19	Total
0 - 0.5	-	4	616	3,576	6,832	3,644	1,051	625	246	168	139	46	25	13	1	-	-	-	-	16,986
0.5 - 1	-	-	40	3,309	13,788	19,856	11,327	2,272	1,010	479	124	51	22	8	-	-	-	-	-	52,286
1 - 1.5	-	-	-	9	831	3,420	6,747	5,338	812	284	219	73	22	10	-	-	-	-	-	17,765
1.5 - 2	-	-	-	-	10	179	759	2,249	1,415	115	18	8	9	-	1	-	-	1	-	4,764
2 - 2.5	-	-	-	-	-	4	96	410	727	213	1	-	-	-	-	-	-	-	-	1,451
2.5 - 3	-	-	-	-	-	-	13	72	263	263	30	2	-	-	-	-	-	-	-	643
3 - 3.5	-	-	-	-	-	-	-	7	83	191	41	-	-	-	-	-	-	-	-	322
3.5 - 4	-	-	-	-	-	-	-	-	7	90	20	15	-	-	-	-	-	-	-	132
4 - 4.5	-	-	-	-	-	-	-	-	3	27	28	6	-	-	-	-	-	-	-	64
4.5 - 5	-	-	-	-	-	-	-	-	-	8	27	7	-	-	-	-	-	-	-	42
5 - 5.5	-	-	-	-	-	-	-	-	-	3	4	8	-	-	-	-	-	-	-	15
5.5 - 6	-	-	-	-	-	-	-	-	-	-	7	2	-	-	-	-	-	-	-	9
6 - 6.5	-	-	-	-	-	-	-	-	-	-	1	-	-	-	-	-	-	-	-	1
6.5 - 7	-	-	-	-	-	-	-	-	-	-	-	-	-	-	-	-	-	-	-	-
7 - 7.5	-	-	-	-	-	-	-	-	-	-	-	-	-	-	-	-	-	-	-	-
7.5 - 8	-	-	-	-	-	-	-	-	-	-	-	-	-	-	-	-	-	-	-	-
8 - 8.5	-	-	-	-	-	-	-	-	-	-	-	-	-	-	-	-	-	-	-	-
8.5 - 9	-	-	-	-	-	-	-	-	-	-	-	-	-	-	-	-	-	-	-	-
Total	-	4	656	6,894	21,461	27,103	19,993	10,973	4,566	1,841	659	218	78	31	2	-	-	1	-	94,480

Figure 56: Scatter diagram for direction segment 5

Hs(m) \ Tp(s)	0 - 1	1 - 2	2 - 3	3 - 4	4 - 5	5 - 6	6 - 7	7 - 8	8 - 9	9 - 10	10 - 11	11 - 12	12 - 13	13 - 14	14 - 15	15 - 16	16 - 17	17 - 18	18 - 19	Total
0 - 0.5	2	1	249	2,097	1,566	389	107	83	38	13	21	22	7	5	1	-	-	-	-	4,601
0.5 - 1	1	-	33	2,835	10,444	4,870	1,114	244	120	55	35	24	9	11	-	-	-	-	-	19,795
1 - 1.5	-	-	-	15	1,822	5,269	2,456	287	31	25	17	7	4	2	-	1	-	-	-	9,936
1.5 - 2	-	-	-	-	9	492	1,367	607	43	1	4	-	5	1	-	-	-	-	-	2,529
2 - 2.5	-	-	-	-	-	8	193	486	81	10	-	-	-	-	-	-	-	-	-	778
2.5 - 3	-	-	-	-	-	-	9	142	109	22	-	-	-	-	-	-	-	-	-	282
3 - 3.5	-	-	-	-	-	-	-	15	61	27	-	-	-	-	-	-	-	-	-	103
3.5 - 4	-	-	-	-	-	-	-	-	9	46	2	-	-	-	-	-	-	-	-	57
4 - 4.5	-	-	-	-	-	-	-	-	4	19	1	-	-	-	-	-	-	-	-	24
4.5 - 5	-	-	-	-	-	-	-	-	-	9	2	-	-	-	-	-	-	-	-	11
5 - 5.5	-	-	-	-	-	-	-	-	-	1	2	-	-	-	-	-	-	-	-	3
5.5 - 6	-	-	-	-	-	-	-	-	-	-	3	-	-	-	-	-	-	-	-	3
6 - 6.5	-	-	-	-	-	-	-	-	-	-	-	-	-	-	-	-	-	-	-	-
6.5 - 7	-	-	-	-	-	-	-	-	-	-	-	-	-	-	-	-	-	-	-	-
7 - 7.5	-	-	-	-	-	-	-	-	-	-	-	-	-	-	-	-	-	-	-	-
7.5 - 8	-	-	-	-	-	-	-	-	-	-	-	-	-	-	-	-	-	-	-	-
8 - 8.5	-	-	-	-	-	-	-	-	-	-	-	-	-	-	-	-	-	-	-	-
8.5 - 9	-	-	-	-	-	-	-	-	-	-	-	-	-	-	-	-	-	-	-	-
Total	3	1	282	4,947	13,841	11,028	5,246	1,864	496	228	87	53	25	19	1	1	-	-	-	38,122

Figure 57: Scatter diagram for direction segment 6

Direction segment 1 scatter (Figure 52) shows that the highest wave in the 37 years of data is less than 4 meters high. Direction segment 2 highest wave is less than 3 meters. Direction segment 3 waves are up to 7 meters. Direction segment 4 (Figure 55) is the main direction of the waves, with highest wave up to 8.5 meters high. Direction segments 5 and 6 have the highest wave up to 7 and 6.5 meters respectively.

Direction segment 3 (Figure 54) has high waves up to 7 meters, however, it does not have long waves, the longest wave period is 13 seconds. Direction segments 4, 5 and 6 have both the highest waves (largest Hs) and the longest waves (largest Tp). They have wave periods longer than 15 seconds in each direction segment. Longest wave period in location 1 is about 18

seconds, this wave has a height of about 2 meters, and it's oriented in direction segment 5 and occurred in winter season.

The marginal subsets of directional significant wave height can be fitted to a distribution using long-term wave statistics. The distribution may be used to estimate the wave extremes corresponding to specific return periods (say 100-year wave) coming from a specific direction. A comparison of fitted models of significant wave height marginal subsets with the "original" dataset, the omnidirectional set, is made. The probability paper plot is found in Figure 58, comparing the omnidirectional set with direction segments 2 and 4. And the q-q plot is found in Figure 59 comparing the omnidirectional set with direction segment 4.

The probability plot is made by fitting the datasets with Weibull distribution, the Weibull parameters are calculated using MME and are listed in Table 7.

Table 7: Weibull parameters for omnidirectional sea, segment 4 and segment 2 data

	Shape	Scale	Location
Omnidirectional	0.8610111	0.5362840	0.9988873
Direction: Segment 4	0.9061106	0.6345731	0.9812379
Direction: Segment 2	1.0642010	0.2704617	1.0042829

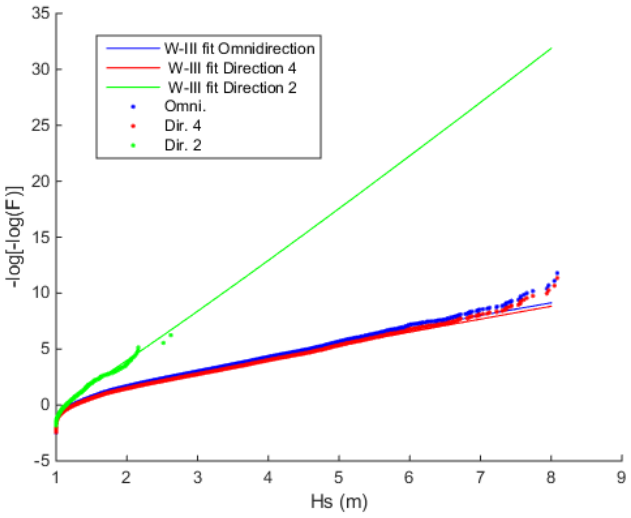

Figure 58: Probability paper for comparison of directional fitted distributions

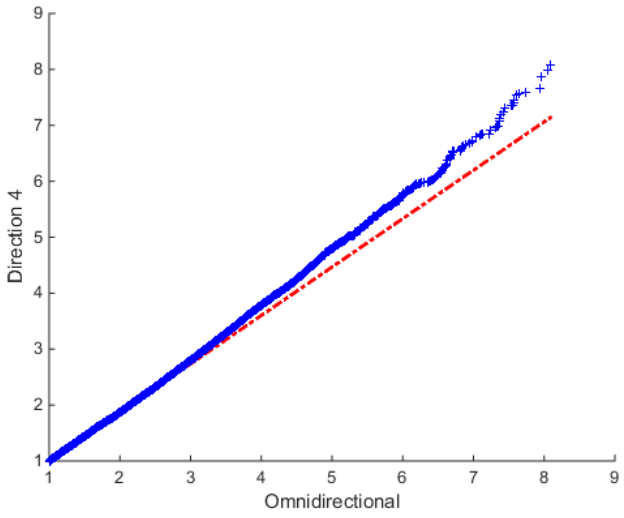

Figure 59: q-q plot for direction 4 data against omnidirectional data

A directional extreme value can never be larger than the omnidirectional value. In other words, a subset cannot imply extremes larger than those of the original set. That is valid for directional subsets as well as seasonal ones. If one particular direction segment is immensely more severe than all other segments, the extreme values for the dominant sector may be equal to the omnidirectional value.

For this case, direction segment 4 is more severe than all other directions. Then the underlying true value could be close to the omnidirectional, but should be lower. However, when the subset and the original set are fitted with a distribution, the subset (Figure 58, red line, direction segment 4) is indicating higher extremes than the original set (blue line, omnidirectional), since the red line is to the right of the blue line at the tail. This is not realistic, but there will always be uncertainties associated with the fitted distribution. In such a case the estimated extremes for the subset (direction segment 4) could end up being slightly higher than the omnidirectional extremes. It is not know which one of the extremes is the correct value, probably none of them due to uncertainties. (Haver, 2013)

Figure 58 also shows that the other subset, direction segment 2, gives much smaller extremes than those of the original dataset (omnidirectional).

The q-q plot in Figure 59 confirms that the subset (direction segment 4) and the original set (the omnidirectional) can be related and described by the same distribution, because the blue line is straight and following the red line, however it confirms with indication seen from probability paper plot that the subset is implying higher extremes (the tail of the blue line is to the left of the red line, given that on the x-axis is the omnidirectional data and on the y-axis is the direction segment 4 data)

Figure 60 shows the average spectral peak period conditional for every class of Hs for the different direction segments for Location 1. It shows that the main directions for Location 1 (segments 4, 5 and 6) have the waves with the highest periods. This figure indicates the periods of the waves (given wave height) for every direction segment. Some lines, such as the red one (direction segment 2) does not continue past Hs = 3 meters, since there are no waves coming from this direction above 3 meters in height. This figure shows that there is one main direction (segment 4), and it governs the highest periods and the highest wave heights. This also agrees with the validity of omnidirectional assumption.

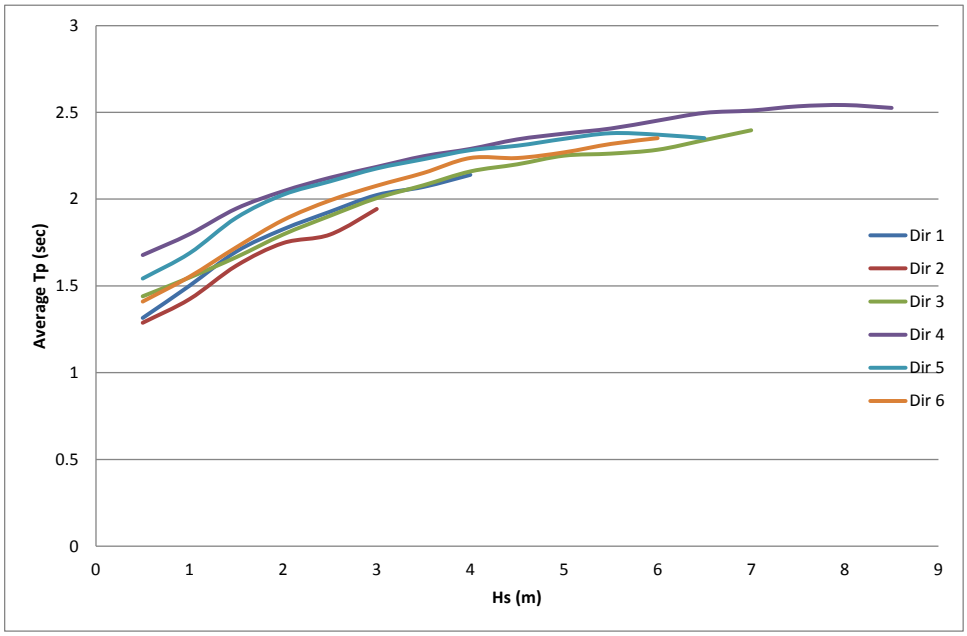

Figure 60: Tp against Hs for the different direction segments (Location 1)

5.3 Swell Waves

In swells, the wave frequency is much less than the Eigen frequency of the vessel ($\omega \ll \omega_0$) thus $\beta \ll 1$. Therefore vertical motions are dominated by stiffness coefficient, this results in an undesired response, where vessel follows the heave motions of the wave, with no damping. Swells are a wave system of their own; they can happen at the same time with wind waves, but with a different direction. This is what makes them important for marine structures design and operations. Typically, swell waves are long crested and wind waves are short crested in nature (Gudmestad, 2015).

This section investigates wind-sea, swell 1 and swell 2 components provided by hindcast. The investigation includes scatter diagrams, correlation scatters, direction roses, and comparisons that include wave heights, wind speed, directions, mean periods and peak periods. The goal is to understand the nature of swells in the area and know the relative direction between swell sea and wind-sea.

According the Wavewatch-III (the wave model used in building the hindcast), the swells waves can be split into three components, swell 1, swell 2 and swell 3 as follows.

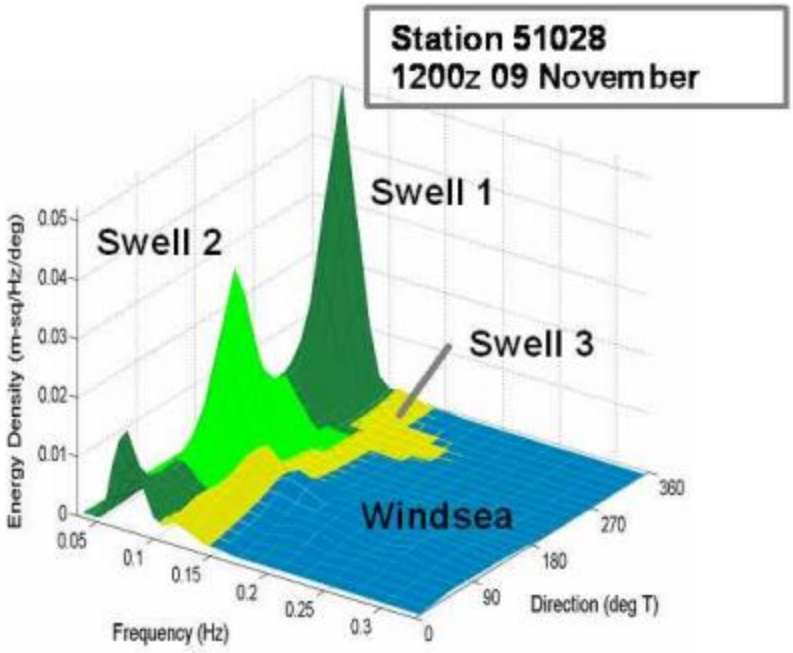

Figure 61: Surface plot of an energy density spectrum showing spectral partitions for wind-sea and three swell trains. This is a snapshot of hincasted conditions at Christmas Island. Copied from Wavewatch III manual (Tolman, 2009)

Definitions of swell components were not found in Wavewatch-III, therefore Figure 61 is interpreted as follows: swell 1 is the swell sea with highest energy density, coming from a particular direction; swell 2 the swell sea with lower energy density, coming from a different direction than swell 1; swell 3 is the transition between swell sea and wind-sea. The hindcast files provided for this thesis include data for swell 1 and swell 2, but they do not include data for swell 3.

Swell sea: This is a sea condition which is not caused by the local wind field. Generated far away and blown by continuous winds to location. It can be realized as rather narrow banded swell wave component or as a decaying wind-sea after the wind is considerably reduced or the wave field has propagated out of the area affected by strong wind.

Wind-sea: A wind-sea is a sea that is a result of the local wind field. Since both the wave field and the wind field are propagating in space, the observed sea at a given site may well be the result of wind induced wave growth over quite some distance.

Combined sea: Most sea-states encountered in practice will include both a pure wind-sea component process and one or more swell components processes. Such seas are referred to as combined seas.

Wind-sea is further separated into fully developed wind-sea and growing wind-sea:
Fully developed wind-sea: the wind and wave fields have reached some sort of an equilibrium condition in the sense that the wave spectrum has reached a form that is not changing. This means that there is a balance between all processes involved in the wave growth process, i. e. wind input process, wave-wave interaction process and dissipation process. This situation is referred to as a fully developed sea (or “old” wind waves). Interpreted strictly, this situation will hardly take place in the real ocean.

Growing wind-sea: Imagine following the growth of waves in space and time from a situation where there is no wind at the beginning (and therefore no wind-sea) to a situation where there is a very strong wind blowing. During this phase waves will grow in height and they will also gradually increase their characteristic wave length (wave period). The spectrum will also change its shape during this process. It will typically be more sharply peaked than the spectrum representing fully developed sea-states. The term decaying is also used to describe a decaying wind-sea.

Swell information is available in the hindcast file provided by DICCA (http://www.dicca.unige.it/), and this information is used for basic swell sea analysis. The analysis includes scatter diagrams and rose diagrams. Graphic plots are presented for visualizing the differences between wind-sea, swell sea 1, and swell sea 2. In this analysis the mean period, Tm, is used instead of the peak period, Tp, therefore it is important to keep in mind that the peak period is almost always higher (except for swell waves). Figure 77 shows the relation between Tp and Tm, for Location 1.

Initial representation is shown in Figure 1 below. It shows the three wave systems, i.e. swell 1, swell 2 and wind-sea, in the same scatter plot. It is noted that swell 2 wave system is limited to very low wave heights (about 2 meters). The swell 1 wave system is also consecrated at low wave heights, but higher than swell 2 system (about 6 meters). The wind-sea takes place at the lower mean periods for same wave heights. More details, especially about the extremes (rare waves) can be taken from the scatter diagrams.

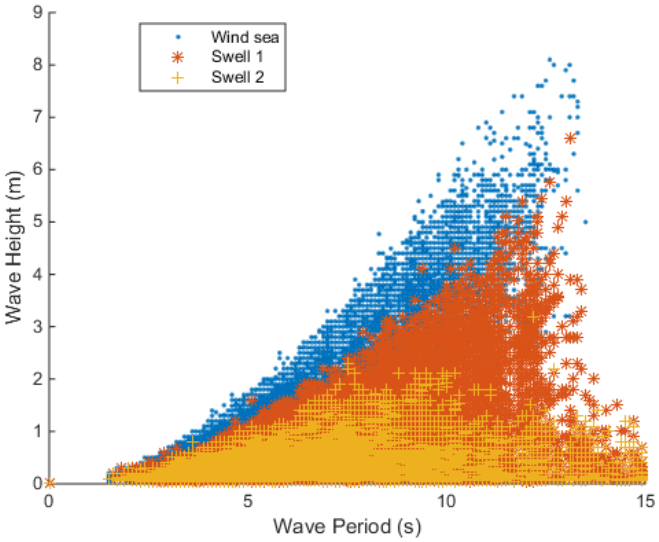

Figure 62: Hs vs. Tm for wind and swell seas

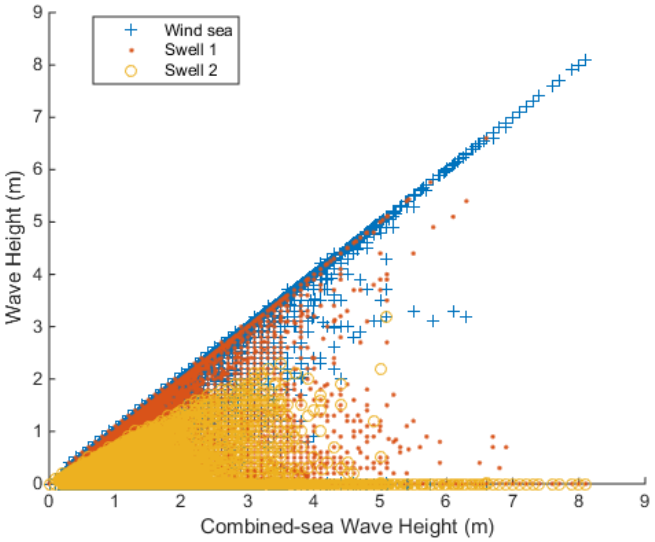

Figure 63: H (of wind and swell seas) vs. Hs (combined sea)

Figure 62 and Figure 63 show that wind waves are higher that swell waves, but for a given height, swell waves are longer (have longer periods). The figures also show that swell 2 component is considerably smaller than swell 1 component in terms of wave height. Pairs of significant wave height, Hs, versus mean period, Tm, are used to generate the scatter diagrams. Four scatter diagrams are presented below: for combined sea, wind-sea, swell sea 1 and swell sea 2.

Hs(m) \ Tm(s)	0 - 1	1 - 2	2 - 3	3 - 4	4 - 5	5 - 6	6 - 7	7 - 8	8 - 9	9 - 10	10 - 11	11 - 12	12 - 13	13 - 14	14 - 15	15 - 16	16 - 17	17 - 18	18 - 19	Total
0 - 0.5	-	-	1,674	12,181	8,748	1,734	446	102	11	6	-	-	-	-	-	-	-	-	-	24,902
0.5 - 1	-	-	359	28,992	72,415	41,963	5,419	608	105	24	12	-	-	-	-	-	-	-	-	149,897
1 - 1.5	-	-	-	792	22,381	41,385	19,696	2,783	474	100	15	-	-	-	-	-	-	-	-	87,626
1.5 - 2	-	-	-	-	1,185	10,482	13,044	4,298	782	126	17	-	-	-	-	-	-	-	-	29,934
2 - 2.5	-	-	-	-	5	1,454	5,212	3,575	771	144	12	1	-	-	-	-	-	-	-	11,174
2.5 - 3	-	-	-	-	-	57	1,925	2,625	771	135	14	7	-	-	-	-	-	-	-	5,534
3 - 3.5	-	-	-	-	-	-	288	1,654	956	130	11	-	-	-	-	-	-	-	-	3,039
3.5 - 4	-	-	-	-	-	-	23	672	815	160	18	-	-	-	-	-	-	-	-	1,688
4 - 4.5	-	-	-	-	-	-	-	120	496	192	10	-	-	-	-	-	-	-	-	818
4.5 - 5	-	-	-	-	-	-	-	9	287	201	15	-	-	-	-	-	-	-	-	512
5 - 5.5	-	-	-	-	-	-	-	-	71	143	18	-	-	-	-	-	-	-	-	232
5.5 - 6	-	-	-	-	-	-	-	-	9	81	30	-	-	-	-	-	-	-	-	120
6 - 6.5	-	-	-	-	-	-	-	-	-	15	30	-	-	-	-	-	-	-	-	45
6.5 - 7	-	-	-	-	-	-	-	-	-	12	14	1	-	-	-	-	-	-	-	27
7 - 7.5	-	-	-	-	-	-	-	-	-	1	11	3	-	-	-	-	-	-	-	15
7.5 - 8	-	-	-	-	-	-	-	-	-	-	5	-	-	-	-	-	-	-	-	5
8 - 8.5	-	-	-	-	-	-	-	-	-	-	3	-	-	-	-	-	-	-	-	3
8.5 - 9	-	-	-	-	-	-	-	-	-	-	-	-	-	-	-	-	-	-	-	-
Total	-	-	2,033	41,965	104,734	97,075	46,053	16,446	5,548	1,470	235	12	-	-	-	-	-	-	-	315,571

Figure 64: Hs-Tm scatter diagram of combined sea, location 1

Hs(m) \ Tm(s)	0 - 1	1 - 2	2 - 3	3 - 4	4 - 5	5 - 6	6 - 7	7 - 8	8 - 9	9 - 10	10 - 11	11 - 12	12 - 13	13 - 14	14 - 15	15 - 16	16 - 17	17 - 18	18 - 19	Total
0 - 0.5	684	1,475	9,875	12,165	5,989	1,404	168	29	5	1	-	-	-	-	-	-	-	-	-	31,795
0.5 - 1	-	-	397	14,135	26,687	22,636	10,013	928	153	25	2	-	-	-	-	-	-	-	-	74,976
1 - 1.5	-	-	-	43	5,094	13,442	16,024	6,804	774	189	42	2	1	-	-	-	-	-	-	42,415
1.5 - 2	-	-	-	-	33	2,066	5,386	7,022	2,024	315	53	18	1	-	-	-	-	-	-	16,918
2 - 2.5	-	-	-	-	-	75	1,371	2,983	2,439	684	120	17	1	-	-	-	-	-	-	7,690
2.5 - 3	-	-	-	-	-	1	128	1,170	1,659	1,096	206	30	5	-	-	-	-	-	-	4,295
3 - 3.5	-	-	-	-	-	-	1	270	814	1,036	371	54	22	3	-	-	-	-	-	2,571
3.5 - 4	-	-	-	-	-	-	-	28	262	746	372	85	18	-	-	-	-	-	-	1,511
4 - 4.5	-	-	-	-	-	-	-	-	56	243	314	122	17	1	-	-	-	-	-	753
4.5 - 5	-	-	-	-	-	-	-	-	2	96	229	136	23	-	-	-	-	-	-	486
5 - 5.5	-	-	-	-	-	-	-	-	-	25	84	83	23	1	-	-	-	-	-	216
5.5 - 6	-	-	-	-	-	-	-	-	-	3	34	46	31	2	-	-	-	-	-	116
6 - 6.5	-	-	-	-	-	-	-	-	-	-	5	7	29	2	-	-	-	-	-	43
6.5 - 7	-	-	-	-	-	-	-	-	-	-	2	11	12	1	-	-	-	-	-	26
7 - 7.5	-	-	-	-	-	-	-	-	-	-	-	3	5	7	-	-	-	-	-	15
7.5 - 8	-	-	-	-	-	-	-	-	-	-	-	-	3	2	-	-	-	-	-	5
8 - 8.5	-	-	-	-	-	-	-	-	-	-	-	-	2	1	-	-	-	-	-	3
8.5 - 9	-	-	-	-	-	-	-	-	-	-	-	-	-	-	-	-	-	-	-	-
Total	684	1,475	10,272	26,343	37,803	39,624	33,091	19,234	8,188	4,459	1,834	614	193	20	-	-	-	-	-	183,834

Figure 65: Hs-Tm scatter diagram of wind-sea, location 1

Hs(m) \ Tm(s)	0 - 1	1 - 2	2 - 3	3 - 4	4 - 5	5 - 6	6 - 7	7 - 8	8 - 9	9 - 10	10 - 11	11 - 12	12 - 13	13 - 14	14 - 15	15 - 16	16 - 17	17 - 18	18 - 19	Total
0 - 0.5	322	7	1,143	15,744	29,383	24,101	11,794	8,522	3,406	1,566	784	449	234	104	74	-	-	-	-	97,633
0.5 - 1	-	-	1	535	10,752	35,609	37,252	10,856	3,828	1,878	638	199	98	56	15	-	-	-	-	101,717
1 - 1.5	-	-	-	-	20	1,773	12,345	16,375	4,203	1,702	744	299	94	11	6	-	-	-	-	37,572
1.5 - 2	-	-	-	-	-	8	264	2,820	3,973	1,534	398	175	55	7	1	-	-	-	-	9,235
2 - 2.5	-	-	-	-	-	-	1	77	857	1,137	376	126	26	5	-	-	-	-	-	2,605
2.5 - 3	-	-	-	-	-	-	-	2	70	347	257	116	41	5	-	-	-	-	-	838
3 - 3.5	-	-	-	-	-	-	-	-	8	45	140	48	51	3	-	-	-	-	-	295
3.5 - 4	-	-	-	-	-	-	-	-	-	5	32	28	27	3	-	-	-	-	-	95
4 - 4.5	-	-	-	-	-	-	-	-	-	1	4	20	12	-	-	-	-	-	-	37
4.5 - 5	-	-	-	-	-	-	-	-	-	-	1	11	7	-	-	-	-	-	-	19
5 - 5.5	-	-	-	-	-	-	-	-	-	-	-	3	4	1	-	-	-	-	-	8
5.5 - 6	-	-	-	-	-	-	-	-	-	-	-	-	1	-	-	-	-	-	-	1
6 - 6.5	-	-	-	-	-	-	-	-	-	-	-	-	-	-	-	-	-	-	-	-
6.5 - 7	-	-	-	-	-	-	-	-	-	-	-	-	-	1	-	-	-	-	-	1
7 - 7.5	-	-	-	-	-	-	-	-	-	-	-	-	-	-	-	-	-	-	-	-
7.5 - 8	-	-	-	-	-	-	-	-	-	-	-	-	-	-	-	-	-	-	-	-
8 - 8.5	-	-	-	-	-	-	-	-	-	-	-	-	-	-	-	-	-	-	-	-
8.5 - 9	-	-	-	-	-	-	-	-	-	-	-	-	-	-	-	-	-	-	-	-
Total	322	7	1,144	16,279	40,155	61,491	61,656	38,652	16,345	8,215	3,374	1,474	650	196	96	-	-	-	-	250,056

Figure 66: Hs-Tm scatter diagram of swell sea 1, location 1

Tm(s) / Hs(m)	0 - 1	1 - 2	2 - 3	3 - 4	4 - 5	5 - 6	6 - 7	7 - 8	8 - 9	9 - 10	10 - 11	11 - 12	12 - 13	13 - 14	14 - 15	15 - 16	16 - 17	17 - 18	18 - 19	Total
0 - 0.5	11	21	4,241	25,660	26,885	22,093	15,282	11,711	5,251	2,952	1,644	954	470	237	112	-	-	-	-	117,524
0.5 - 1	-	-	-	149	2,028	4,229	3,853	2,476	1,326	794	360	123	78	38	17	-	-	-	-	15,471
1 - 1.5	-	-	-	-	1	34	263	374	260	84	23	16	33	10	4	-	-	-	-	1,102
1.5 - 2	-	-	-	-	-	-	9	36	45	31	10	2	2	-	-	-	-	-	-	135
2 - 2.5	-	-	-	-	-	-	-	3	1	9	2	-	1	-	-	-	-	-	-	16
2.5 - 3	-	-	-	-	-	-	-	-	-	-	-	-	-	-	-	-	-	-	-	-
3 - 3.5	-	-	-	-	-	-	-	-	-	-	-	-	1	-	-	-	-	-	-	1
3.5 - 4	-	-	-	-	-	-	-	-	-	-	-	-	-	-	-	-	-	-	-	-
4 - 4.5	-	-	-	-	-	-	-	-	-	-	-	-	-	-	-	-	-	-	-	-
4.5 - 5	-	-	-	-	-	-	-	-	-	-	-	-	-	-	-	-	-	-	-	-
5 - 5.5	-	-	-	-	-	-	-	-	-	-	-	-	-	-	-	-	-	-	-	-
5.5 - 6	-	-	-	-	-	-	-	-	-	-	-	-	-	-	-	-	-	-	-	-
6 - 6.5	-	-	-	-	-	-	-	-	-	-	-	-	-	-	-	-	-	-	-	-
6.5 - 7	-	-	-	-	-	-	-	-	-	-	-	-	-	-	-	-	-	-	-	-
7 - 7.5	-	-	-	-	-	-	-	-	-	-	-	-	-	-	-	-	-	-	-	-
7.5 - 8	-	-	-	-	-	-	-	-	-	-	-	-	-	-	-	-	-	-	-	-
8 - 8.5	-	-	-	-	-	-	-	-	-	-	-	-	-	-	-	-	-	-	-	-
8.5 - 9	-	-	-	-	-	-	-	-	-	-	-	-	-	-	-	-	-	-	-	-
Total	11	21	4,241	25,809	28,914	26,356	19,407	14,600	6,883	3,870	2,039	1,095	585	285	133	-	-	-	-	134,249

Figure 67: Hs-Tm scatter diagram of swell sea 2, location 1

It is noted that swell 2 wave system is limited to very low wave heights (up to 3.5 meters), with peak occurrence at the mean period, Tm, around 4 seconds, with mean period of 12.5 seconds for the highest wave. The swell 1 wave system is also consecrated at low wave heights, but higher than swell 2 system (up to 6 meters), with peak occurrence at Tm around 7 seconds, with mean period of 13.5 seconds for the highest wave.

According to DNV, there is an equation that related the total sea to the wind-sea and swell sea components. This relation is applied to the components provided in the hindcast file, the wave height of the total sea is calculated and compared against the given significant wave height (Hs). Figure 68 shows the relation between the calculated and the given significant wave heights.

Total sea wave height (35)

$$h_{s,total} = \sqrt{h_{swell\ 1}^2 + h_{swell\ 2}^2 + h_{wind}^2}$$

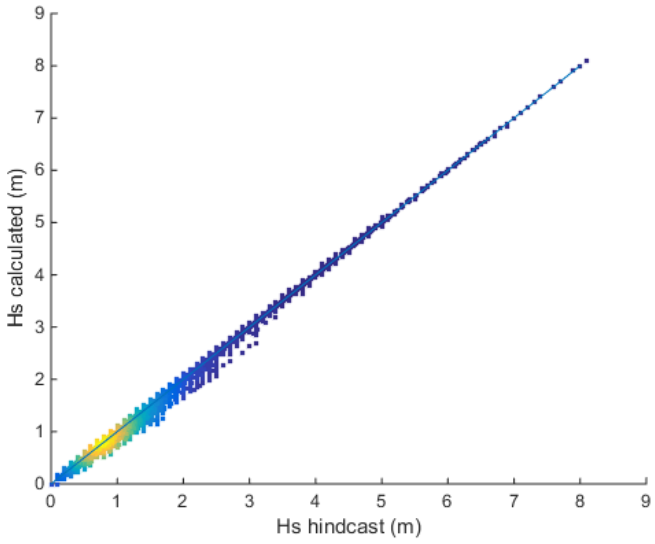

Figure 68: Calculated Hs against hindcast given Hs

Figure 68 shows a 45º straight line, that means that the calculated wave height equals the given wave height. This check is valid, therefore, in a reverse manner, the following relationships between the wave components spectra are validated as well (DNV-RP-C205, 2007, p.34):

Combined wind-sea and swell may be described by a double peak frequency spectrum, where components are assumed to be uncorrelated:

Combined sea double peak spectrum (36)

$$S(\omega) = S_{wind\ sea}(\omega) + S_{swell}(\omega)$$

And the spectral moments are additive:

Combined sea spectral moments (37)

$$M_n = M_{n,wind\ sea} + M_{n,swell}$$

Figure 69 to Figure 72 check amplitude correlation between wind speed and wave height. Four figures are presented to show the correlation of wind speed with combined sea and the correlations with the individual wave components.

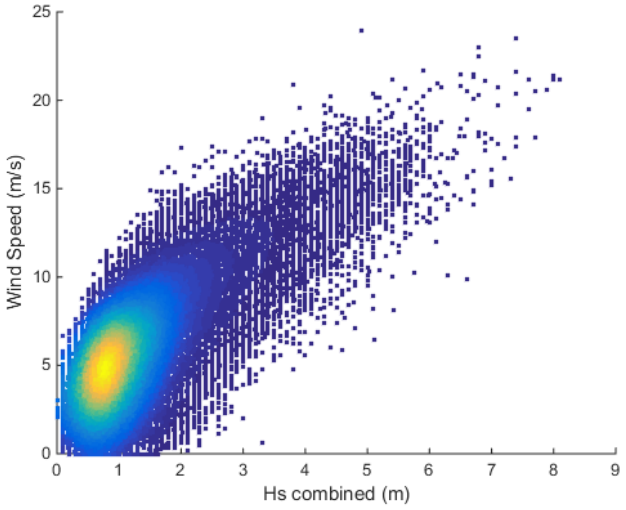

Figure 69: Wind speed vs. combined Hs scatter

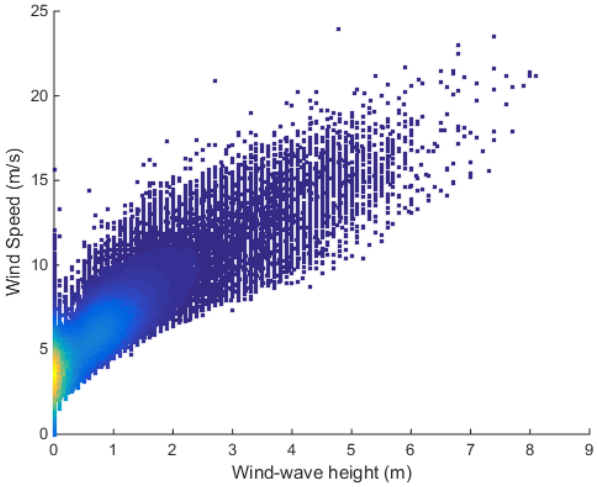

Figure 70: Wind speed vs. wind wave Hs scatter

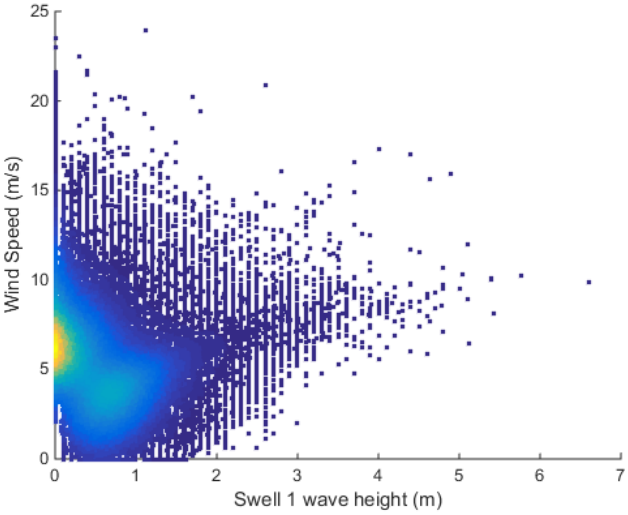

Figure 71: Wind speed vs. swell 1 Hs scatter

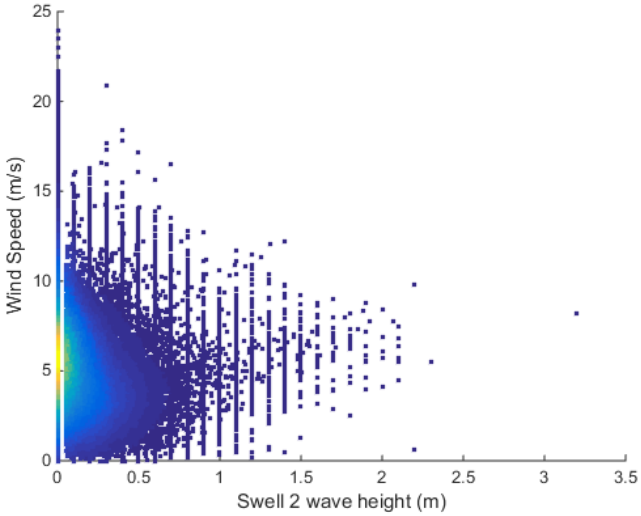

Figure 72: Wind speed vs. swell 2 Hs scatter

Figure 69 and Figure 70 show correlation between wind speed and wave height of combined sea and wind-sea respectively. Since the wind-sea is generated by local winds, it is expected to have a clear correlation, and indeed Figure 70 shows that, for every 5 m/s increase in wind speed there is roughly 2 meters increase in wind-sea wave height.

Figure 71 and Figure 72 show weak correlation between swell components and wind speed. This approves the definition of swell waves (not related to local winds). The figures may be interpreted in two parts: part 1 is that swell wave heights will increase with an increase in wind speed (lower edge of the scatter cloud), and part 2 is that swell heights will decrease with an increase in wind speed (upper edge of the scatter cloud). Part 2 is the more dominant than part

1. This decay of swells by local wind may indicate that swells are mainly coming from a different direction than wind-sea waves. This will be more investigated.

Figure 73 to Figure 76 check direction correlation between winds and waves. Four figures are presented to show the correlation of wind direction with combined sea direction and the correlations with the individual wave components. Angles in figures are given anticlockwise from north and indicate the directions towards which both winds and waves are going.

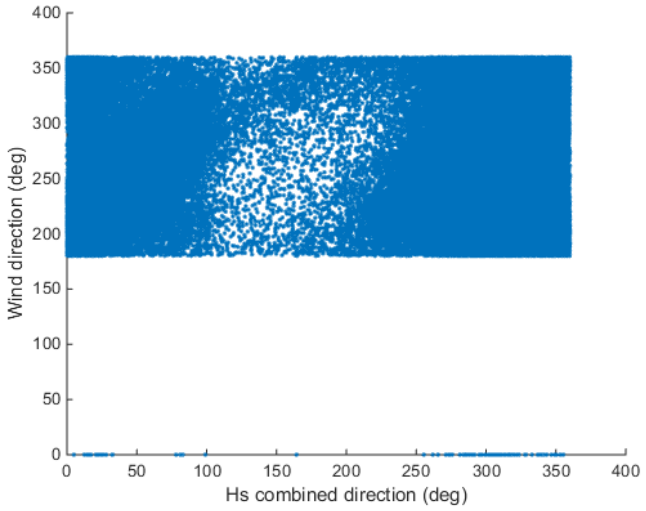

Figure 73: Wind direction vs. combined wave direction scatter

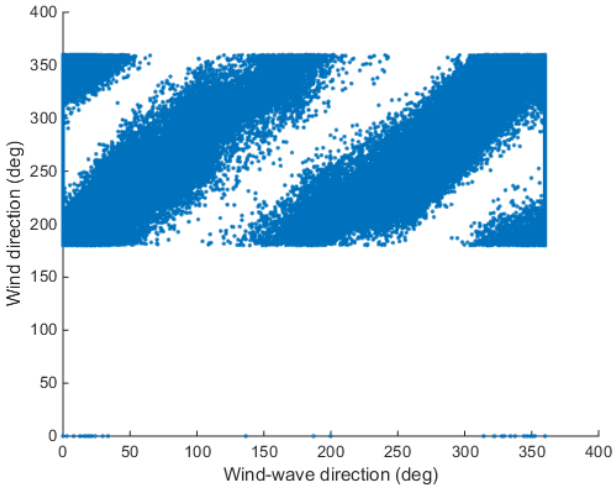

Figure 74: Wind direction vs. wind-sea direction scatter

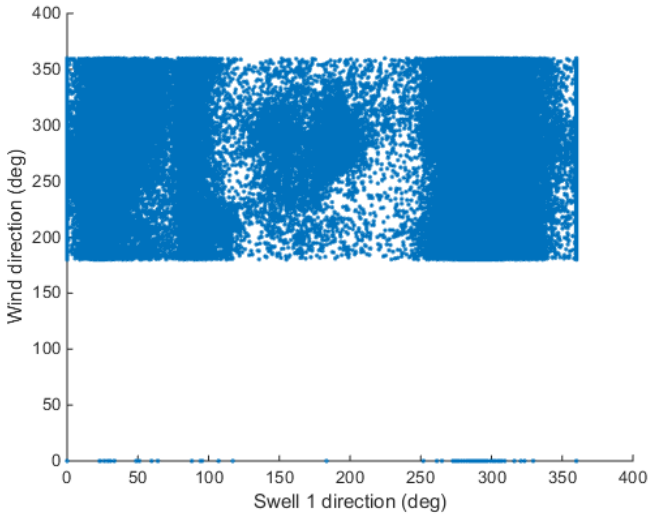

Figure 75: Wind direction vs. swell 1 direction scatter

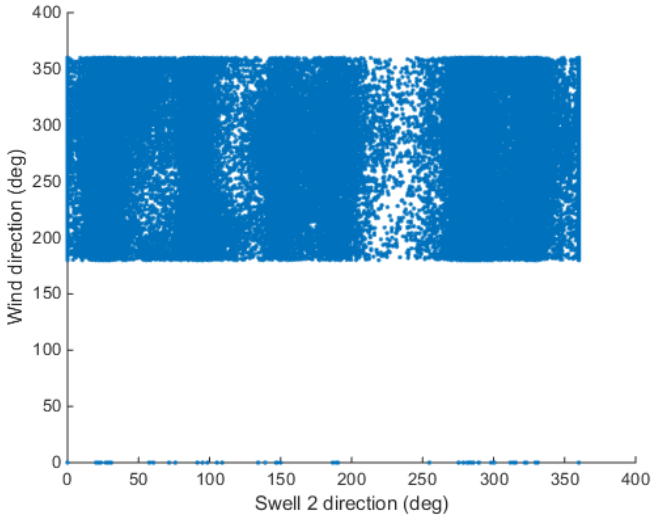

Figure 76: Wind direction vs. swell 2 direction scatter

Figure 73 to Figure 76 show clouds of blue dots, each with a different white shape inside. This white shape is area with no data point within. It means that the directions indicated by the white

shapes are combinations of directions (wind against wave) that are not allowed by nature (have never happened in the past 37 years of hindcast data). The main white areas are interpreted. First there is the main white block present in the figures that means that there is no wind (at all) blowing west (from 0 to 180 degrees), this finding could be a result of a limitation of hindcast model. Figure 74 shows with the inclined white areas that winds and wind-sea waves cannot be 90 degrees out of phase of each other. Figure 75 shows less correlation for swell 1 waves than wind-sea waves. It shows with the circular white area that swell 1 waves are not likely to go neither SW nor SSE. Plus that at times when winds are heading south or north, swell 1 waves are not likely to go south. Figure 76 shows that swell 2 waves direction are less correlated to wind direction than swell 1 waves, and the figure shows that for all directions of wind, swell 2 waves are not likely to go SSE. As definition suggests, wind-sea wave directions are the most correlated with wind directions.

Figure 77 to Figure 80, with combined sea mean period in the x-axis, show the relationship between periods (of wave components) to mean period Tm (of combined sea). The scatter plots show the points of the (Tm, T) pairs for all waves in the hindcast file. The 45 degrees line is the line where T = Tm. Figure 77 shows clearly that usually the Tp of combined sea is higher than Tm of combined sea, it can reach up to triple times the value of Tm. Figure 78 shows that there is correlation between wind-sea mean period and combined mean period, whereas it shows that there is a number of waves with combined mean period higher than that of wind-sea. Figure 79 shows that there is a correlation between swell 1 mean period and combined mean period, whereas it shows that there is a number of waves with combined mean period lower than that of swell 1 component mean period. Figure 80 shows the least correlation is between swell 2 component and combined sea mean periods. Mean periods of components can be higher or lower than combined mean periods. The main motive of the following figures is to have a relation between components mean periods and combined mean period, and a relation between combined mean period with combined peak period.

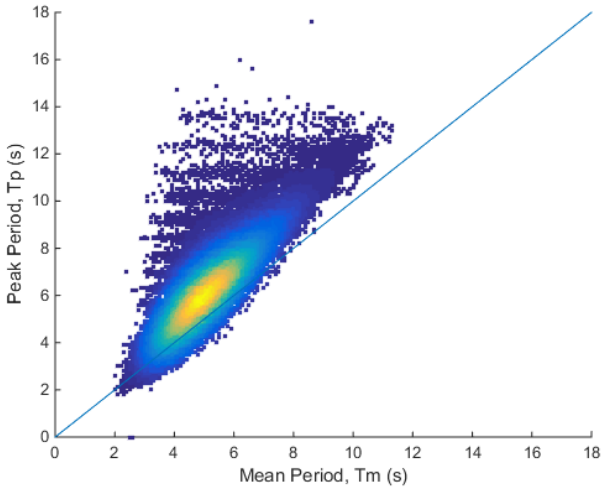

Figure 77: Combined peak period vs combined mean period scatter

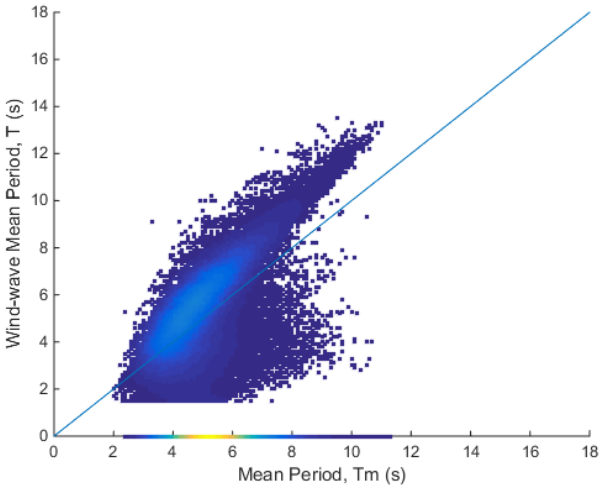

Figure 78: Wind-sea mean period vs combined mean period scatter

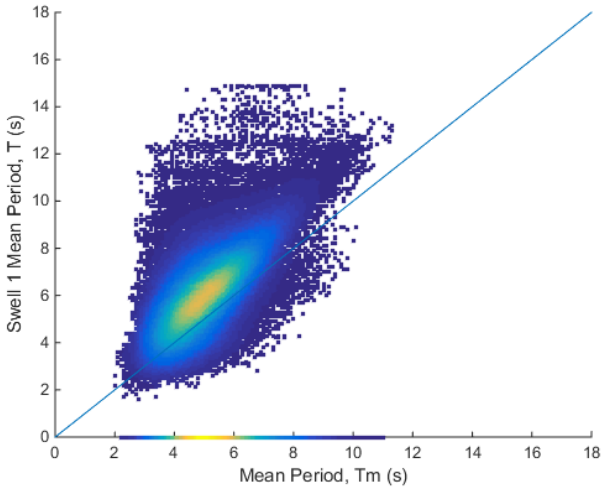

Figure 79: Swell 1 mean period vs combined mean period scatter

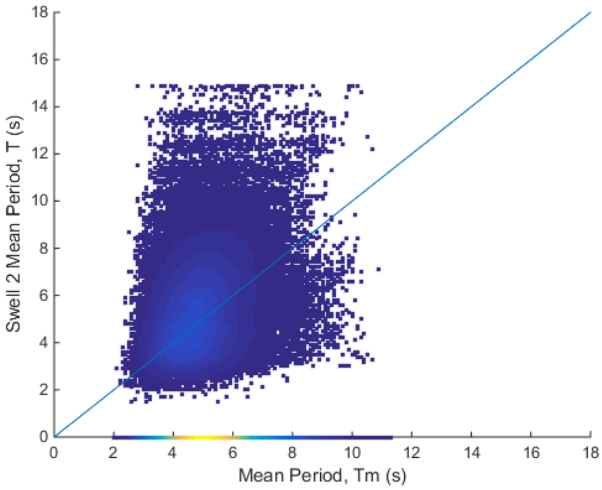

Figure 80: Swell 2 mean period vs combined mean period scatter

Figure 81 to Figure 86 show directional rose diagrams comparing wind-sea, swell 1 and swell 2 wave components. Wind-sea and swell 1 waves are mainly coming from the same direction as the main direction of the sea. However, the swell 2 component of the waves is distributed into three main directions, according to Figure 85; around 30% of the waves are coming from direction WNW, around 20% of the waves are coming from direction NNE, and around 12% of the waves are coming from NNW. Swell 2 waves in the three directions are ranging in the same wave height range, with largest mean periods associated with waves are coming from WNW, refer to Figure 86.

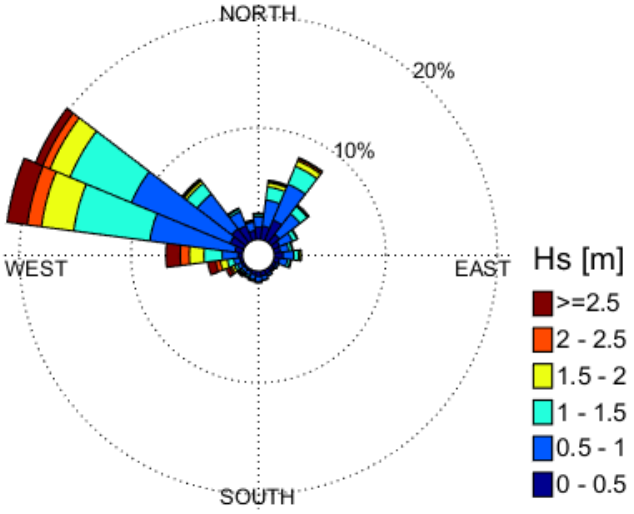

Figure 81: Hs rose diagram for wind-sea

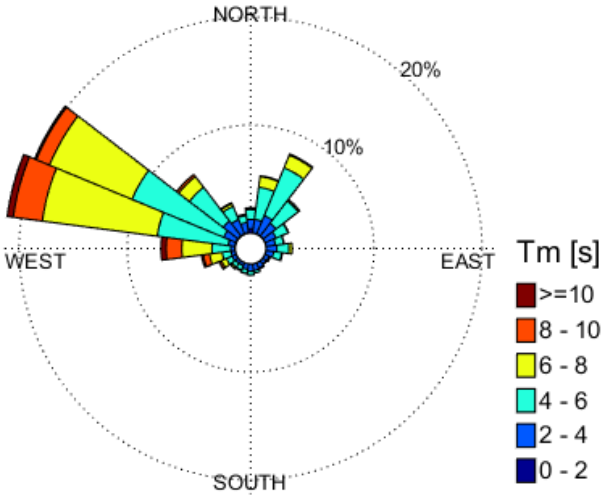

Figure 82: Tm rose diagram for wind-sea

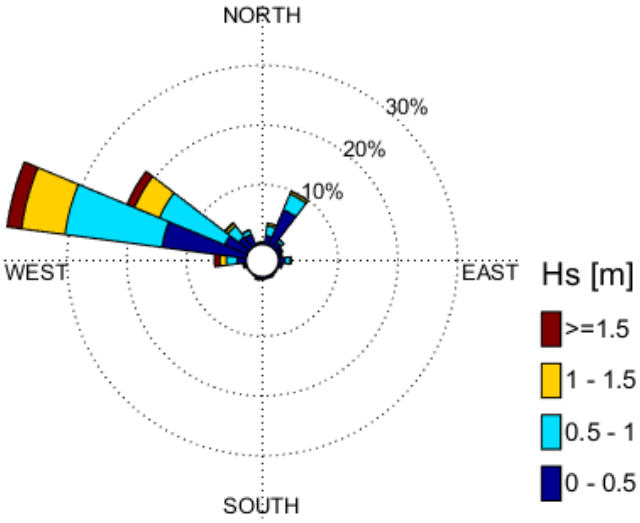

Figure 83: Hs rose diagram for swell sea 1

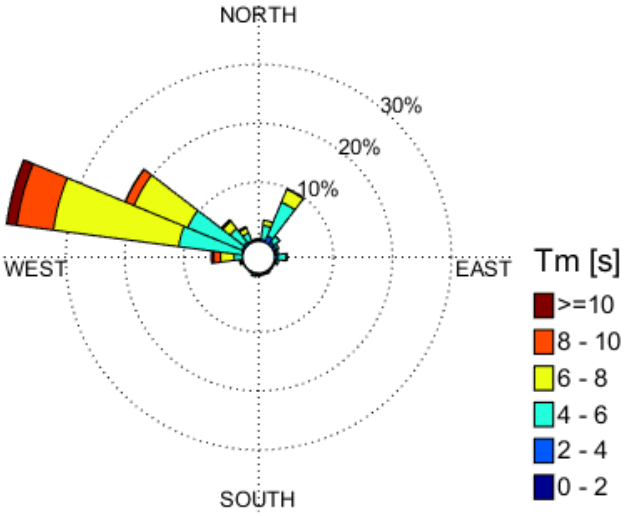

Figure 84: Tm rose diagram for swell sea 1

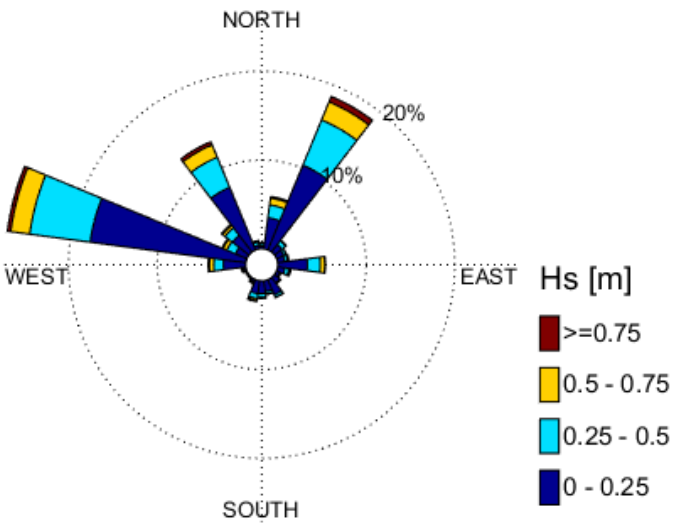

Figure 85: Hs rose diagram for swell sea 2

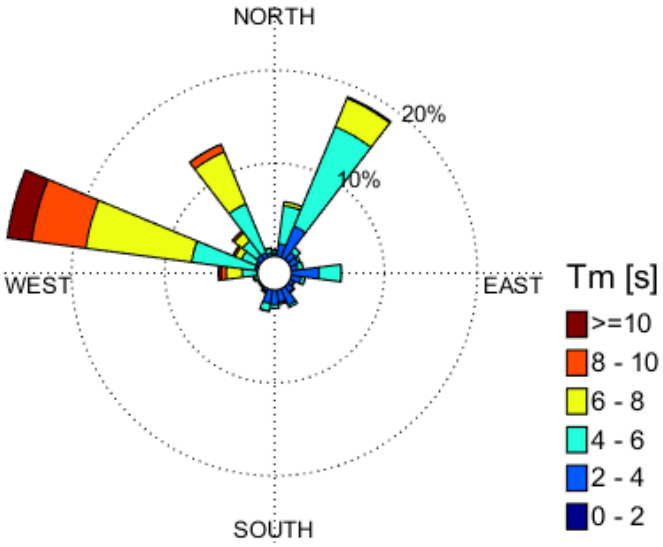

Figure 86: Tm rose diagram for swell sea 2

From previous section, the sea was concluded to be an omnidirectional sea. Swell 1 waves are coming from same direction as the omnidirectional sea. Swell 2 waves come from three different directions; WNW, NNE, and NNW. The main direction of swell 2 waves is WNW and coming from the same direction as the omnidirectional sea. The question is, how significant are the two other directions of swell 2 component? The answer depends on the operation type and operation criteria.

To distinct between a wind dominated and a swell dominated sea-state, a criteria is given by DNV, it is defined by introducing a variable T_f as (Torsethaugen, 1996; DNV-RP-C205, 2007):

Tf (used in wind/swell sea dominated criteria) (38)

$$T_f = \alpha_f H_s^{1\backslash 3}$$

Where α_f depends on fetch length, in this case fetch is estimated to be 400 km and the corresponding α_f is $\alpha_f = 7\ (sm^{-\frac{1}{3}})$. Estimated fetch is a little conservative value, the actual for Location 1 can reach up to 600 km.

$$if\ T_p < T_f \rightarrow wind\ dominated$$

$$and\ if\ T_p > T_f \rightarrow swell\ dominated$$

T_f is calculated and is plotted against T_p in Figure 87. 79% of the data points satisfy the criteria of a wind dominated sea.

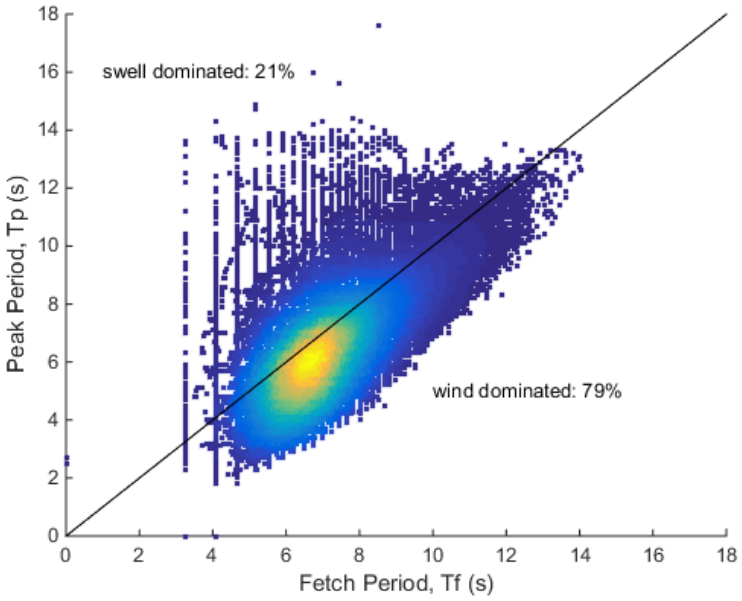

Figure 87: Tp against Tf plot

Figure 87 shows that 79% of the waves are valid as wind dominated waves according to DNV criteria, that is, for 79% of time the sea is wind dominated. Direction rose diagrams show that swells travel in the same direction as the wind-sea (except a third of swell 2 waves flow in different directions, this part has very small wave heights, refer to Figure 67).

5.4 Location Analysis

Directional comparison of the different locations, Location 1 to 5, is made. A change in the main direction is noted in locations 2 and 3, the rose diagrams for Hs of these locations are found in Figure 88 and Figure 89. Figure 88 shows that the main direction at Location 2 is direction segment 5 (NW), and the main direction at location 3 is still within segment 4 but shifted towards WSW, whereas in the other locations main direction is segment 4 (WNW).

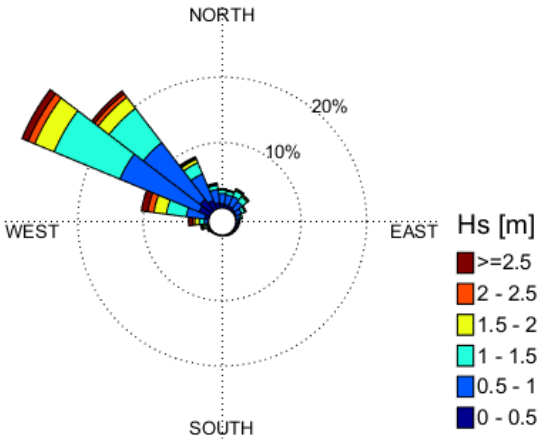

Figure 88: Rose diagram of Hs for Location 2

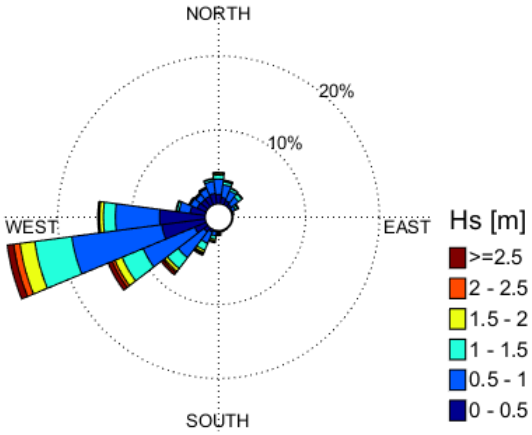

Figure 89: Rose diagram of Hs for Location 3

Figure 88 and Figure 89 show the locations that have waves coming from different directions. Location 2 and Location 3 have most of their waves coming from NW and WSW respectively. Figure 90 shows the percentage of waves against the direction for every location. It shows that the five locations under study are very similar, except Location 2, is different with main direction is segment 5. Further investigation for Location 2 sea-state is recommended.

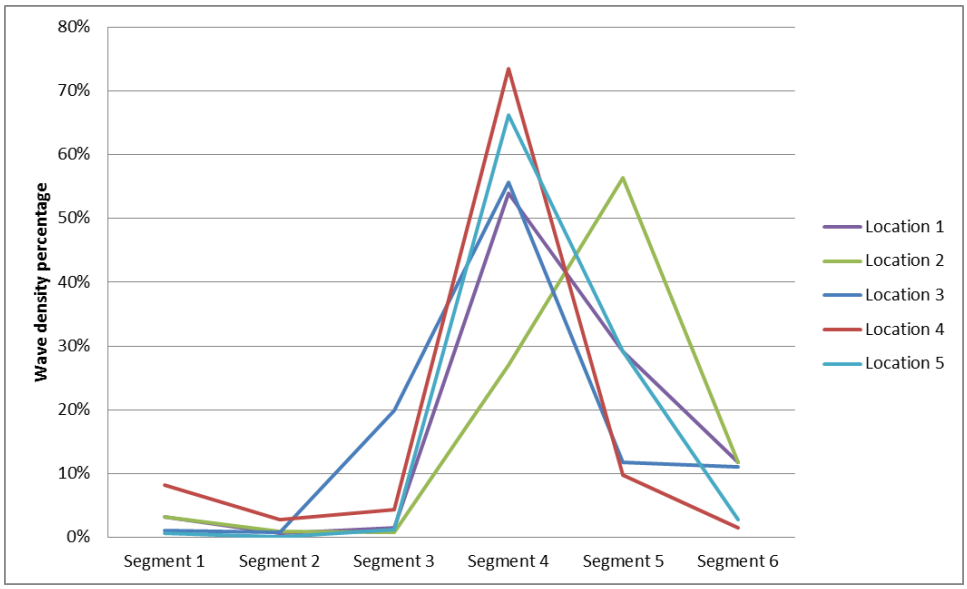

Figure 90: Distribution of waves among direction segments

By taking a look at the maps in Figure 92 and Figure 91 and comparing them with Figure 88 and Figure 89 respectively. It is obvious that the locations with different directions are the south-most and north-most locations, i.e. locations 2 and 3. The possible reason for wave coming from NW (instead of W) for Location 2, is thought to be related to the location, since this point is south-most and west-most among all others, which makes this location open in straight fetch to

shores of Italy (largest distance comparing to other locations, because this fetch is not available for others), and recalling the wind rose diagram (Figure 48), that shows that there are winds coming from that direction, together with this long fetch, waves could develop and main direction of waves possibly shift to NW (Figure 91).

And the other point with different direction than other locations is Location 3. Main waves here are coming from WSW, and the reason is thought to be that refraction of waves coming from west approaching shores of Lebanon will take place as waves approach shallow waters and continue their flow between Syria and Cyprus north towards shores of Turkey (Figure 92).

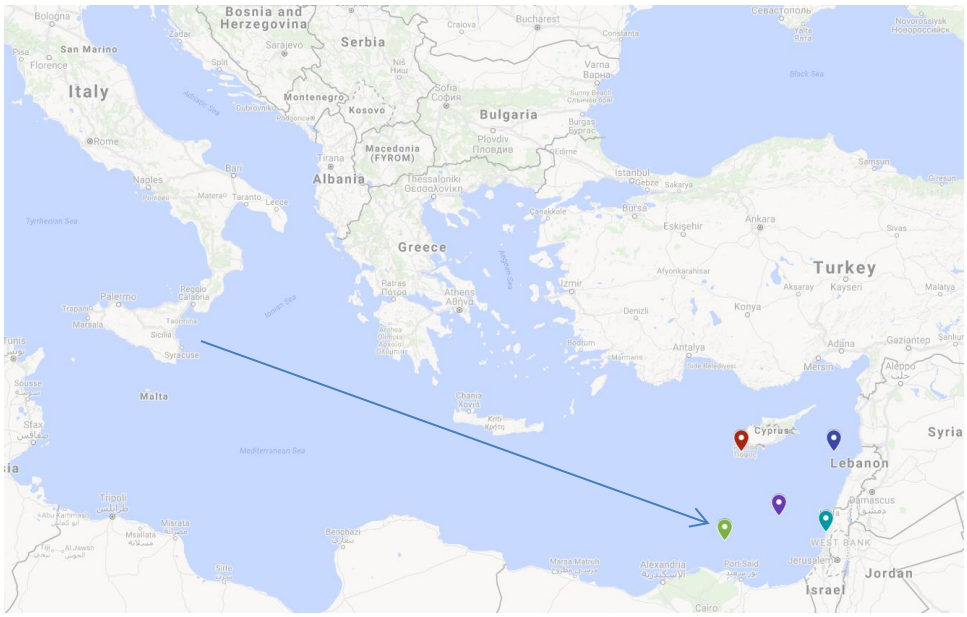

Figure 91: Zoomed out map of the area (Google Maps, 2016)

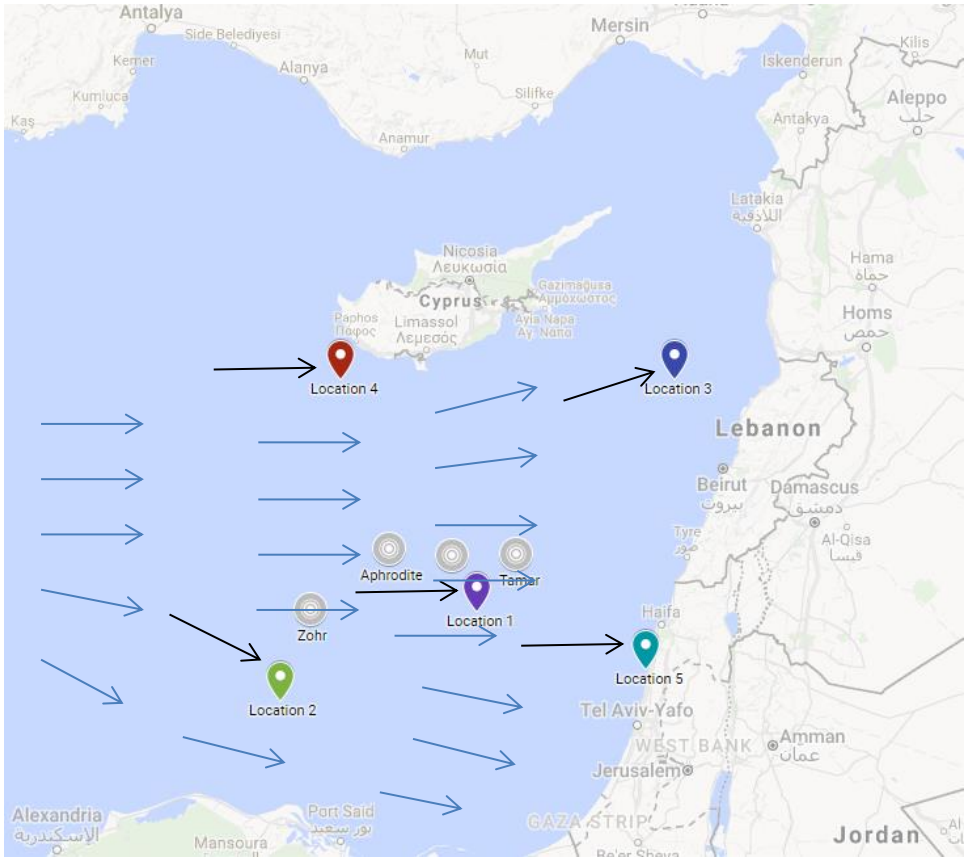

Figure 92: Propagation of waves map (Google Maps, 2016)

Directional analysis also confirms the omnidirectional assumption (for all locations). For all locations being studies, segment 4 is the main direction, except for Location 2, it is segment 5. Extremes of Location 2 may be higher than extremes of the other locations, therefore further investigation on Location 2 extremes is recommended. Omnidirectional assumption validity is shown in Table 8.

Swell waves directions are also checked for locations 2 and 3 to investigate for the relative direction between swell waves and omnidirectional wave. Figure 93 to Figure 96 show the directions of swell 1 and swell 2 wave components of locations 2 and 3 in directional rose diagrams.

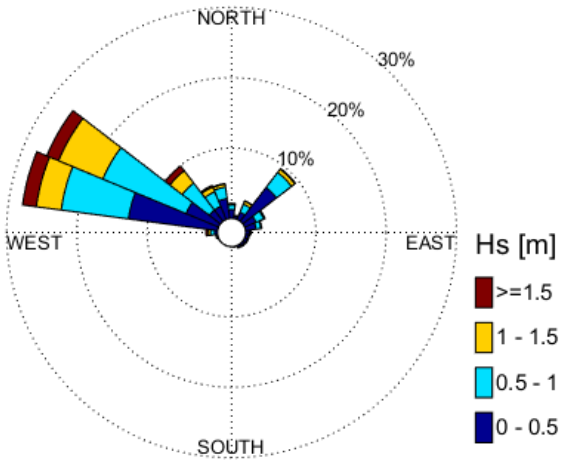

Figure 93: Hs rose diagram for swell 1, Location 2

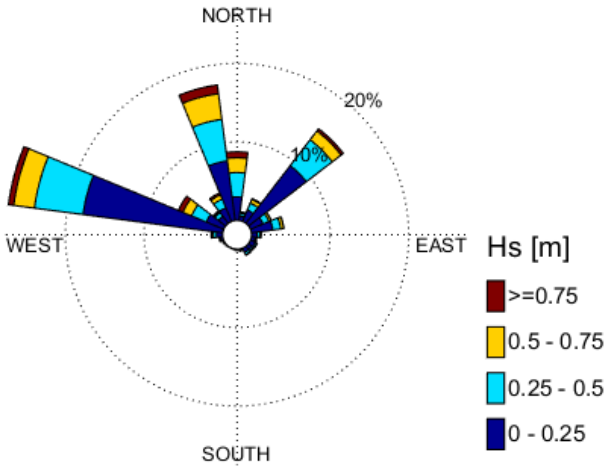

Figure 94: Hs rose diagram for swell 2, Location 2

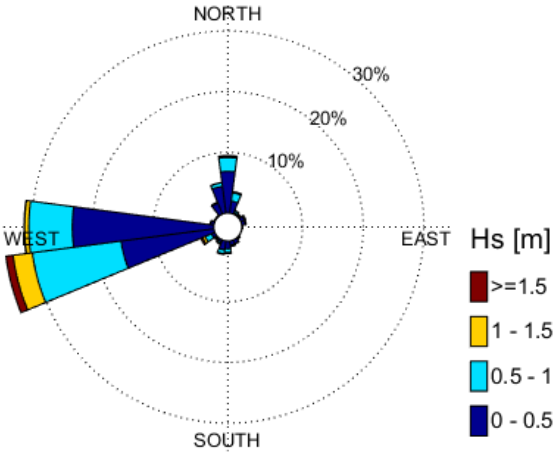

Figure 95: Hs rose diagram for swell 1, Location 3

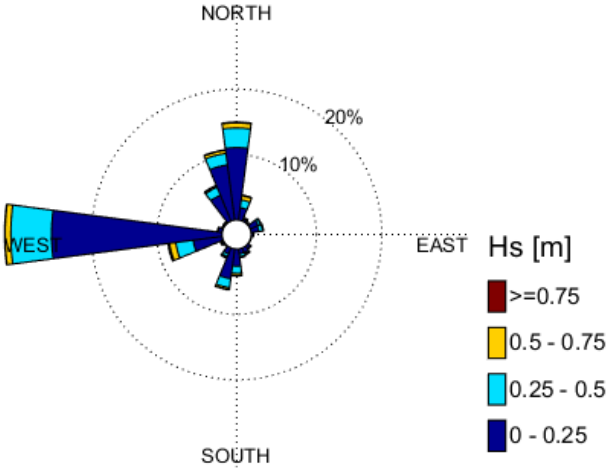

Figure 96: Hs rose diagram for swell 2, Location 3

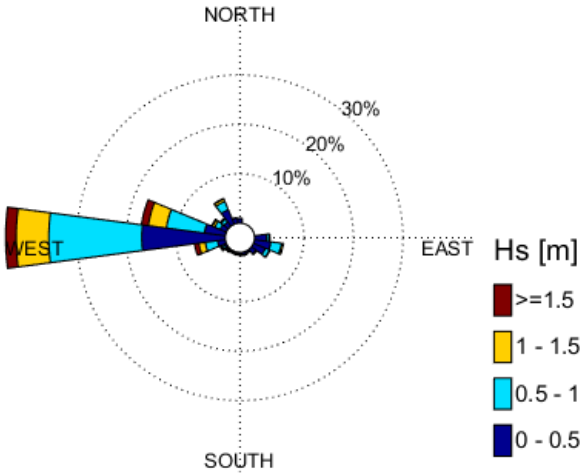

Figure 97: Hs rose diagram for swell 1, Location 4

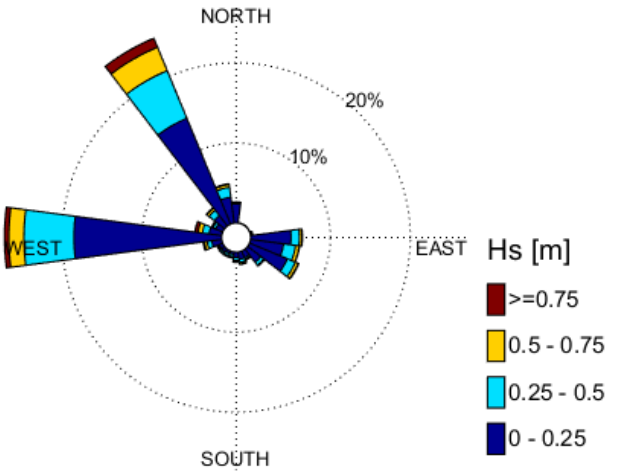

Figure 98: Hs rose diagram for swell 2, Location 4

Figure 93 and Figure 95 show that swell 1 component in locations 2 and 3 are coming from the same directions as the omnidirectional sea. Swell 2 components mainly come from the same direction as well, however, there are portions of swell 2 components coming from different directions. Table 8 summarizes the validity of omnidirectional assumptions for the locations under study and notes a warning for swell 2 component portions that come from different directions. If the assumption of omnidirectional sea is made, this table points out the sea main directions (that governs the majority of wind-sea and swell sea) and the directions where a tiny portion of swells may come from, that is given for the engineers to check the stability of the structures and operations.

Table 8: Omnidirectional assumption validity

Locations	Omnidirectional Sea	Swell
	The large majority of waves	Tiny portions of swell 2 component
	Directions: where the waves are coming from	
Location 1	**W**	NNE, NNW
Location 2	**NW**	NNW, NE
Location 3	**WSW**	N
Location 4	**W**	NNW
Location 5	**W**	swell info not available

Table 8 simplifies the sea-state; it gives the engineers the confidence to assume an omnidirectional sea for their analysis, gives the direction of the omnidirectional sea, and points out the direction of swells waves that have to be checked for maintaining analysis integrity.

6 Wave Extreme Estimations

6.1 Introduction

A joint academic task has been set up between University of Stavanger and University of Genova to analyze wave extremes in the Eastern-Mediterranean. Focus has been put to assess uncertainties in the estimation of extremes, applying 90 unique probabilistic models with different combinations of:

1. Extreme estimation approach

Three approaches are used: Annual maxima (AM), Peak-over threshold (POT) and All Sea States (ID)

2. Probabilistic distributions
   Five distributions are used: 3-par Weibull (W-III), Gamma, Generalized Extreme Value (GEV), Lognormal (LogN), and Gumbel
3. Parameter Estimation Methods
   Two estimation methods are used: Maximum likelihood estimation (MLE) and Method of Moments (referred to as MOM or MME)
4. Data sampling rate
   Three sampling rates are used: 1 hourly sampling (1Hr), 3 hourly sampling (3Hr) and 6 hourly sampling (6Hr)

This chapter will present probability paper plots of the fitted distributions, and proceeds with filtering them into a short list of the best fits. Probability plots are used as the tool to evaluate the integrity of the fitted distributions. Gumbel scale plots are used. Each plot shows the scatter data points and the fitted distribution being evaluated on the same graph. Evaluation of the fitted distributions is done by visual comparison, and is followed by decision-making whether a distribution should be filtered in or out.

In this study 90 models were fitted and evaluated, 36 were shortlisted for further uncertainty investigation. Average extremes of the 36 shortlisted models are presented in Table 9, first averages according to each approach (ID, POT or AM) are presented, and then in the last column on the right, the overall averages are given.

Table 9: Summary of Extreme Estimations (Location 1)

Return Period (years)	Significant wave height extremes (m)			
	ID	POT	AM	Average
100	8.2	8.2	8.6	8.3
10,000	11.5	11.0	11.4	11.3

Extreme estimates performed by others for roughly same location:

- $Hs_{100} = 8.7\ m$ (by Israel National Institute of Oceanography 2001)
- $Hs_{100} = 8.7\ m$ (by Kit and Kroszynski, 2014, Technion)
- $Hs_{100} = 8.2\ m$ (by EIA of Tamar Field by CSA International, 2012)
- No reported estimates found for the 10^4-year extreme wave.

- $Hs_{200} = 9.2\ m$ (from ATOS report final by Levin et al 2012)

6.2 Methodology

The procedure of data processing for each model is simplified as follows: first sampling the raw data, applying an approach for extreme estimations, assigning empirical cumulative probabilities for the resulting dataset, selecting a parameter-estimation method, fitting the dataset with probabilistic distributions, estimating the extremes, then fitting evaluations for filtering the models. Brief description of the steps is found below:

Sampling the raw data (Hs) as 1, 3, or 6-hourly sampled data

Sampling 1 hourly: is taking the original hindcast Hs input as is, without doing any change, since the hindcast is provided with hourly readings.

Sampling 3 hourly: is implemented by taking the values of Hs every third entry, e.g. taking the 1st, 4th, 7th value and so on. That is, taking the first and ignoring the second and third of every three values of Hs. Sampling 6 hourly is implemented in the same manner but with taking first value in every 6 values of Hs.

The main point of this section is checking the sensitivity of extremes to sampling rate, because some widely used hindcast data are provided in 1, 3 or 6-hourly patterns, e.g. DICCA hindcast is 1-hourly sampled dataset, the NORA10 hindcast (Norwegian Reanalysis by the Norwegian Meteorological Institute) is 3-hourly sampled and the ERA-Interim (archive of global atmospheric reanalysis ranging from 1989, by the European Centre for Medium-Range Weather Forecasts, ECMWF) is 6-hourly sampled. Therefore it is important to appreciate the effect of duration sampling (of available hindcast datasets) on extreme estimations.

Applying an approach for extreme estimations (AM, POT, or ID)

The three following approaches are data extraction methods, where the raw Hs dataset is processed into a tailored dataset before applying statistical fitting analysis.

First the raw data is cleaned from the low values, in this project the cleaning-threshold selected is 1 meter, and all values below this threshold are removed from dataset. After cleaning the low values, one extraction method is followed. Extraction methods are explained below:

Annual Maxima approach is implemented by sorting the sampled Hs yearly and simply taking the maximum Hs value in every year. Hence, *Hs,am* dataset is created. The calendar year (from beginning of January until end of December) is considered in this study, whereas it is recommended by DNV to consider the year from beginning of June until end of May. Referred to as *Annual Extremes* method, (DNV-RP-C205, 2007, p.38).

Peak over Threshold method is implemented as follows:

a. Sorting the sampled *Hs* yearly

   The calendar year is considered in this sorting. But less attention is given to sorting in POT approach; the challenging part of this approach is to get the threshold that well represents the storms.

b. Setting a threshold, *Hs,t*

   Threshold selection is crucial part in extreme estimation. There is no internationally accepted procedure for the selection criteria. DNV recommends a sensitivity analysis.

   The selection of the “right” threshold is not a straightforward procedure, there should be multiple distribution fittings with different thresholds, and attention to estimated extremes and number of storms for every threshold. This chapter includes a section for POT threshold selection.

c. Finding, for every year all the *Hs* values that are higher than the threshold *Hs,t,* calling the dataset *Hs,ot*

d. Assuming that the inter-arrival time of storms in the given area is 12 hours.

   Inter-arrival time is the minimum time between two consecutive storms, Hence, for every 12 hours there can maximum be 1 storm data point in the dataset.

e. Sorting the values of *Hs,ot* by storm

f. Taking the maximum *Hs* value of every storm, *Hs,pot*

All sea states approach is implemented by taking all values of sampled Hs. Hence, *Hs,id* is created. Note that the all sea state dataset is highly correlated. The use of extreme value theory requires datasets consisting of independent random variables. The use of highly correlated data (ID approach) violates this basic condition, therefore this approach is not preferred, but is still used for marine operation, because it can be used for both estimating extremes and planning day to day operations. The correlation means that adjacent data points tend to vary together. In wave height data, average time of uncorrelated data, is around 24 – 48 hours (Wang 1983).

Assigning empirical cumulative probabilities

As explained in the literature review, the extracted dataset is given empirical cumulative probabilities by the *ecdf.* For instance, if *Hs,am* is a dataset with N values, and *i* is the index of *Hs,am* that runs from 1 to N, then the empirical cumulative probability of *Hs,am (i)* is defined by the following equation, that is only valid if the dataset is sorted in an ascending manner.

Empirical CDF for Hs dataset (39)

$$F[Hs, am\ (i)] = \frac{i}{N+1}.$$

Selecting a parameter-estimation method

Distribution parameters can be estimated by different methods, the most common methods for extreme value applications are “Maximum Likelihood Estimator” MLE and “Method of Moments” MME. In this thesis only MME and MLE are considered.

MLE method estimates the parameters by maximizing the likelihood function, a function that maximizes the probability agreement of the selected model with the sample dataset. MLE is the best possible estimator method if the sample being modelled is of a very large size (given that the data is independent).

MME method estimates the parameters by setting the moments of the selected model equal to those of the sample dataset. Model moments are the mean, variance, skewness and kurtosis. MOM approach gives more weight to tail observations than MLE, it fits the moments of the population to those of the distribution.

Fitting the dataset with probabilistic distributions

This section lists the five distributions being considered in this study. These distributions are considered based on industry best practices in relevant offshore engineering applications (Haver, 2013).

Distributions: Weibull (3-parameter), Gamma, Generalized Extreme Value (GEV), Lognormal, and Gumbel. Their functions and parameters are defined in the literature review section.

Estimating the extremes

Extreme events are rare, their chance of occurrence is often rated with return periods, say the 100 year wave, defined as the wave that on average occurs once in a period of 100 years. However this can also be defined as the wave that has the annual probability of exceedance of 0.01, i.e. there is 1% percent chance that the 100 year wave happens every year.

In order to find extremes that correspond to certain return period, this relation between the return period T_r, and cumulative probability F_{Hs} is used.

Cumulative probability with return period relation (40)

$$F_{Hs} = 1 - \frac{1}{Na \times T_r}$$

Where Na is the annual average number of data points (in the dataset being fitted).

The resulted cumulative probability is used in the equation of every distribution to find the corresponding extreme.

Fitted distribution evaluations and filtering the models.

Models are used to estimate Hs in respect to return period. The focus is to find the distributions that best describe the data, especially in the tail (extreme Hs) where there is lack of data points. The lack of data at the tail leads to uncertainty. It is crucial to find a way of evaluating the fitted models, in this project, *Gumbel-scale Probability Paper Plots* are used with linear H_s in the x-axis and $-\log[-\log(F_{Hs}(h)]$ in the y-axis. The plots include scatter (data points) and fitted models in the same plot. Visual evaluation is made to decide whether a model should be filtered out or stay in the study. The goal of this part is to create a shortlist of models to proceed with for the rest of the study. For every approach only the best two distributions are shortlisted, and the rest are filtered out. All fitted distributions are presented in sections 6.3, 6.5 and 6.6. They are

made with 1-hourly sampled datasets, and MME parameter estimation method. Table 10 includes the parameters of all models used.

Table 10: Distribution parameters for the 90 models applied

	Appr-oach	Par. Est.	Sampling (hourly)	Weibull-III			Gamma		GEV			Lognormal		Gumbel	
				Shape	Scale	Location	Shape	Rate	Location	Scale	Shape	Mean	SD	Location	Scale
1	ID	MLE	1	1.0480954	0.6409021	1.0000000	8.2990750	5.0987600	1.2804816	0.2529241	0.5585736	0.4257532	0.3266215	1.3721909	0.3725644
2			3	1.0489930	0.6412818	1.0000000	8.3079980	5.1038010	1.2808211	0.2527742	0.5579940	0.4258562	0.3264852	1.3723747	0.3723514
3			6	1.0493360	0.6411983	1.0000000	8.3121440	5.1066800	1.2800357	0.2521189	0.5627767	0.4257650	0.3264789	1.3721941	0.3723421
4		MME	1	0.8610111	0.5362840	1.0000000	5.8095580	3.5692810	1.2807543	0.2529942	0.5572360	0.4077291	0.3985257	1.3237455	0.5265241
5			3	0.8610111	0.5362840	1.0000000	5.8111560	3.5693440	1.2812560	0.2534695	0.5555339	0.4080067	0.3984750	1.3241258	0.5265912
6			6	0.8610111	0.5362840	1.0000000	5.8102190	3.5699750	1.2798178	0.2524569	0.5618036	0.4076565	0.3985047	1.3236499	0.5264616
7	POT	MLE	1	1.3710890	1.3053340	2.8654640	22.0257590	5.4372870	3.5264132	0.4715887	0.4500132	1.3760906	0.2070405	3.6563166	0.6126892
8			3	1.4386010	1.3220630	2.8654640	23.6300350	5.8262920	3.5500991	0.4468066	0.4568328	1.3788186	0.1998405	3.6753887	0.5871181
9			6	1.5107220	1.3502450	2.8654640	25.4980330	6.2585190	3.6182684	0.4830891	0.3125593	1.3849222	0.1925383	3.7068685	0.5741777
10		MME	1	1.2239590	1.2136740	2.8654640	18.8905200	4.6637330	3.5252153	0.4749721	0.4469945	1.3730530	0.2271190	3.6304817	0.7277085
11			3	1.2239590	1.2136740	2.8654640	20.3170670	5.0084910	3.5564731	0.4561289	0.4302831	1.3763033	0.2191957	3.6508850	0.7027720
12			6	1.2239590	1.2136740	2.8654640	22.1564460	5.4357810	3.6189431	0.4770043	0.3235399	1.3830530	0.2101064	3.6856966	0.6762663
13	AM	MLE	1	2.2176730	2.2919170	3.7387540	37.0459170	6.4160950	5.3848426	0.8677134	-0.1489275	1.7397950	0.1645462	5.3168255	0.8457785
14			3	2.1749740	2.2250830	3.7387540	37.4315980	6.5507780	5.3244617	0.8439994	-0.1319361	1.7295121	0.1634131	5.2658660	0.8247411
15			6	2.1282850	2.1439810	3.7387540	38.5345900	6.8236650	5.2717658	0.8310087	-0.1399195	1.7181589	0.1611834	5.2103750	0.8153715
16		MME	1	2.2012590	2.2464200	3.7387540	37.4336940	6.4758080	5.3963985	0.8542688	-0.1483458	1.7413161	0.1623678	5.3494827	0.7468145
17			3	2.2012590	2.2464200	3.7387540	36.7966940	6.4380220	5.3367427	0.8590471	-0.1573845	1.7297798	0.1637487	5.2856412	0.7447788
18			6	2.2012590	2.2464200	3.7387540	37.9281050	6.7208760	5.2677396	0.8217967	-0.1339282	1.7174619	0.1613198	5.2252507	0.7243193

6.3 Annual Maxima Fitted Distributions

Starting with the AM approach, the fitted models are presented in Figure 99 to Figure 106, including a histogram, an empirical CDF (ecdf) of the dataset and a Cullen and Frey graph. In this case, AM dataset consists of 37 data points, which are the maximum significant wave heights for every year.

The Cullen and Frey graph

The kurtosis (degree of "peakedness") and skewness (degree of asymmetry) are the second and third moments of a particular distribution, and often are used to compare behaviors of distributions and datasets. In this study the Cullen and Frey graphs are presented, graphs that relate to kurtosis and skewness, however they are not the tool used in the filtering process, they are rather used like a reference.

Cullen and Frey graphs present the Hs dataset in kurtosis-skewness plot with kurtosis in the y-axis against square of skewness in the x-axis, and compares location of the dataset (the dark blue circle) with the theoretical locations of various standard probabilistic distributions. For some

of the standard distributions there is only one possible value of the kurtosis and skewness, such as the normal and exponential distributions. For instance, the normal distribution has kurtosis = 3 and skewness = 0, hence it is marked on Figure 106 by a star on point (0, 3). However other distributions have multiple possible values of kurtosis and skewness, thus they are represented by lines, such as lognormal distribution. Weibull distribution is not there on the graph but theoretically it falls close to the gamma distribution, since both are extensions of the exponential distribution and involve a certain integral called the gamma function. Nonparametric bootstrapping of the dataset is shown by the yellow/orange dots, bootstrapping is done by random resampling 1000 datasets of same size as original dataset (there are 1000 yellow dots on the graph). Nonparametric bootstrapping is a method of resampling subsets of data from the original dataset without making assumptions about probability distributions of the variable being assessed. These bootstraps are key indicator for evaluating the robustness of the proposed distribution and deriving the statistical (epistemic) uncertainty and variability of the model. Bootstrapping of 1000 samples and plotting them on the same graph shows the range of uncertainty on parameter estimation of the original sample that is plotted as the yellow/orange cloud. (Cullen and Frey, 1999)

Figure 104 shows that the five fitted models are representing the data in a fine way, and are close to each other. With dataset size of 37 points, in spite of the high independency of the variables in the list, the small number of data points in AM method makes the statistical uncertainty higher, and this can be seen in the yellow dots (1000 bootstraps of the same sample size) in Figure 106 where the size of the cloud is larger than that of other approaches.

In Figure 104: AM Multi-Plot, it was noted that there is a particular distribution that best represents the dataset of annual maxima, and that distribution is the Gumbel, see Figure 103. Gamma fit is filtered out because it is the furthest from the data scatter. Weibull-3, GEV and Lognormal are quite the same in this case therefore it is decided to include Lognormal (Figure 102) and exclude the rest from the shortlist. Theory supports that Gumbel is a best fit for a sample of maxima (Haver 2013, p.79)

The two shortlisted distributions for AM approach are Gumbel and Lognormal.

Probability plots in Gumbel Scale for Annual Maxima approach and MME parameter estimations

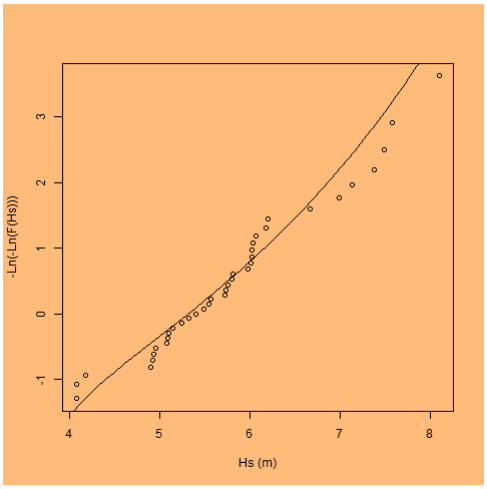

Figure 99: AM Weibull-3

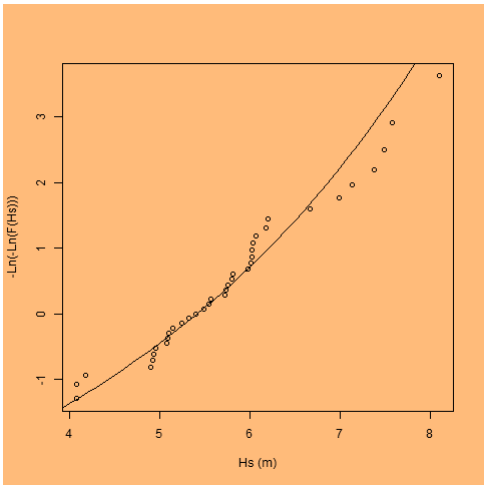

Figure 100: AM Gamma

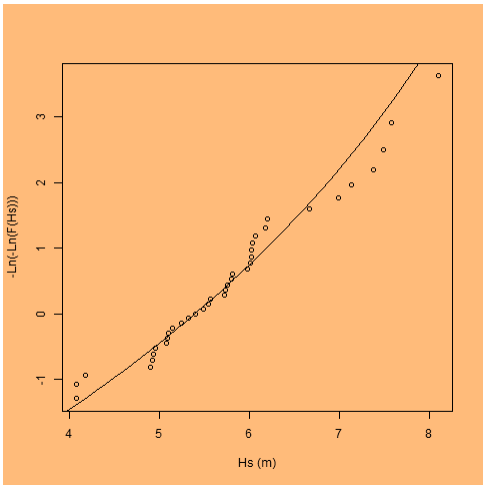

Figure 101: AM GEV

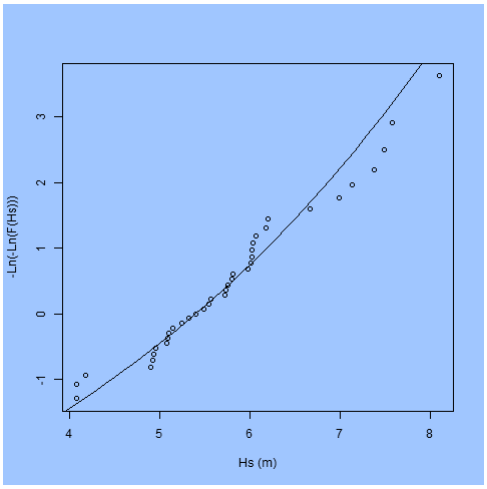

Figure 102: AM LogNormal

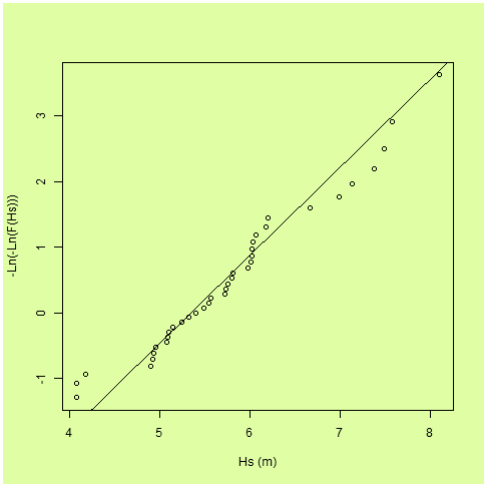

Figure 103: AM Gumbel

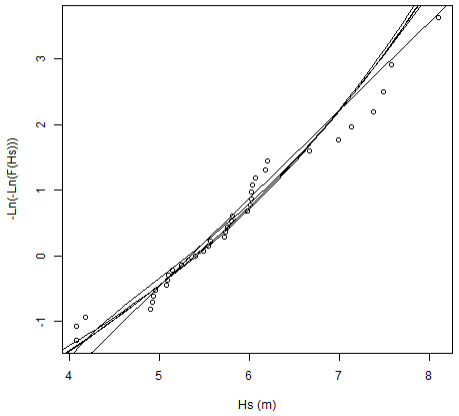

Figure 104: AM Multi-Plot

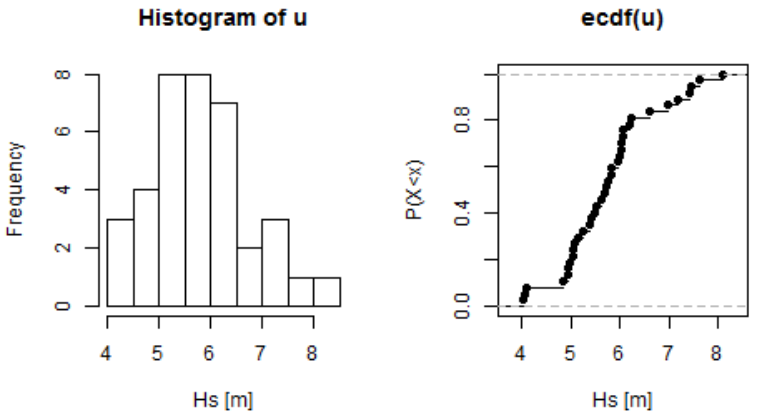

Figure 105: Histogram and CDF for AM Dataset (37 data points)

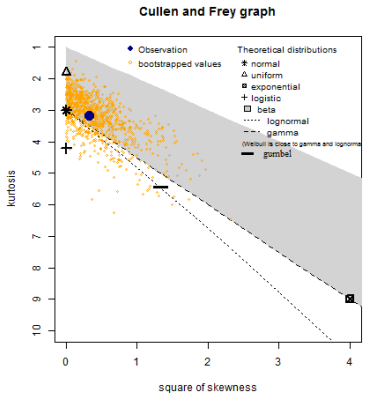

Figure 106: AM Cullen and Frey

6.4 Threshold Selection

It may be valid to state that the POT is the most widely used approach for extreme estimations. Because POT-processed variable is believed to be independent and the number of data points is not critically small (such as AM). However this approach is sensitive to threshold selection. According to DNV, in case a POT should be used, a sensitivity analysis with respect to threshold level should be performed (DNV-RP-C205, 2007, p. 37).

The threshold selection is discussed in this section, sensitivity analysis is performed and at the end of the section a threshold selection is concluded. Factors considered while investigating pros and cons of threshold level are listed below. There are a number of documents addressing the issue, but still there is no universally accepted procedure. Therefore there is a certain degree of subjectivity in the recommended criteria given in this section. The criteria addressing the important factors for threshold selection is set as follows:

I. Number of storms

The number of storms basically is the number of points being fitted, at the end, and used for extreme estimation, there is a general interest of having data points as much as possible, but attention should be given to the effects of a too low number and a too high number of data points. A too high number of data points will increase correlation (dependency) between the points and will disturb the quality of the fit, since more weight in fitting will be given to lower waves hence the quality of the fit will be weaker in honoring of high waves, the waves of interest. However, the effects of a too low number of data points include an increase in the statistical uncertainties in the extreme. As the threshold is increased, the number of data points is decreased, until it reaches the same as the number of years in the data being studied, then the POT approach dataset will be equal to AM dataset and will probably have few tens of data points (10 – 50 points) and it is not recommended to go below this range.

Recommendations regarding number of storms according to discussion with Prof. Haver:

- Setting the range of number of storms (points) in a POT dataset:

The number of storms is recommended to be between somewhere between: $[(1.5-10)\times num.years]$; for example, if there are 40 years of data, then the recommended range for number of points is $[60-\ 400\ points]$.
The lower limit is given to justify the use of POT approach, otherwise an AM approach could be used with 1 data point per year. The upper limit is given to keep the focus concentrated in the tail of the scatter. A lower threshold leads to an increase in the number of points included in a POT dataset and this increase is basically including storms with lower peak heights to the dataset. The inclusion of the lower storms is believed to disturb the tail-honoring of the fitted distribution. And the range is set large enough to allow for further testing.

- [Tentative criterion] At least 1 storm from every year to be included in the dataset. A calm year may be under-represented by POT, if the threshold was higher than the calm year's highest storm peak height. This recommendation ensures that there is data from every year.

  This criterion has a room for discussion, some scientists argue for a time-dependent version of POT (see, e.g., Smith, 2001; Katz et al., 2002; Davison and Smith, 1990). Time-dependency promote independent variables with equal spacing, e.g. yearly (or seasonally) data by the use of annual quantile threshold. For example an annual quantile threshold of 98% is selected, then the whole dataset is separated into annual subsets, and a corresponding threshold value of the quantile is calculated for every subset, leading to different yearly thresholds but with equal representation of the time span selected. Some other specialists argue for time-independent version of POT. A fixed threshold is set over the span of the whole dataset to capture exceeding storms. Regardless of spacing between the captured storms, some years may not be represented at all (Coles, 2001). A time-independent version of POT is considered for this thesis (after trying working with both versions).

II. Sensitivity analysis

The behavior of the extreme wave (say 100-year wave) in respect to changes in threshold level is important to be investigated. This understanding helps locate the threshold ranges where the extreme estimation is most stable. Recommendations for sensitivity consideration in the selection of threshold:

- Locate the (most) stable threshold range(s)
- Limit the threshold selection to those ranges

III. Distribution fitting

The quality of the fitted distribution is a key indicator for the quality of the threshold selected. By looking at a probability paper one can tell whether the fitted distribution is acceptable, underrating or overrating the extremes. Combining the criteria considerations from two previous points (number of storms and sensitivity), a preference of few threshold values will be established. Note that, unlike AM method, there is no theoretical distribution that best fits the POT data. Thus recommendations regarding fitting are crucial, and are summarized as follows:

- Limit threshold options to two or three values
- Execute the POT approach for the three values and fit them with multiple distributions
- Select the distribution of the best fit
- Compare it for the limited thresholds selected
- Select the threshold with the best tail-honoring fit

Attention was given to three considerations above in the threshold selection process. Procedure and graphics are shown below.

First, a sensitivity analysis is performed, where thresholds from 1 meter to 8 meters with 0.5 meters increments are used for POT approach. The resulting POT datasets are fitted with Gumbel distribution (it is best for AM, and it is believed from past experience that it behaves relatively well with POT). The 100-year wave extreme is estimated for every threshold. A plot showing wave extremes vs thresholds is generated and shown below. This plot is a key for selecting the (most) stable ranges of threshold levels.

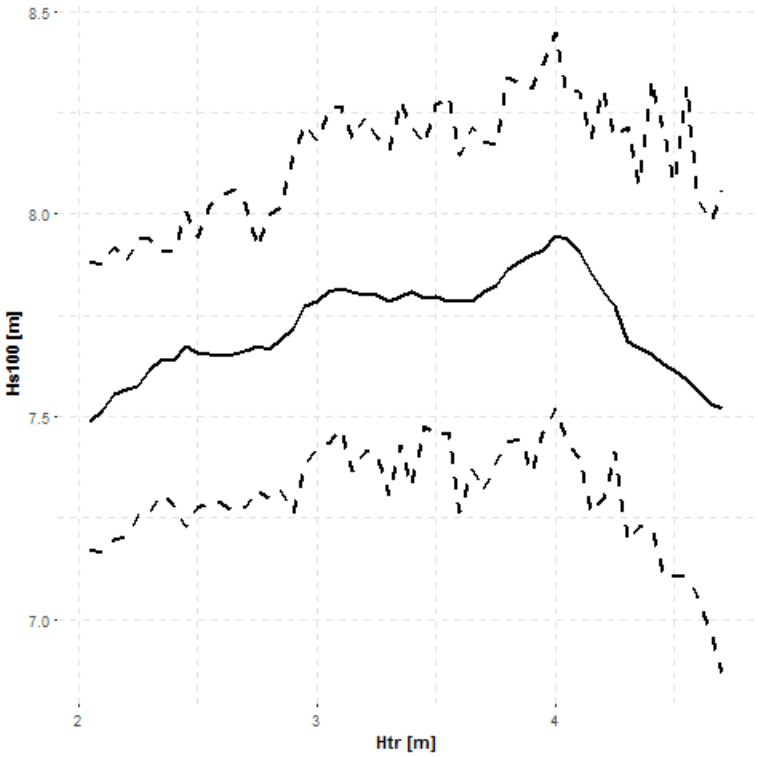

Figure 107: Sensitivity plot, wave extreme vs POT threshold

The black line in Figure 107 is the line representing the extremes for every threshold increment used. The dashed lines are the 90% confidence interval band, which is generated by Gumbel bootstrapping 100 samples and plotting the 5% and 95% quantiles for every threshold. The figure shows that the most stable regions (where the extreme does increase or decrease rapidly) can be pointed out as follows:

- Stable threshold range 1: 2.5 – 2.8 meters
- Stable threshold range 2: 3.0 – 3.7 meters

Integrating the number of points consideration with the stable ranges above, a plot is generated showing number of points associated with every threshold selected, the plot is shown in Figure 108. The number of points is decreasing with an increase in threshold; therefore the first check is done on the lower limits of the two ranges above, because the lower threshold limits correspond to the higher number of points in a POT dataset.

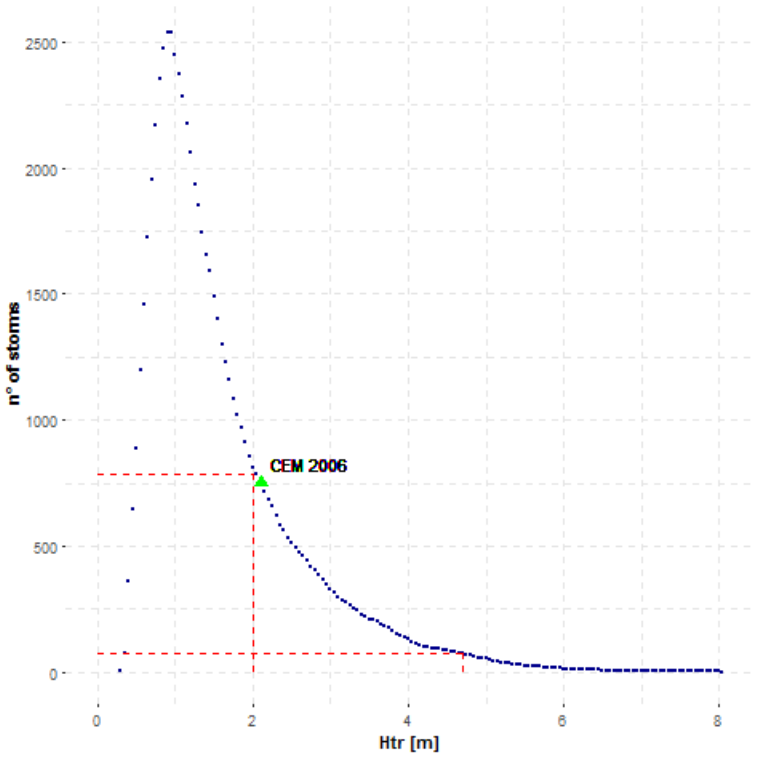

Figure 108: Number of storms against threshold

The marked CEM 2006 is the recommendation of selecting the 6% exceedance limit of the recorded long-term Hs time-series as the threshold according to *the US Army Coastal Engineering Manual* (CEM, 2006). Checking the two lower limits of the ranges above, the 2.5 and 3 meters, they result in 526 and 338 data points respectively. Threshold 2.5 meters results in 526 data points which is a quite large number, in addition to a less conservative extreme estimation (as seen in Figure 107), thus, 2.5 meters falls out as an invalid threshold. 300 is a relatively high as well, but is still valid for the criteria, thus threshold 3 meters is recommended.

Since 3 meters threshold results in a relatively large (but acceptable) number of points, another threshold from the same range will be considered, say 3.7 meters that results in 185 points. The mid-point of the stable range can be considered as well (3.35m). Nevertheless, a comparison of distribution fitting is to be performed to ensure the quality of the thresholds.

Deeper investigation for thresholds 3 and 3.7 meters is found below. Distributions selected for fitting comparisons are Weibull-III, Gumbel and GEV distributions.

Threshold 3.7 meters results in 1 storm only for the years 1989 and 2014, and these storms are 4.09 m and 3.99 m high respectively. According to this section's criteria (at least 1 storm per year), the threshold cannot reach 3.99 m, else the year 2014 will be un-represented in the POT dataset. The distribution parameters are listed at the end of this section in Table 12. Fitted distributions are presented in Figure 109 to Figure 114.

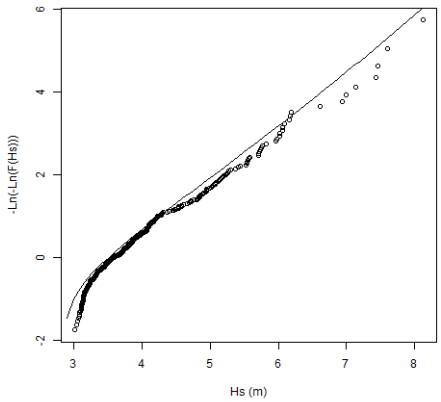

Figure 109: Wei-III fit (3 m threshold)

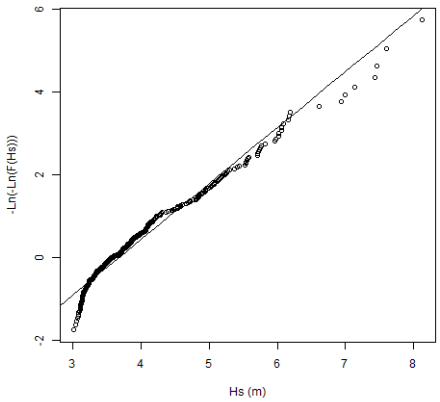

Figure 110: Gumbel fit (3 m threshold)

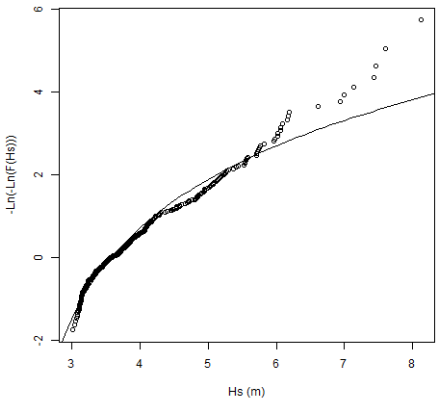

Figure 111: GEV fit (3 m threshold)

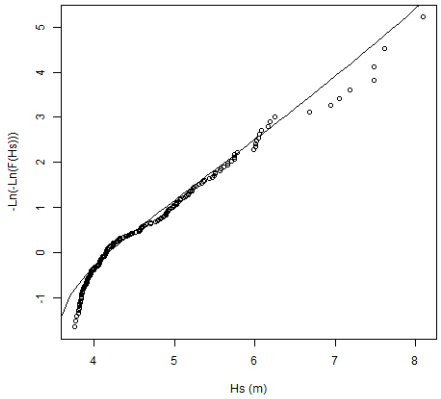

Figure 112: Wei-III fit (3.7 m threshold)

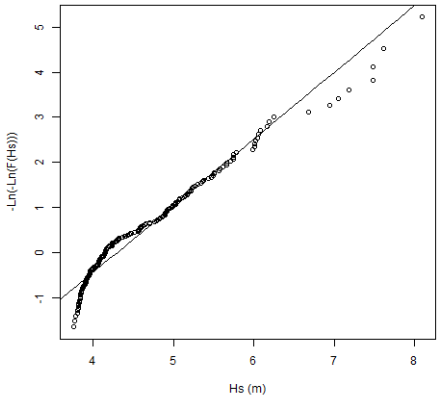

Figure 113: Gumbel fit (3.7 m threshold)

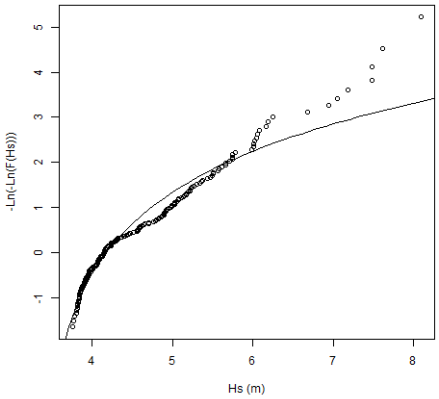

Figure 114: GEV fit (3.7 m threshold)

Looking at the fitted distribution above, an interest is created after noticing the performance of the data scatter on the probability plot is different in the body that in the tail, a decision is made, based on the fitting, to include another threshold in the study. The selection of the third threshold is based on visual evaluation of the behavior of the POT scatter, see Figure 115. The threshold will cut the lower part of the points that behave differently than the tail, and at the same time, keeping enough points in the study. The selected threshold may violate with the pre-set criteria of minimum 1 storm per year, if selected larger than 3.98 m. Therefore, the third

threshold is selected to be 3.98 meters and the information and plots associated with it are found below.

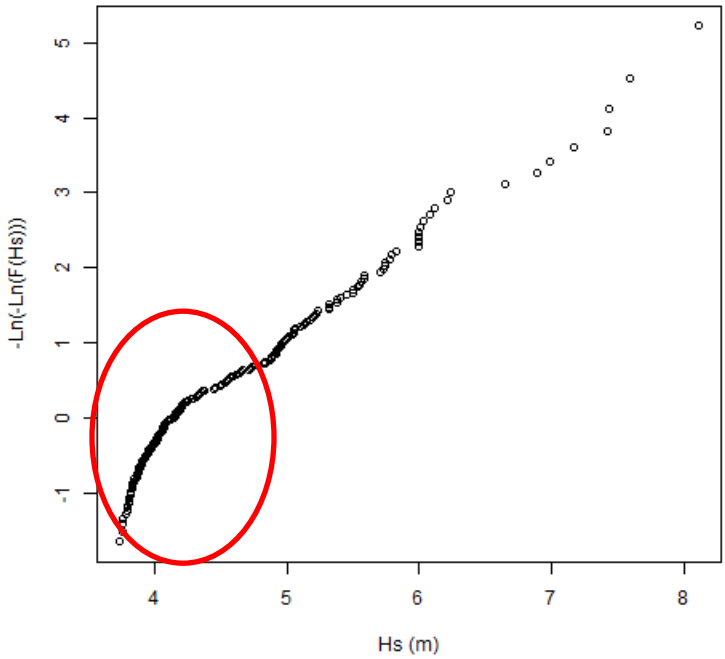

Figure 115: POT scatter

The red circle in the figure above shows the data that is noted to behave different than the rest of the sample, and this data is the motive for the investigation of a third threshold that is higher than the first two. The third threshold information and graphics are found in Table 11 and Figure 116 to Figure 118.

Table 11: Basic information specific to different thresholds

Threshold	**3 meters**	**3.7 meters**	**3.98 meters**
Total number of storms (data points)	338	185	137
Annual Average number of storms	9.1	5	3.7
Minimum annual number of storms	3 storms	1 storm	1 storm
Year(s) of minimum annual number of storms	2014	1989; 2014	89; 95; 98; 99; 05; 10; 14
Maximum annual number of storms	16 storms	11 storms	9 storms
Year of maximum annual number of storms	1992	2012	2012

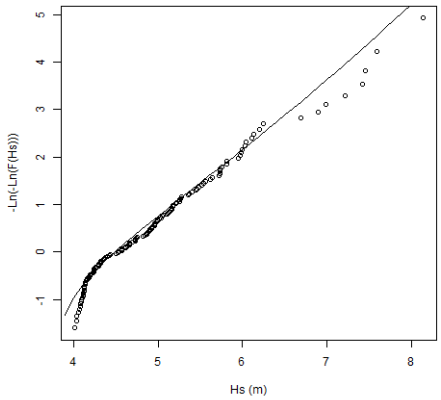

Figure 116: Wei-III fit (3.98 m threshold)

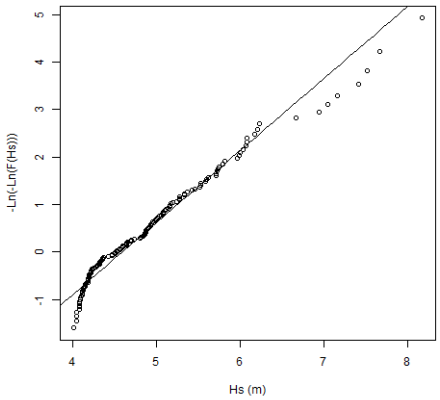

Figure 117: Gumbel fit (3.98m threshold)

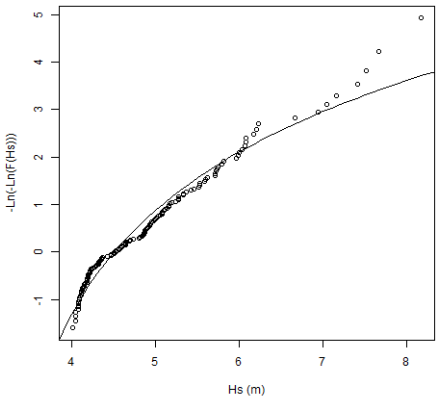

Figure 118: GEV fit (3.98 m threshold)

After a close look at the fitted distributions for the three thresholds being investigated above, Weibull-III is selected to be the best distribution. Gumbel was also good, whereas GEV was not acceptable. When the solid line of the distribution is below the data scatter dots in the plot, then the extreme will be over-estimated, i.e. for a given probability, the resulted distribution extreme will be higher than that of the data set. Comparing the three Weibull-III distributions, even if the difference is small, it is possible to use the probability paper plots as a tool for selection of a threshold that the user feels comfortable with (since it is subjective, the feeling of comfort towards the threshold is believed to be required). The three Weibull-III plots are similar, small differences exist, the lower threshold fit was the most impressive one, and the gap between the fitted line and the data scatter increases with the higher thresholds. The highest threshold was included in the study in hopefulness to have a better fit that the other two, and this was not the case, therefore it is discarded. Threshold 1 fitted distribution is visually judged to be (slightly) better than that of threshold 2. The selected threshold for POT analysis is threshold 1 (3 meters). That corresponds to 98% quantile of the raw data. Distribution fittings parameters are listed in the Table 12.

Table 12: Distribution parameters for fitting the different thresholds

Threshold (m)	Weibull-III			Gumbel		GEV		
	Shape	Scale	Location	Location	Scale	Location	Scale	Shape
3	1.2239590	1.2136740	2.8654640	3.6754956	0.7412947	3.5788642	0.5132192	0.3839778
3.7	1.2638552	1.1683200	3.5508610	4.3058132	0.6812263	4.1883080	0.4396568	0.4965283
3.98	1.3042556	1.1748942	3.8344165	4.6135784	0.6648653	4.5400065	0.5145639	0.2857731

Threshold selected is: 3 meters.

6.5 Peak-Over-Threshold Fitted Distributions

With the selected threshold of 3 meters there are 338 data points. They also have the quality of being statistically independent, and the other quality of having fairly large number of data points (around 10 times larger than that of AM). The distribution of data points is shown in the histogram in Figure 125. The yellow cloud in Figure 126 shows indication of size of uncertainties (smaller cloud than that of AM, see Figure 106). Looking at the multi plot of Figure 124, it is clear that all the fits tend to deviate at the tail. Honoring the tail is the main feature of a fitted distribution. Comparing fitted models with scatter tails, it is concluded that Gumbel (Figure 123) and Weibull (Figure 119) are the shortlisted models. Weibull as the best fit. GEV and Gamma deviate considerably from the dataset. DNV recommendations for POT approach are Weibull and exponential. Figure 119 to Figure 124 show the fitted distributions.

The two shortlisted distributions for POT approach are Weibull and Gumbel.

Probability plots in Gumbel Scale for POT approach and MME parameter estimations

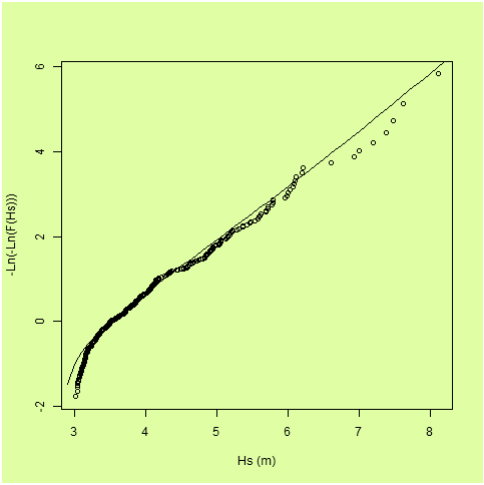

Figure 119: POT Weibull-3

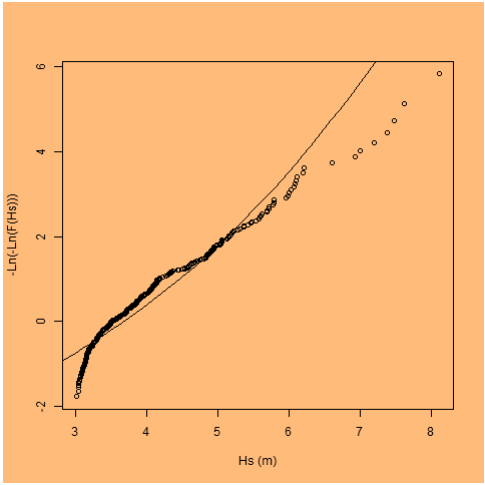

Figure 120: POT Gamma

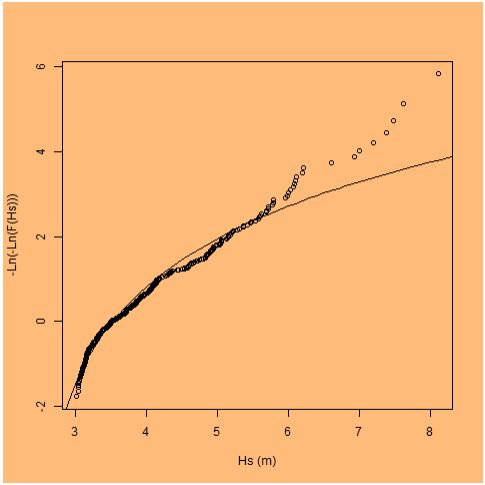

Figure 121: POT GEV

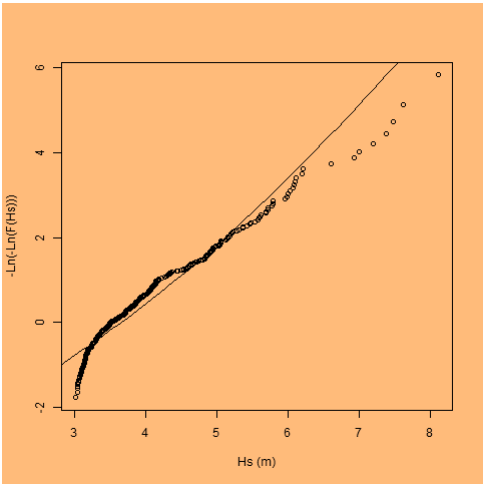

Figure 122: POT LogNormal

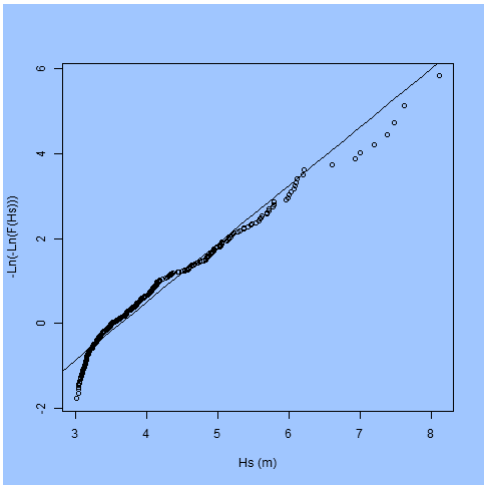

Figure 123: POT Gumbel

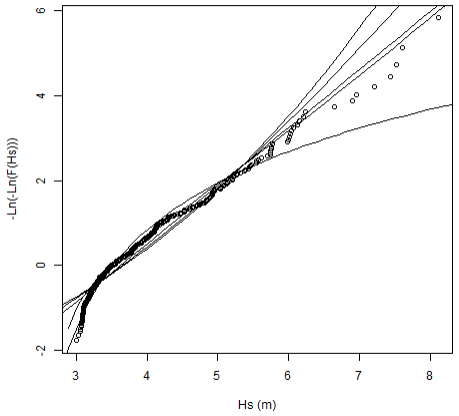

Figure 124: POT Multi-Plot

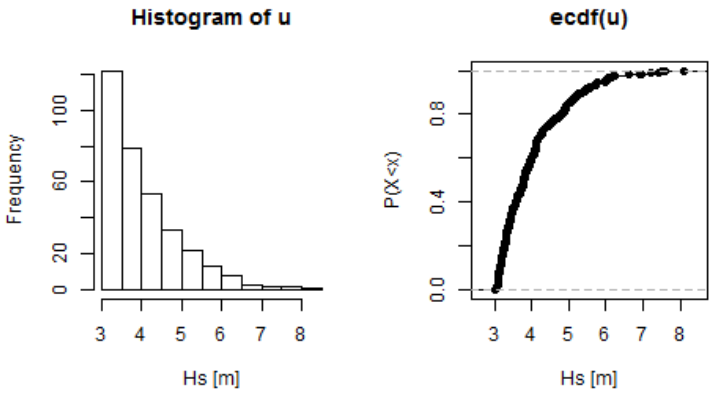

Figure 125: POT Dataset Representation (338 data points)

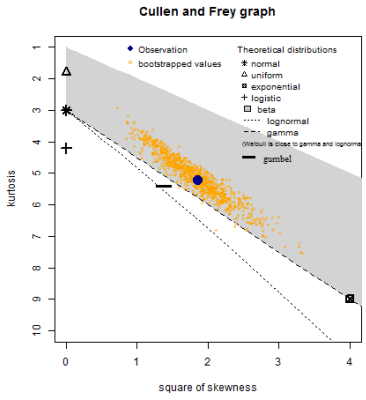

Figure 126: POT Cullen and Frey

6.6 All Sea-states (ID) Fitted Distributions

Figure 127 to Figure 132 show fitted distributions. ID dataset size is 107145. Looking at Figure 132, a larger deviation exists between fitted distributions and the data scatter, the best two fits are the Weibull (Figure 127) and the Lognormal (Figure 130) distributions and those are the selected models for the shortlist, with Weibull as the best fit. Histogram in Figure 133 shows the distribution of the 107145 values, where most of them are below 2 meter. The yellow cloud in Figure 134 shows indication of size of uncertainties. The cloud is very narrow; it is the smallest among other approaches, which reflects higher correlation and smaller uncertainties in this dataset. The result of best fit agrees with DNV recommendations.

The two shortlisted distributions for ID approach are Weibull and Lognormal.

Probability plots in Gumbel Scale for ID approach and MME parameter estimations

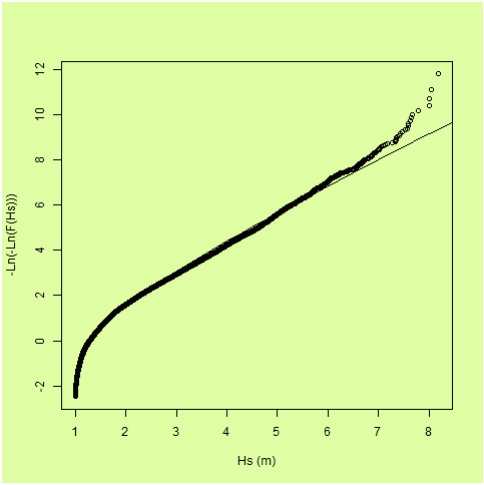

Figure 127: ID Weibull-3

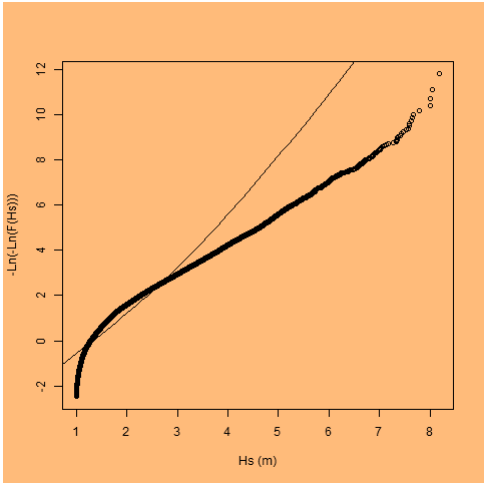

Figure 128: ID Gamma

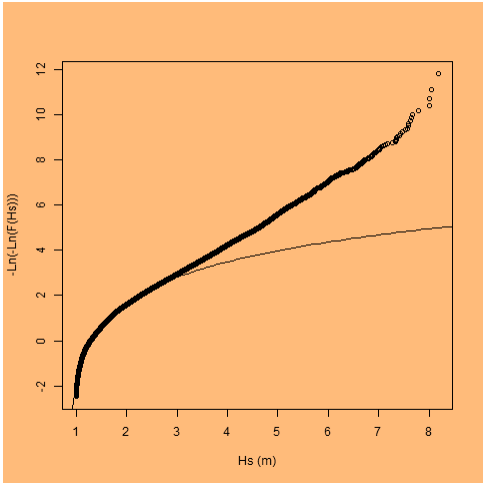

Figure 129: ID GEV

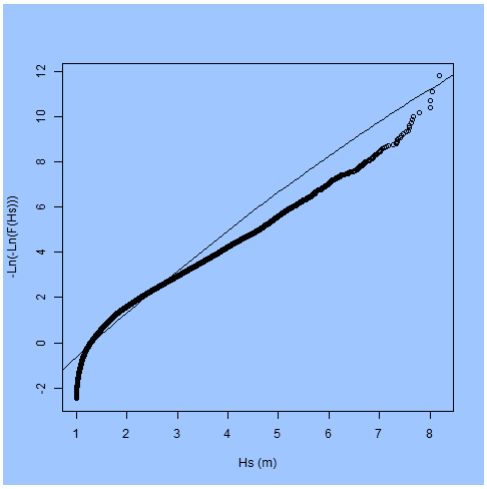

Figure 130: ID LogNormal

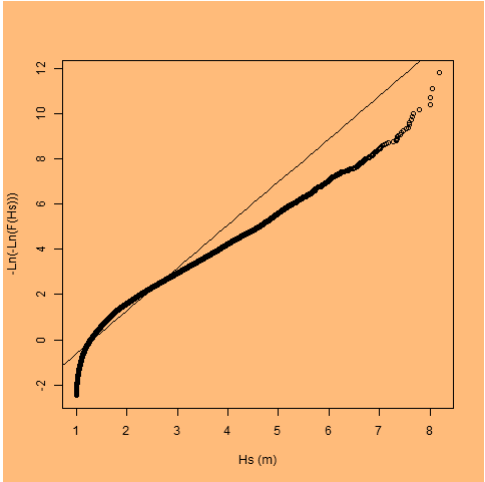

Figure 131: ID Gumbel

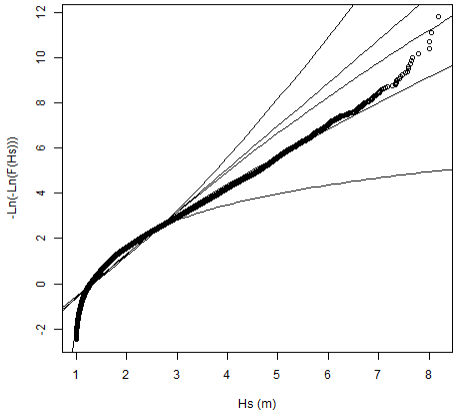

Figure 132: ID Multi-Plot

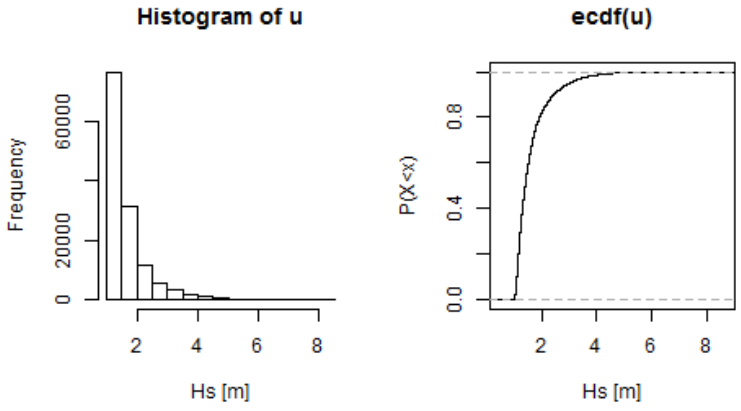

Figure 133: ID Dataset Representation (~110,000 data points)

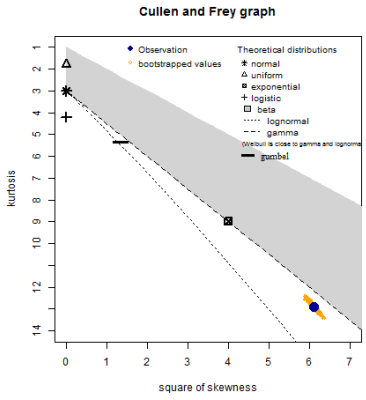

Figure 134: ID Cullen and Frey

6.7 Summary of Fitted Distribution Evaluations

Summary of models (Table 13), shows a summary of the filtering process of the 90 different combinations, and points out the shortlisted ones. There are 36 shortlisted models out of 90. The rows represent unique combinations of Approach, Parameter Estimation Method and Sampling Rate. The columns have the five distributions being considered in this study. With 18 rows and 5 columns there are 90 cells that represent the unique models within the scope of this study. Values inside the matrix correspond to the status of every particular model. Two options are available, first is *out*, that means that the model is filtered out because was proved relatively not good enough. Second is *SL*, that means that the model is shortlisted, to proceed with extreme uncertainty assessment.

Table 13 shows that for ID approach, Weibull and Lognormal distributions are selected. For POT approach, Weibull and Gumbel are selected, and for AM approach Lognormal and Gumbel are selected. Two main advantages gained with this wide-range of model-fitting. First is the experience gained in dealing with the most common extreme-value-relevant distribution and learning about which distributions are behaving best in representing the extremes. Second is narrowing down the uncertainty that will be assessed further on in this report, instead of using results from 90 different models, only the most suitable are selected for the uncertainty assessment.

Table 13: Summary of different models; SL: shortlisted; out: filtered out

	Approach	Parameter Estimation Method	Sampling (hourly)	Distribution				
				1_w3	2_gamma	3_gev	4_log-n	5_gum
1	ID	MLE	1	SL	out	out	SL	out
2			3	SL	out	out	SL	out
3			6	SL	out	out	SL	out
4		MME	1	SL	out	out	SL	out
5			3	SL	out	out	SL	out
6			6	SL	out	out	SL	out
7	POT	MLE	1	SL	out	out	out	SL
8			3	SL	out	out	out	SL
9			6	SL	out	out	out	SL
10		MME	1	SL	out	out	out	SL
11			3	SL	out	out	out	SL
12			6	SL	out	out	out	SL
13	AM	MLE	1	out	out	out	SL	SL
14			3	out	out	out	SL	SL
15			6	out	out	out	SL	SL
16		MME	1	out	out	out	SL	SL
17			3	out	out	out	SL	SL
18			6	out	out	out	SL	SL

7 Assessment of Extremes

7.1 Introduction

A control experiment is presented in this chapter; the shortlisted models are compared, comparisons are based on keeping all factors relating to a model set-up unchanged, except one factor, to see the effect of this factor on the estimated extremes.

7.2 Parameter Estimation Method

This section compares the effect of parameter estimation method on estimated extremes. Hs-Tr relationships for return periods from 1 year to 10,000 years are plotted. Figure 135 to Figure 140 show this comparison for the different approaches adopted and the distributions shortlisted. It is obvious from the results that AM and POT are not sensitive to parameter selection method. POT approach is a little bit more sensitive than AM approach, but still considered not sensitive to parameters selection. ID is very sensitive to parameter estimation method.

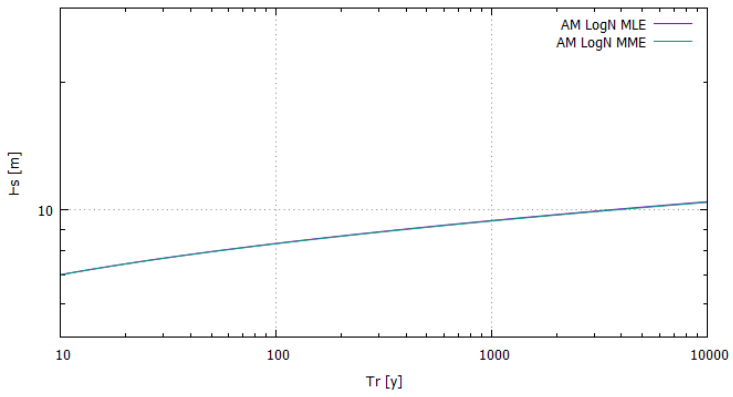

Figure 135: MLE vs. MME for AM approach fitted with Lognormal distribution

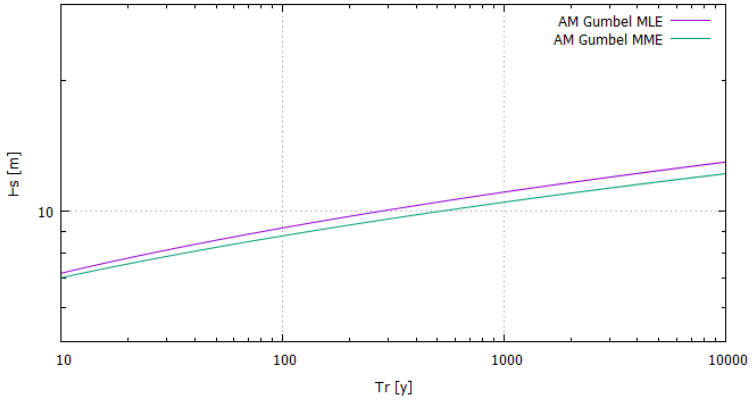

Figure 136: MLE vs. MME for AM approach fitted with Gumbel distribution

Table 14: Extreme estimations for parameter estimation methods comparison with AM approach

	Hs (m), 100 year	Hs (m), 10,000 year
Annual Maxima, LogN, MLE	8.3	10.4
Annual Maxima, LogN, MME	8.3	10.4

Annual Maxima, Gumbel, MLE	9.2	13.0
Annual Maxima, Gumbel, MME	8.8	12.2

Looking at Figure 135 and Figure 136, Lognormal distribution with AM approach is not sensitive at all to parameter estimation method. While Gumbel is slightly sensitive (0.4 meters error in 100-year wave and 0.4 meters error in 10,000-year wave). Distribution with MLE estimated parameters tend to give higher extremes.

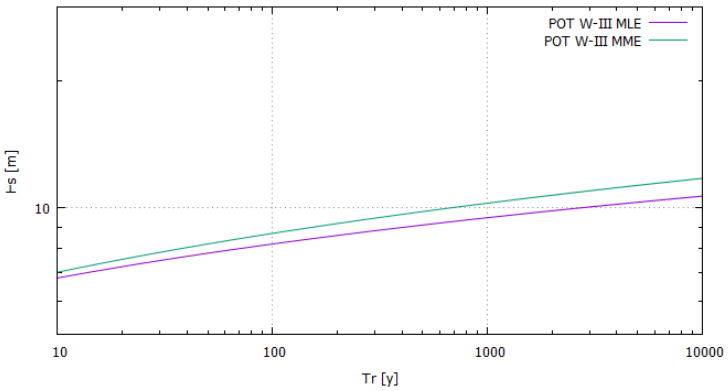

Figure 137: MLE vs. MME for POT approach fitted with Weibull distribution

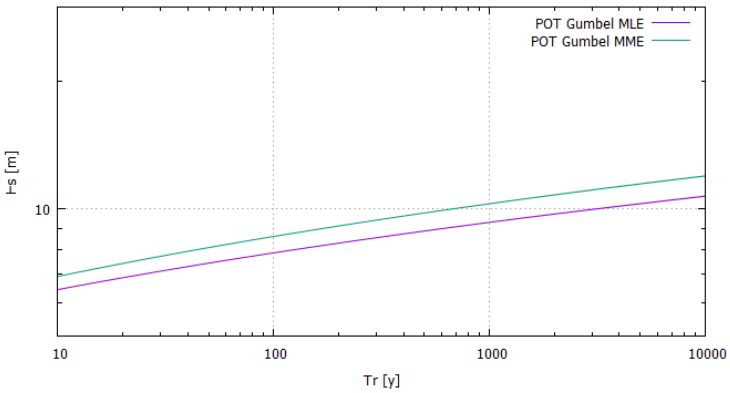

Figure 138: MLE vs. MME for POT approach fitted with Gumbel distribution

Table 15: Extreme estimations for parameter estimation methods comparison with POT approach

	Hs (m), 100 year	Hs (m), 10,000 year
POT, W-III, MLE	8.2	10.7
POT, W-III, MME	8.7	11.7
POT, Gumbel, MLE	7.9	10.7
POT, Gumbel, MME	8.6	12.0

Looking at Figure 137 and Figure 138, Weibull and Gumbel distributions with POT approach are a little bit sensitive to parameter estimation method. Weibull is slightly less sensitive than Gumbel. Unlike AM approach, with POT, distribution with MLE estimated parameters tend to give lower extremes.

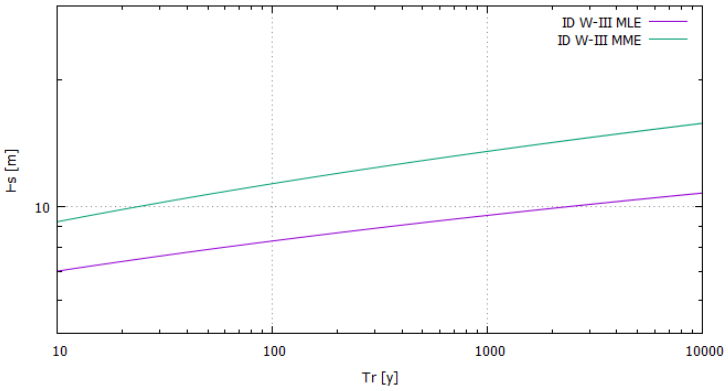

Figure 139: MLE vs. MME for ID approach fitted with Weibull distribution

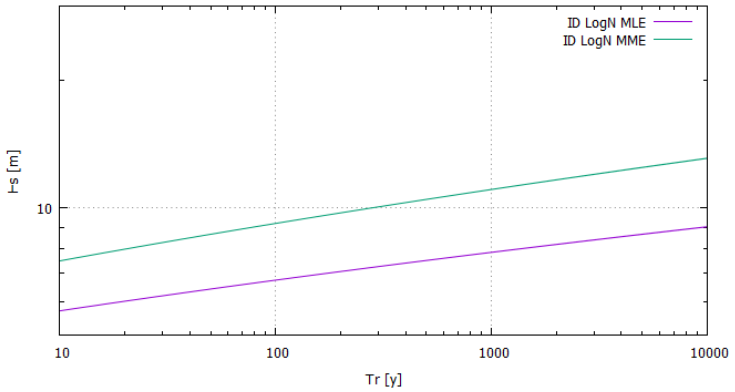

Figure 140: MLE vs. MME for ID approach fitted with Lognormal distribution

Table 16: Extreme estimations for parameter estimation methods comparison with ID approach

	Hs (m), 100 year	Hs (m), 10,000 year
ID, W-III, MLE	8.3	10.8
ID, W-III, MME	11.3	15.8
ID, LogN, MLE	6.7	9.0
ID, LogN, MME	9.2	13.1

Looking at Figure 139 and Figure 140, Weibull and Lognormal distributions with ID approach are very sensitive to parameter estimation method. Lognormal is slightly less sensitive than Weibull. Like POT approach, with ID, distributions with MLE estimated parameters tend to give lower extremes.

The approach that has the largest number of data points (ID), has the highest sensitivity to parameter estimation method, with MME as the method resulting in higher wave extremes. POT and AM approaches are not sensitive to parameter estimation methods.

7.3 Distribution Selection

This section compares the effect of distribution selection on estimated extremes. Hs-Tr relationships for return periods from 1 year to 10,000 years are plotted. This comparison is made for the different approaches adopted and the parameter estimation methods applied. It is obvious from the results that POT approach is not sensitive to distribution selection, given that

the quality of the fit of the selected distribution is approved. AM approach is more sensitive than POT approach. ID is very sensitive to distribution selection.

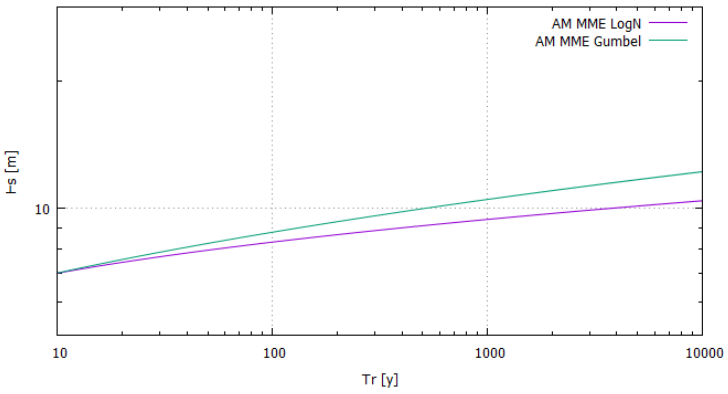

Figure 141: Lognormal vs. Gumbel for AM approach with MME parameters

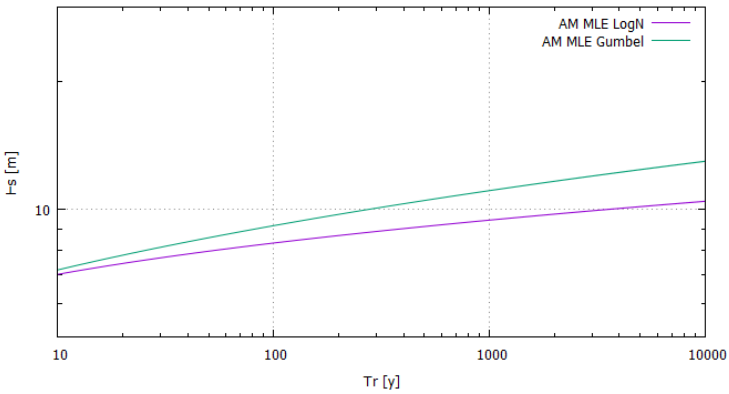

Figure 142: Lognormal vs. Gumbel for AM approach with MLE parameters

Table 17: Extreme estimations for distribution selection comparison with AM approach

	Hs (m), 100 year	Hs (m), 10,000 year
AM, MME, LogN	8.3	10.4
AM, MME, Gumbel	8.8	12.2
AM, MLE, LogN	8.3	10.4
AM, MLE, Gumbel	9.2	13.0

Looking at Figure 141 and Figure 142, MME and MLE parameter estimation methods with AM approach are sensitive to distribution selection. Distribution selection effect for MME parameter estimation method is slightly less sensitive than MLE parameter estimation method. Gumbel distribution, in both cases, MLE and MME parameter estimation methods, tend to give higher extremes.

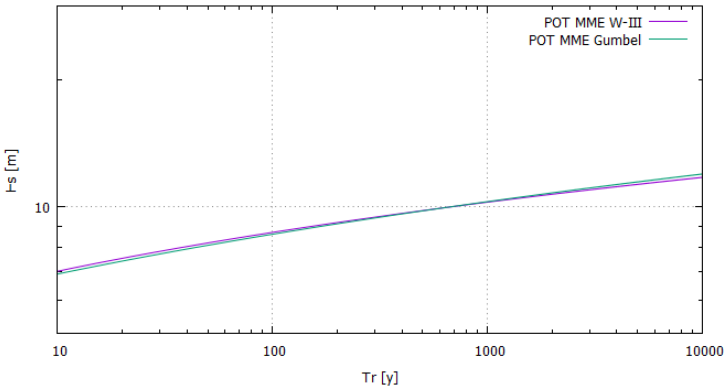

Figure 143: Weibull vs. Gumbel for POT approach with MME parameters

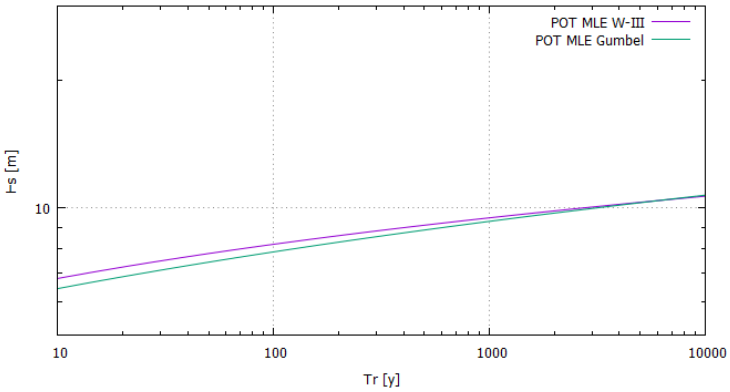

Figure 144: Weibull vs. Gumbel for POT approach with MLE parameters

Table 18: Extreme estimations for distribution selection comparison with POT approach

	Hs (m), 100 year	Hs (m), 10,000 year
POT, MME, W-III	8.7	11.7
POT, MME, Gumbel	8.6	12.0
POT, MLE, W-III	8.2	10.7
POT, MLE, Gumbel	7.9	10.7

Looking at Figure 143 and Figure 144, neither MME nor MLE parameter estimation methods with POT approach are sensitive to distribution selection. Distribution selection effects for POT approach are negligible. Gumbel and Weibull distributions, roughly give the same results.

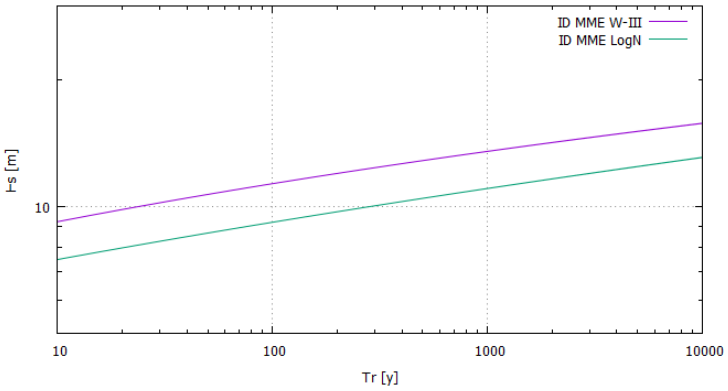

Figure 145: Weibull vs. Lognormal for ID approach with MME parameters

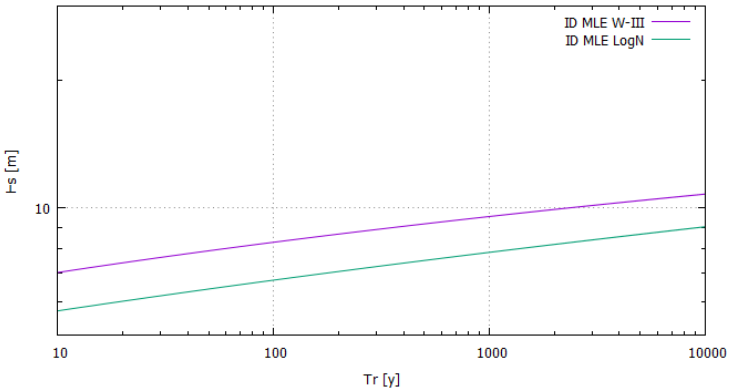

Figure 146: Weibull vs. Lognormal for ID approach with MLE parameters

Table 19: Extreme estimations for distribution selection comparison with ID approach

	Hs (m), 100 year	Hs (m), 10,000 year
ID, MME, W-III	11.3	15.8
ID, MME, Log-N	9.2	13.1
ID, MLE, W-III	8.3	10.8
ID, MLE, Log-N	6.7	9.0

Looking at Figure 145 and Figure 146, MME and MLE parameter estimation methods with ID approach are sensitive to distribution selection. Weibull distribution, in both cases, MLE and MME parameter estimation methods, tend to give higher extremes.

AM and ID approaches are sensitive to distribution selected. In AM approach, Gumbel is giving higher extremes than Lognormal, and in ID approach Weibull is giving higher extremes than Lognormal. POT approach is not sensitive to distribution selected.

7.4 Sampling Rate

The point in this section is to appreciate reduction of extremes accompanied with longer sampling rates. It is surely recommended to use the highest resolution possible (for AM and POT approaches), that is, if 1 hourly data is available, therefore the user must use that dataset without performing any de-sampling such as 3 hourly or 6 hourly sampling. Because de-

sampling will affect results obtained. The main point of this section is checking the sensitivity of extremes to sampling rate, because some widely used hindcast data are provided in 1, 3 or 6-hourly patterns, e.g. DICCA hindcast is 1-hourly sampled dataset, the NORA10 hindcast is 3-hourly and the ERA-Interim is 6-hourly sampled.

This section compares the effect of sampling rate on estimated extremes. Hs-Tr relationships for return periods from 1 year to 10,000 years are plotted. Figure 148 to Figure 153 show this comparison for the different approaches adopted and the distributions shortlisted. It is obvious from the results that AM and POT are a little sensitive to sampling rate. For POT and AM approaches, sampling may cause storms to be overlooked, and thus lower the storm peak values and would cause a reduction in the extreme estimates.

Figure 147 below shows the effect of sampling rate on annual maxima, compares 1 hourly with 6 hourly sampling, and shows the difference in macro-scale in a time series plot that covers the period from 1980 to 2015.

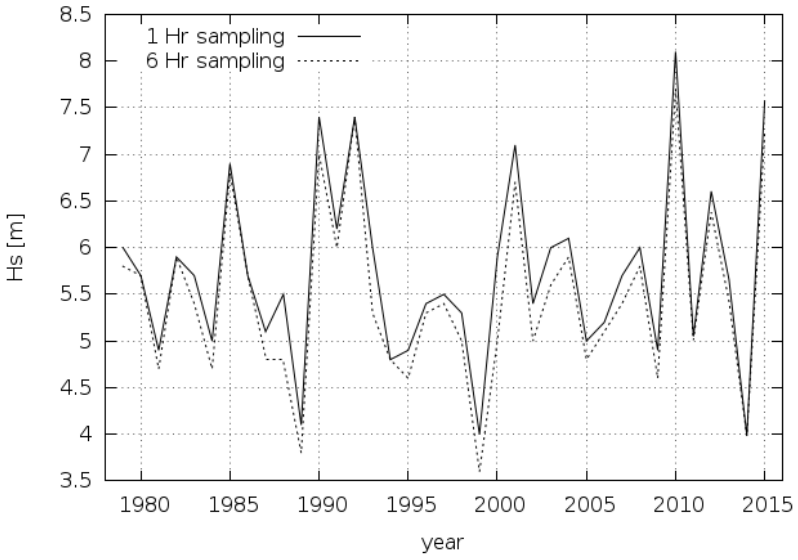

Figure 147: Annual Maxima: Effect of sampling rate on AM dataset

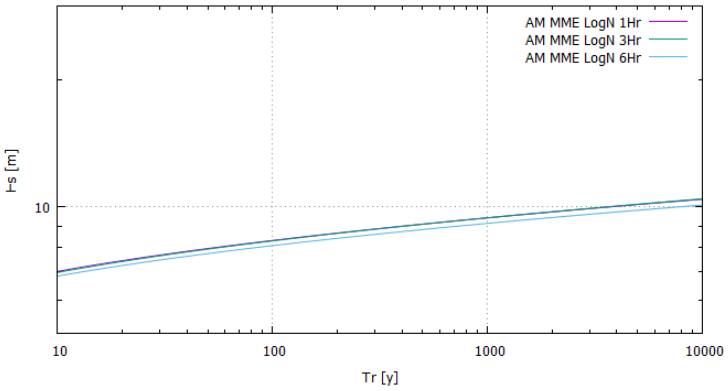

Figure 148: Sampling rate comparison for AM approach, MME parameters and Lognormal distribution

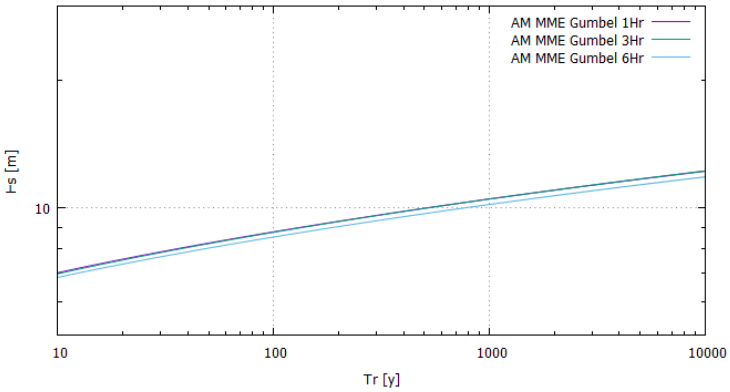

Figure 149: Sampling rate comparison for AM approach, MME parameters and Gumbel distribution

Table 20: Extreme Estimations of sampling rate comparisons for AM approach

	Hs (m), 100 year	Hs (m), 10,000 year
AM, LogN, 1Hr	8.3	10.4
AM, LogN, 3Hr	8.3	10.4
AM, LogN, 6Hr	8.1	10.1
AM, Gumbel, 1Hr	8.8	12.2
AM, Gumbel, 3Hr	8.8	12.2
AM, Gumbel, 6Hr	8.5	11.8

Looking at Figure 148 and Figure 149, both Gumbel and Lognormal distributions with AM approach are not sensitive to sampling rate. However there is a reduction in estimated extremes as the sampling rate increases. For an increase of sampling rate from 1-hourly to 3-hourly there is no reduction, and for an increase from 3-hourly to 6-hourly the reduction is around 3%.

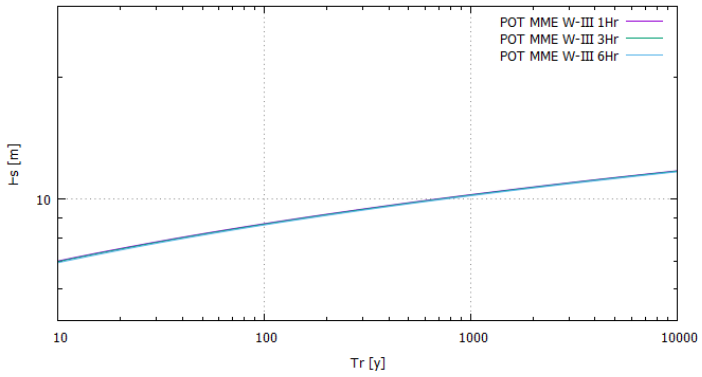

Figure 150: Sampling rate comparison for POT approach, MME parameters and Weibull distribution

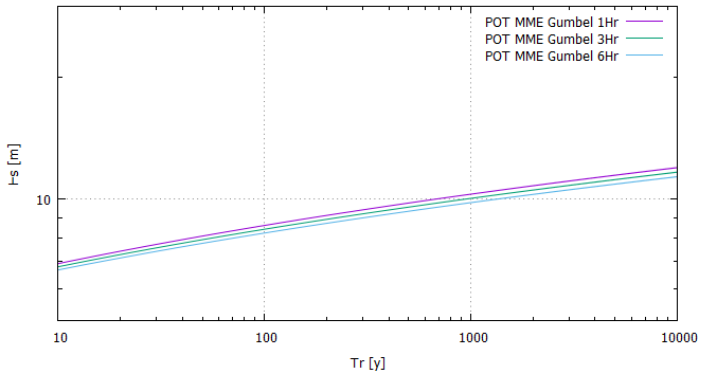

Figure 151: Sampling rate comparison for POT approach, MME parameters and Gumbel distribution

Table 21: Extreme estimations of sampling rate comparisons for POT approach

	Hs (m), 100 year	Hs (m), 10,000 year
POT, W-III, 1Hr	8.7	11.7
POT, W-III, 3Hr	8.7	11.7
POT, W-III, 6Hr	8.6	11.7
POT, Gumbel, 1Hr	8.6	12.0
POT, Gumbel, 3Hr	8.4	11.7
POT, Gumbel, 6Hr	8.2	11.4

Weibull with MME estimated parameters is not tested against sampling rate. The parameters were assumed not sensitive to sampling rate, and that is the reason of Figure 150 showing 3 identical lines. Looking at Figure 151, Gumbel distribution with POT approach is not sensitive to sampling rate. However there is a reduction in estimated extremes as the sampling rate increases. For an increase of sampling rate from 1-hourly to 3-hourly there is no reduction, and for an increase from 3-hourly to 6-hourly the reduction is around 2.5%.

It was expected that sampling rate has larger effect on POT approach, because as sampling rate increases, storms may be overlooked if a sampling rate larger or equal than the storm duration is selected and this will undermine the extreme estimations. But in fact sampling has a very small effect on POT approach estimated extremes (2.5% decreases)

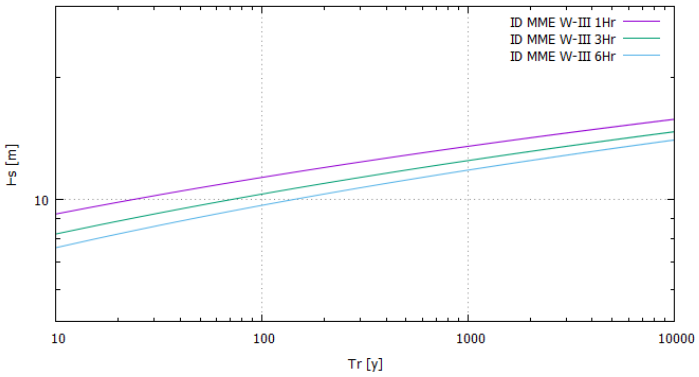

Figure 152: Sampling rate comparison for ID approach, MME parameters and Weibull distribution

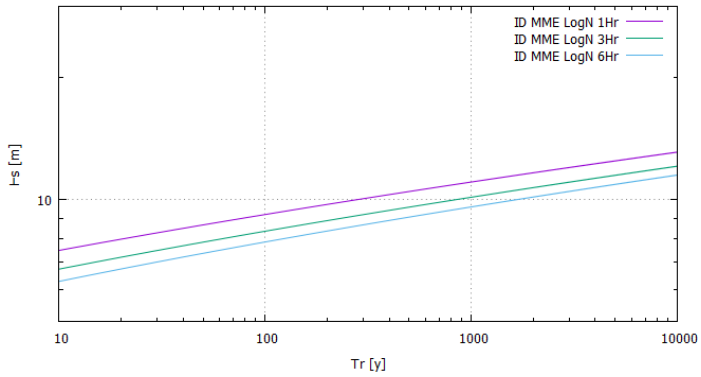

Figure 153: Sampling rate comparison for ID approach, MME parameters and Lognormal distribution

Table 22: Extreme estimations of sampling rate comparisons for ID approach

	Hs (m), 100 year	Hs (m), 10,000 year
All Sea States, W-III, 1Hr	11.3	15.8
All Sea States, W-III, 3Hr	10.3	14.7
All Sea States, W-III, 6Hr	9.7	14.0
All Sea States, LogN, 1Hr	9.2	13.1
All Sea States, LogN, 3Hr	8.4	12.1
All Sea States, LogN, 6Hr	7.9	11.5

Looking at Figure 152 and Figure 153, both Weibull and Lognormal distributions with ID approach are sensitive to sampling rate. There is a reduction in estimated extremes as the sampling rate increases. For an increase of sampling rate from 1-hourly to 3-hourly the reduction is around 9%, and for an increase from 3-hourly to 6-hourly the reduction is around 6%. Summary of expected reduction factors is found in Table 23.

Table 23: Summary of reduction factors of extremes based on sampling rate

Sampling rate	**Extreme Estimation Reduction Factors**		
	AM	**POT**	**ID**
1 hourly	1	1	1
3 hourly	1	1	0.91
6 hourly	0.97	0.97	0.86

7.5 Approach Selection

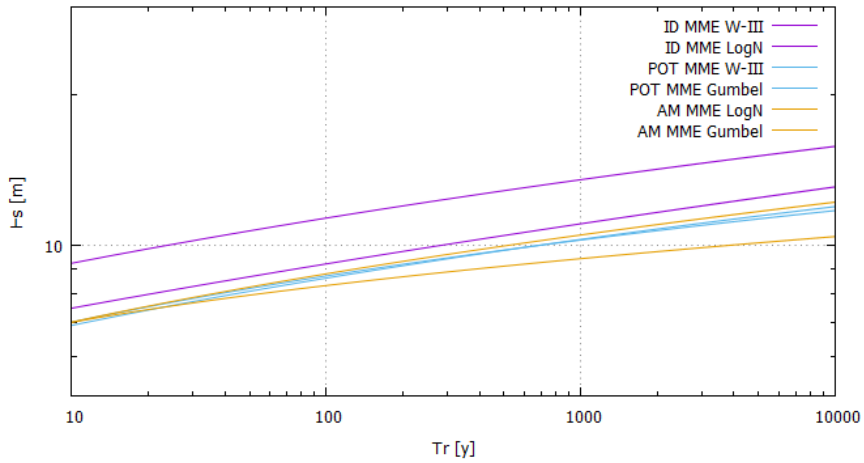

Figure 154: Comparison of different methods

Figure 154 is confusing, the curves in it were previously presented, and the purpose of this plot is only to show the range of the shortlisted extremes. It shows that different models give different results, and the differences are not small. This change in extreme estimation is a motive for extensive investigation about uncertainties that underlie in the procedures that are recommended by standards, and their effects in design. The figure shows that ID approach gives the highest extremes and the AM approach gives the lowest ones.

Table 24 summarizes the results obtained for all different shortlisted models. Average values are given according to data extraction approach (ID, POT and AM) where Hs100 is the 100-year wave and Hs10000 is the 10,000-year wave. And the last column, Average, is the average extreme estimation of all shortlisted models together.

Table 24: Summary of Extreme Estimations Averages per Method

	ID	POT	AM	Average
Hs100 (m)	8.2	8.2	8.6	8.3
Hs10000 (m)	11.5	11.0	11.4	11.3

Given the natural variability of the environment, Hs extremes are better represented as variables instead of single values. Section below elaborates on 100-year and 10,000-year wave heights variability.

7.6 Presentation of Uncertainties

In this section, focus on uncertainties of extreme estimation for the 100 year and 10000 year waves, taking into consideration the shortlisted models. A summary of the shortlisted models values of wave height extremes are shown in the two figures below.

Shortlisted models provide different extreme estimations. There is no documented method in literature that points to the right model to choose for this study due to the fact that the environment is a variable process, it differs from a location to another, and the scope is to find the best estimate to extremes. Therefore, efforts are focused in this study to model the possible variability of environment extremes that are resulted only from shortlisted best-fit model, in this way engineers would appreciate the variability for extremes and adjust the design safety level accordingly.

Table 25: 100-year Hs (m) extremes estimated by shortlisted models in green

	Approach	Parameter Estimation Method	Sampling (hourly)	100-year wave				
				1_w3	2_gamma	3_gev	4_log-n	5_gum
1	ID	MLE	1	8.3	out	out	6.7	out
2			3	7.7	out	out	6.2	out
3			6	7.3	out	out	5.9	out
4		MME	1	11.3	out	out	9.2	out
5			3	10.3	out	out	8.4	out
6			6	9.7	out	out	7.9	out
7	POT	MLE	1	8.2	out	out	out	7.9
8			3	7.9	out	out	out	7.7
9			6	7.6	out	out	out	7.6
10		MME	1	8.7	out	out	out	8.6
11			3	8.7	out	out	out	8.4
12			6	8.6	out	out	out	8.2
13	AM	MLE	1	out	out	out	8.3	9.2
14			3	out	out	out	8.3	9.1
15			6	out	out	out	8.1	8.9
16		MME	1	out	out	out	8.3	8.8
17			3	out	out	out	8.3	8.8
18			6	out	out	out	8.1	8.5

Table 26: 10000-year Hs (m) extremes estimated by shortlisted models in green

	Approach	Parameter Estimation Method	Sampling (hourly)	10000-year wave				
				1_w3	2_gamma	3_gev	4_log-n	5_gum
1	ID	MLE	1	10.8	out	out	9.0	out
2			3	10.2	out	out	8.4	out
3			6	9.8	out	out	8.1	out
4		MME	1	15.8	out	out	13.1	out
5			3	14.7	out	out	12.1	out
6			6	14.0	out	out	11.5	out
7	POT	MLE	1	10.7	out	out	out	10.7
8			3	10.1	out	out	out	10.4
9			6	9.6	out	out	out	10.2
10		MME	1	11.7	out	out	out	12.0
11			3	11.7	out	out	out	11.7
12			6	11.7	out	out	out	11.4
13	AM	MLE	1	out	out	out	10.4	13.0
14			3	out	out	out	10.4	13.0
15			6	out	out	out	10.1	12.7
16		MME	1	out	out	out	10.4	12.2
17			3	out	out	out	10.4	12.2
18			6	out	out	out	10.1	11.8

According to Prof. Haver, estimates of POT approach with Weibull distribution should be very close to estimates of AM approach with Gumbel distribution. This is checked with the estimates in the Table 25 and Table 26 above, it is found that for MME they are very close to each other (8.7 m to 8.8 m for the 100-year wave, and 11.7 m to 12.2 m for the 10,000-year wave). The importance of this check is that the two datasets of POT and AM approaches are independent subsets, different from each other, with different fitted distributions, leading to almost same results. This provides a sense of agreement. Figure 155 and Figure 156 show the variability of Hs extreme estimations if form of histograms, *ecdf* plots and Cullen and Frey graphs.

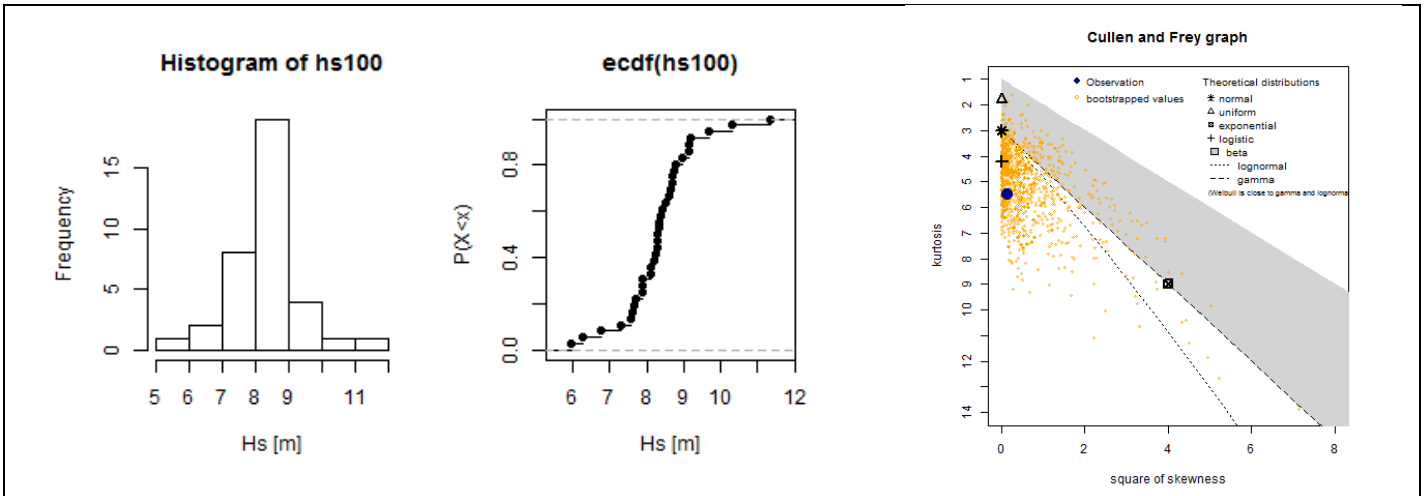

Mean	Standard Dev.	Maximum	Minimum	Range %
8.3	0.99	11.3	5.9	33

Figure 155: 100 year wave variability presentation

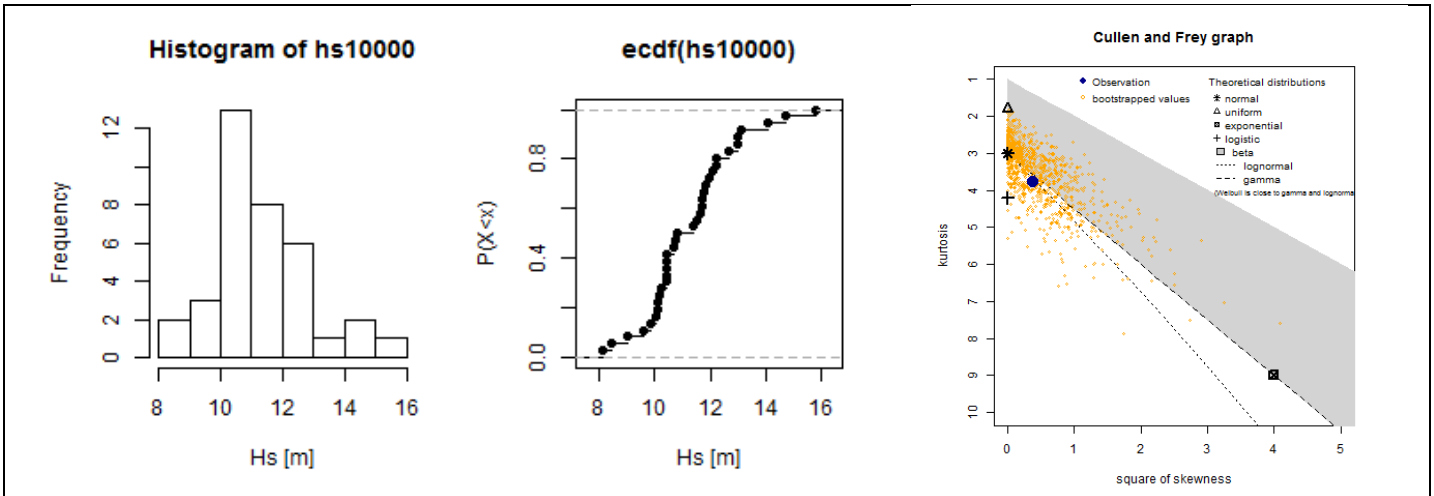

Mean	Standard Dev.	Maximum	Minimum	Range %
11.3	1.64	15.8	8.1	34

Figure 156: 10000 year wave variability presentation

The mean, SD, maximum, minimum and range values are included in Figure 155 and Figure 156. The range percentage is the calculated as follows:

Range of estimated extremes (41)

$$Range(\%) = \frac{Maximum - Minimum}{2 \times Mean} \times 100\%$$

There are 36 shortlisted models. It is interesting to note from the histogram that the 100 year wave looks almost like a normally-distributed random variable! With the highest probability of occurrence is in the middle with high agreement from most of the estimates (from 8m to 9m). And the histogram of the 10000 year wave looks less concentrated, most estimates fall in the range of 10m to 13m.

Given the variation of the 36 estimates of both the 100-year and the 10,000-year wave, shown in Figure 155 and Figure 156, there is a concentration of estimates around the mean value, and that is a positive clue, however does not erase the possible uncertainties underlying in the estimates. Therefore a 70% confidence interval is computed and is summarized

Table 27: Summary of Extremes with a Confidence Interval

Extreme	70% Confidence Interval for Extreme Estimations		
	Lower edge	Mean	Upper edge
100-year wave	7.6	8.3	9.1
10,000-year wave	10.0	11.3	13.0

7.7 Extreme Estimation Conclusions

- Extreme waves are used as a design input; they are the main factor of environmental loading for offshore structures. The uncertainties behind extreme estimations are risky and it is recommended that the uncertainties are given more attention.
- Some of the shortlisted models agree with recommendations by others
    - For AM approach: Gumbel distribution (Coles, 2001; DNV-RP-C205, 2007). Gumbel distribution is supported by theory to represent a sample of independent equally spaced extremes
    - For POT: Weibull (DNV-RP-C205, 2007)
    - For ID: Lognormal and Weibull distributions (Haver, 2013; DNV-RP-C205, 2007)
- Some of the shortlisted models are not mentioned by others as recommended distributions
    - For AM: Lognormal

- For POT: Gumbel

Both have proved that they are able to fit the dataset better than the others (5 distribution fittings were compared for every approach)

- Worst fitted distributions are:
    - For AM: all of the five tested distributions are acceptable for AM approach
    - For POT: GEV and Gamma are unacceptable fitted distributions.
    - For ID: GEV and Gamma are unacceptable fitted distributions.
    - Gamma is always under estimating the extremes and GEV is over estimating (Except in AM approach)
- Different data extraction methods (AM, POT, and ID) are essential to be deployed on the dataset. Because as shown in Figure 154 one method can be over-estimating or under-estimating the extremes relevant to others. In this study, ID approach estimates are higher than other estimates. Those estimates are coming from ID approach with Weibull distribution with MME parameter estimation method. They are recommended to be filtered out.
- Weibull MME in ID approach is over-estimating the extremes while Weibull MME in POT approach is giving stable estimations (trustworthy, because they are validated by their agreement with AM Gumbel MME estimates).
    - When two different datasets, with different size, that include independent variables, agree on the extreme of the same return period, then that is considered a validation of the results.
- POT is the preferred model that enjoys the luxury of highly independent data points, and reasonable number of data points. Plus it has very low sensitivity to parameter estimation methods, distribution selection, and sampling rate. Nevertheless, POT approach cannot be reliably used unless a threshold investigation (sensitivity test) is done.
- The probability plot is a handy tool for visually evaluating the quality of a fitted distribution
- To know if the selected distribution underrates of overrates the extremes, go check the probability paper plot. If the distribution fit is to the right of the data scatter at the tail, then the distribution will overrate the extremes and vice versa.
- DNV and this study highly agree on the distribution selection part, however, if DNV recommendations are followed without uncertainty analysis, a user may go to DNV-RP-

C205 page 37 and select a 3-parameter Weibull, apply it on ID approach and get 11.3 meters as the 100-year wave, while the most probable 100-year value is 8.3 meters. (More than 30% error).

- A higher sampling rate would reduce the extreme estimation in 3 – 14 %.
- ID approach is very sensitive to distribution selection and parameter estimation method.

8 Design and Operations

8.1 Environmental Contours

Significant wave height Hs, maybe is the dominant parameter in structure response design, however is not the only one. Some structures or vessels are sensitive to specific ranges of peak period Tp, and may face undesirable responses at that range, such as resonance; which causes the structure to have large oscillations with the wave period that is close to the structure's natural period. Hence, introduction of Tp in defining the environmental extreme sea state condition is required.

According to DNV, the environmental contours are a rational procedure for defining the extreme sea state condition. The contour line is a line with equal probability, usually corresponds to the standard safety levels, the 100-year or 10,000-year return period. This probability is a joint probability of two parameters, mainly significant wave height Hs, and spectral peak period Tp. The contour defines the borders of safety, for instance, if a weather condition (described by Hs and Tp pair) is located inside the contour, then that condition is said to be within design consideration. Whereas, if a weather condition is located outside the contour, then that condition is said to be an extreme condition (rare condition) that may cause undesired action effects (response).

The extreme sea state conditions are defined by the safety levels, thus they are independent of structure type. Structures behave differently to extreme conditions, and extreme conditions vary (along the contour). For example, a semisubmersible platform will respond to an extreme wave differently than an FPSO would respond to that wave. Along the contour line, there exists a point, where the structure's response is the largest (most critical response). This maximum response point for the semisubmersible is different than that of the FPSO, while two of them lie

on the same contour. Therefore environmental contours are used for determining extreme wave conditions that causes extreme structural responses (Winterstein et al.,1993).

For the offshore industry, environmental contours are mainly constructed with Hs and Tp. However they can be connecting any two relevant variables, such as wave and wind, or, wave and current. The *Inverse First Order Reliability Method (IFORM)* approach is used for creating the contours (DNV-RP-C205, 2007), and is explained as follows:

Calculating the radius of the Gaussian space:

The Gaussian space is a standard normal space (normally distributed on each axis with mean equal to zero and standard deviation equal to one), involving two variables, u1 and u2 (bivariate).

The required radius is supposed to correspond to the 100-year wave, therefore, cumulative probability can be found by Equation 40:

Cumulative Probability (42)

$$F_{Hs} = 1 - \frac{1}{\frac{Na}{n} \times T_r}$$

Where n is independence factor (n-factor), for example, if n = 1, then annual average number of independent observations is set equal to N_a, and if n=12, then the annual average number of independent observations is set equal to $\frac{N_a}{12}$. For ID approach it may be reasonable to add the factor n > 1, but the actual value is unknown. The n-factor reduces the effect of correlation between data points. A value of n = 1 and another value of n > 1 are tested in environmental contours.

And Gaussian space radius is found by:

Gaussian space radius (43)

$$u = \Phi^{-}\left(F_{H_s}\right)$$

Building the contour in the Gaussian space:

Since the radius is known, then the variables u1 and u2 can be built.

The first variable, u1, can be any value within the radius u, such as $u1: \{-u, u\}$

The second variable, u2, is found, for every value of u1 by the circle equation, as follows:

Gaussian contour, u2 (44)

$$u2 = \pm\sqrt{u^2 - u1^2}$$

Transforming the Gaussian contour into physical space using the *Rosenblatt-transformation:*

Each point on the Gaussian contour has equal probability to a point in the physical contour. This translates into:

Transformation equation 1, Hs (45)

$$F(u1) = F_{H_s}(h_s)$$

Transformation equation 1, Tp (46)

$$F(u2) = F_{T_p|H_s}(t_p|h_s)$$

The marginal distribution function $F_{H_s}(h_s)$ can be any of the shortlisted models. Weibull distribution functions are selected because they give extreme estimates close to the average of the 36 shortlisted estimates. The conditional distribution function $F_{T_p|H_s}(t_p|h_s)$ is recommended to be an lognormal function. Therefore the functions will develop as follows:

Transformation equation 2, Hs (47)

$$F(u1) = F_{H_s}(h_s) = 1 - e^{-\left(\frac{h_s-\lambda}{\rho}\right)^{\beta}}$$

Transformation equation 3, Hs (48)

$$\rightarrow h_s = F^{-}(u1|\beta,\rho,\lambda)$$

Where $\beta > 0$ is the shape parameter, $\rho > 0$ is the scale parameter, and λ is the location parameter. The parameters used here are a result of Weibull fitted distribution being applied on the marginal dataset, given the approach (AM, POT, or ID) selected. Hs variable is transformed by the equations above. Tp variable is described by a conditional function, a lognormal function, where its parameters (μ,σ) are also conditional parameters, i.e. the parameters are functions of Hs. The transformation of Tp develops as follows:

Transformation equation 2, Tp (49)

$$F(u2) = \Phi[u2] = F_{T_p|H_s}(t_p|h_s) = \Phi\left[\frac{\ln(t_p) - \mu_{\ln t_p}(h_s)}{\sigma_{\ln t_p}(h_s)}\right]$$

Transformation equation 3, Tp (50)

$$\rightarrow t_p = \exp\left[u2 \times \sigma_{\ln t_p}(h_s) + \mu_{\ln t_p}(h_s)\right]$$

Solutions for the conditional mean and standard deviation functions are required. They are achieved by finding the mean and standard deviation of $\ln(tp)$ for every class of Hs, using the scatter diagrams (ref. to Figure 38). Once found, they can be plotted and fitted. Fitting is recommended to be performed with functions in the following form:

Mean of ln(Tp) as a function of Hs (51)

$$\mu_{\ln T_p(h_s)} = a_1 + a_2 \ln(h_s + a_3)$$

SD of ln(Tp) as a function of Hs (52)

$$\sigma_{\ln T_p(h_s)} = \sqrt{(b_1 + b_2 \exp(b_3 . hs^{b_4}))}$$

The constants of the equations above are found by minimizing the overall error. The fitted functions are found in Figure 157 and Figure 158.

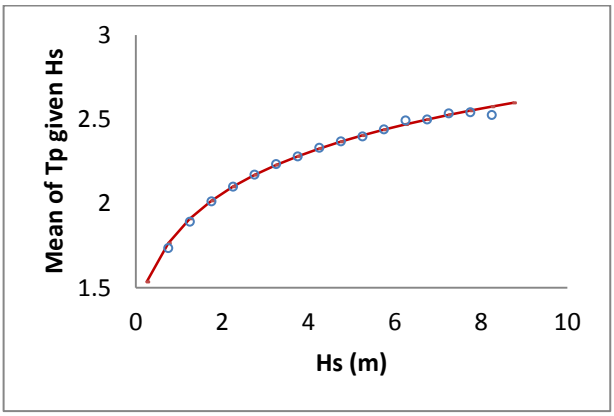

Figure 157: Mean of Tp given Hs

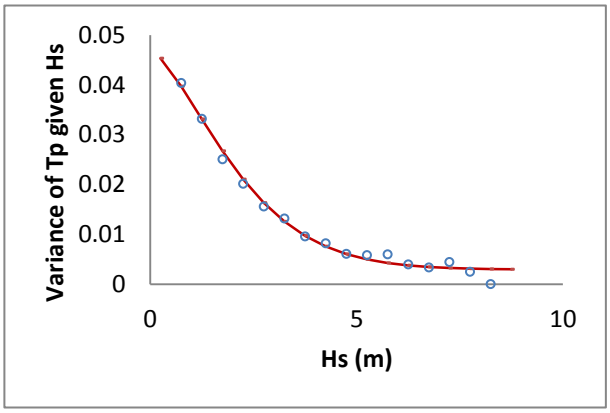

Figure 158: Variance of Tp given Hs

The values of the constants of the mean and standard deviation of $\ln(tp)$ are found in Table 28.

Table 28: Constants for minimum-error fitted functions of mean and SD (contour)

Mean	a1	a2	a3	
	1.7089	0.4016	0.3982	
SD	b1	b2	b3	b4
	0.0029	0.0440	-0.2700	1.4623

The environmental contour of Location 1 is presented in Figure 159. It is created with selected properties to best match the 100-year wave and the 10,000-year wave of previous chapters. Information is found in Table 29.

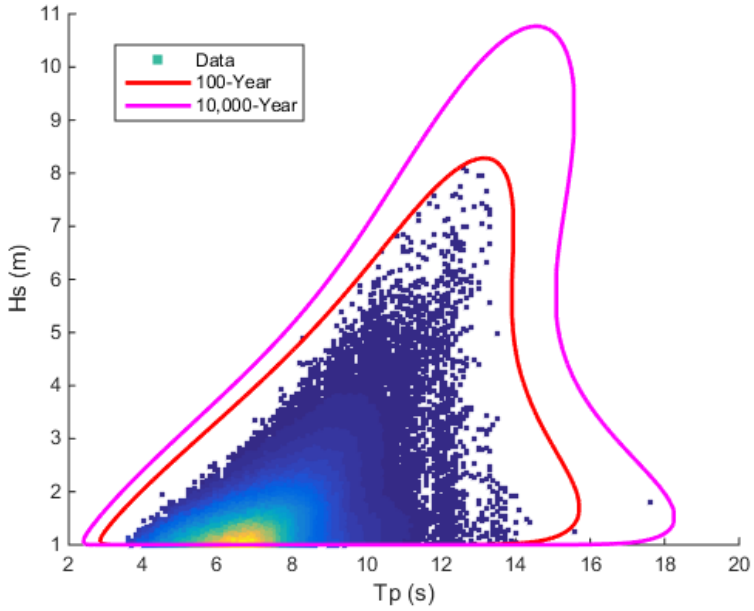

Figure 159: Environmental contours (best estimates) for Location 1

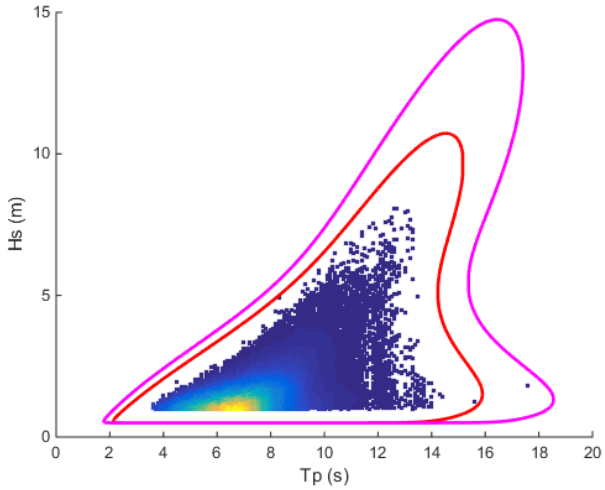

Figure 160: Environment contour (just a test 1) Location 1

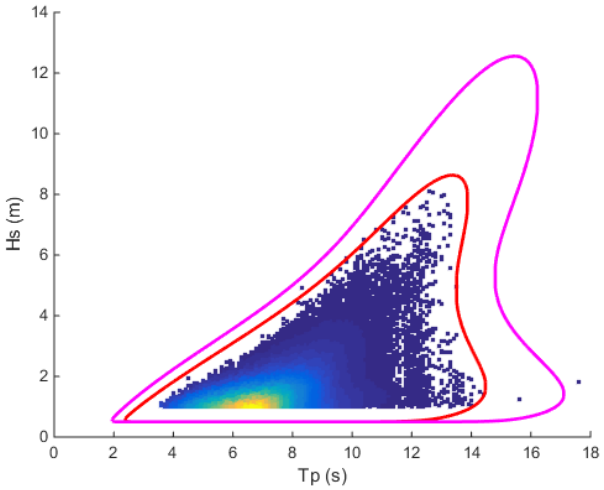

Figure 161: Environment contour (just a test 2) Location 1

The best estimate environmental contour is established with a specific model (for marginal Hs). The model is selected in order to result in extremes equal (or close) to the average extremes found in Table 27.

Table 29: Properties of environmental contours

	Best Estimate	Test 1	Test 2
Approach	ID	ID	ID
Sampling rate	1 hourly	1 hourly	1 hourly
Distribution	Weibull	Weibull	Weibull
Parameter Estimation	MLE	MME	MME
n-factor (equation 42)	1	1	12
Refer to	Figure 159	Figure 160	Figure 161

Figure 159 is the best estimate environmental contour, established with consideration of the 36 shortlisted models, and, as explained earlier, the properties of the marginal distribution of this contour are selected intentionally to give extreme contours that correspond to the best-estimate extremes. Figure 160 (test 1) shows that the selection of the marginal (Hs) distribution affects the contour considerably. Figure 161 (test 2) shows that the n-factor affects the contour considerably as well. The effect of distribution properties to extreme estimation is discussed in Chapter 7. The discussion of this section points out that, also contours, are sensitive to distribution properties, and should be built with special attention, because one small change of properties could lead to considerable change. Figure 159 is given as the best estimate.

Figure 159 describes the environmental extreme conditions as pairs of Hs and Tp as follows:

Table 30: Environmental extreme pairs (Hs and Tp)

Return Period	**Hs (m)**	**Tp (s)**
100 years	8.3	13.1
10000 years	10.8	14.7

Estimates of environmental extreme conditions as pairs of Hs and Tp reported by others are summarized as follows:

Table 31: Environment extreme pairs (Hs and Tp) reported by others.

Return Period	**Hs (m)**	**Tp (s)**	**Reported by:**
100 years	8.2	14.4	CSA, (2012), Tamar Field Project EIA
100 years	8.7	12 – 15	Rosen, (2001), IOLR

The environmental contours in Figure 159 show a couple of data points lying outside the 100-year contour. These two points (in the blue circle) have lower probabilities than any point on the contour line. How did 37 years of data result in 2 occurrences of wave conditions with return periods higher than 100 years?! This question can be answered by calculating the expected number of points lying outside the contour line. This expected number can be found as follows (Haver, 2014):

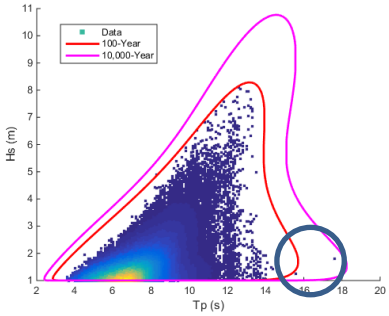

copy of Figure 159

The standard normal PDF for a single variable, say u1, is found by:

Standard normal PDF of 1 variable (53)

$$\Phi(u_1) = \frac{1}{\sqrt{2\pi}}\, e^{-\frac{1}{2}u_1^2}$$

The standard normal PDF for two independant coupled variables, say u1 and u2, is given by:

Standard normal PDF of 2 variables (54)

$$\Phi(u_1, u_2) = \frac{1}{2\pi}\, e^{-\frac{1}{2}(u_1^2 + u_2^2)}$$

Then the probability of a point being inside the contour of radius u, is gives by:

Probability of a point being inside the contour (55)

$$p(u) = \iint_{A(u)} \Phi(u_1, u_2)\, du_1 du_2 = \iint_{A(u)} \frac{1}{2\pi}\, e^{-\frac{1}{2}(u_1^2 + u_2^2)} du_1 du_2$$

$$= \int_0^{2\pi} \int_0^{u} \frac{1}{2\pi}\, e^{-\frac{1}{2}(r^2)}\, r\, d\theta\, dr = \int_0^{u} r e^{-\frac{1}{2}(r^2)} dr$$

$$\rightarrow p(u) = 1 - e^{-\frac{1}{2}u^2}$$

Then the probability of a point being outside the contour is given by:

Probability of a point being outside the contour (56)

$$p_{out}(u) = \exp\left(-\frac{1}{2}u^2\right)$$

Then, the expected number of points outside the contour is given by

Expected number of points outside the contour (57)

$$n_{out}(u) = N_a \times Y \times \exp\left(-\frac{1}{2}u^2\right)$$

Where N_a is the annual average number of observations, Y is the number of years covered by data, and u is the Gaussian space radius that corresponds to a contour of a specific return period. u is given by:

Gaussian space radius (58)

$$u = \Phi^{-}\left(1 - \frac{1}{N_a \times T_r}\right)$$

The expected number of points outside the contour is calculated for environmental contour of Figure 159, and resulted as follows:

i. For the 100-year contour: $n_{out} = 4.4\ points$

ii. For the 100000-year contour: $n_{out} = 0.05\ points$

Therefore, given the number of data points available, the expected number of points outside the 100-year contour is below 5. Concluding that due to the large number of data points available (131889 points after filtering waves below 1 meter height), there empirically exists (less than 5 of them) outliers (or extremes) that fall out of the contour. And since the number that can be visually spotted is less than the expected number of points being outside of the contour, then it is fine. Whereas if the number of visually spotted points outside the contour is larger than the expected, then further investigation about global warming effects and trends in weather conditions is recommended to be taken.

Environmental contours for the other locations are created and presented in Figure 162 to Figure 165. Location 2 is obvious to have higher extreme waves than the other locations. Nevertheless the locations are similar to a high degree.

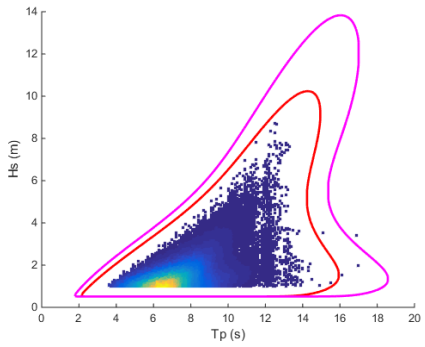

Figure 162: Location 2 environment contour

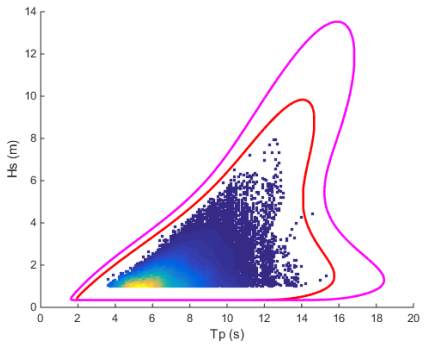

Figure 163: Location 3 environment contour

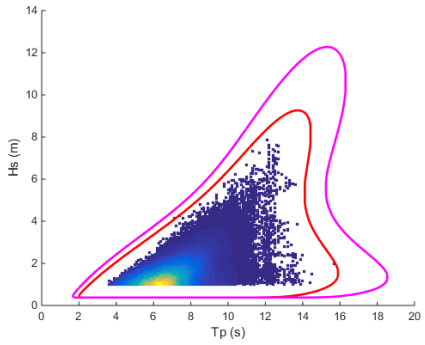

Figure 164: Location 4 environment contour

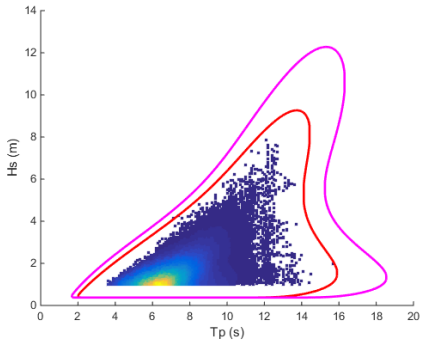

Figure 165: Location 5 environment contour

8.2 Vessel Response

Offshore floating structures can be considered to have six degrees of freedom, three rotation motions and three translation motions as shown in Figure 166. The rotation motions are roll, pitch and yaw. And the translation motions are surge, sway and heave. Structure stability primarily depends on the geometry and dimensions. Structure response depends on study of coupled motions. Nonetheless, study of motions of every degree of freedom on its own it also an indicator of dynamics.

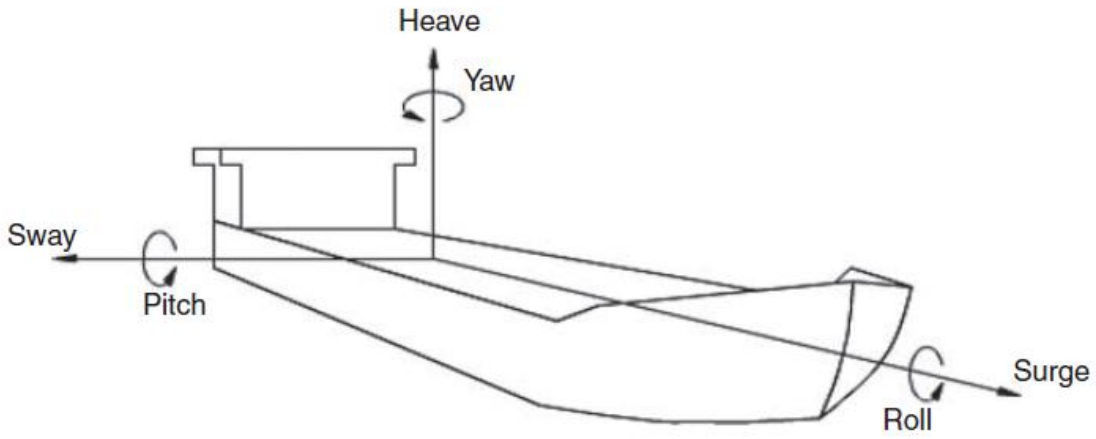

Figure 166: Motion of a vessel

Rotational motions are measured in degrees and are equal for all points of the ship. Translation motions are coupled and they depend on motions of other degrees of freedom, e.g. heave at bow depends on both the heave motion of cog and the pitch motion (equal everywhere on vessel). Among the six the degrees of freedom, heave and roll motions are usually the most critical, others have slower responses and are compensated by dynamic positioning (DP) systems. Acceleration and roll criteria is set for vessel motions (by Nordforsk, 1987) is shown in Figure 167:

Criteria for Accelerations and Roll (NORDFORSK, 1987)			
Description	RMS Vertical Acceleration	RMS Lateral Acceleration	RMS Roll Motion
Light Manual Work	0.20 g	0.10 g	6.0°
Heavy Manual Work	0.15 g	0.07 g	4.0°
Intellectual Work	0.10 g	0.05 g	3.0°
Transit Passengers	0.05 g	0.04 g	2.5°
Cruise Liner	0.02 g	0.03 g	2.0°

Seakeeping performance criteria for human effectiveness - Limiting Criteria with regard to accelerations (vertical and lateral) and roll motion (NORDFORSK, 1987).

Figure 167: Criteria with regard to accelerations and roll (Nordforsk, 1987)

Vertical acceleration is heave acceleration, and lateral is surge. In matter of fact, the displacement, velocity and acceleration of the critical motions have particular importance on the

vessel operation. Motion importance of heave and roll are summarized in Table 32 (Gudmestad, 2015):

Table 32: Importance of vessel motions

Motion	Displacement	Velocity	Acceleration
Heave (meters)	i. Lifting operations (control of loading and unloading) ii. Drilling operations (heave limit = 4 meters) iii. Helicopter operations iv. Influence design of heave compensators	i. Helicopter operations ii. Speed of lifting iii. Hydraulic flow rate in heave compensators	i. Vertical forces ii. Fastening cargo and equipment iii. Sea sickness
Roll (degrees)	i. Comfort in vessel ii. Cargo stability iii. Orientation of vessel	i. Handling cargo ii. Helicopter operations iii. Orientation of vessel	i. Cargo stability (strength of fasteners) ii. Rotational motion induced forces

Vessel response largely depends on natural periods. Table 33 includes some basics about heave and roll natural periods for different type of vessels:

Table 33: Heave and roll natural periods for different types of vessels

Vessel Size	Heave natural period	Stiffness	GM	Roll natural period
Small vessel	5 – 7 sec	Proportional to waterline area	>15 m	$0.8\frac{b}{\sqrt{GM}}$
Large vessel	14 – 18 sec		>0.5 m	$0.6\frac{b}{\sqrt{GM}}$
Rig Type	20 – 24 sec	Low stiffness	>1 m	$0.6\frac{b}{\sqrt{GM}}$
Fixed platform	Low period	High stiffness	-	

The equation for heave natural period is given by:

Heave natural period (59)

$$T_{heave} = 2\pi\sqrt{\frac{M_{barge} + M_a}{k}} = 2\pi\sqrt{\frac{\rho\nabla + M_a}{\rho g A_w}}$$

Where M_{barge} is the mass of the barge, M_a is the added mass, k is the stiffness coefficient, ρ is sea water density, ∇ is submerged volume, g is gravitational acceleration, and A_w is waterline area.

The equation for roll natural period is given by:

Roll natural period (60)

$$T_r = \frac{2\pi}{\sqrt{12g}} \frac{b}{\sqrt{GM}}$$

Where b is the width of the vessel and GM is the metacentric height. GM is a measurement of the initial stability of a floating body (Gudmestad, 2015).

Motions of a vessel are characterized by response amplitude operators (RAOs), RAO is a transfer function of the amplitude of platform motion to the amplitude of wave component for a given frequency, given degree of freedom and a given direction (vessel orientation). RAO is given as follows:

RAO equation (61)

$$RAO(f) = \frac{X_o(f)}{\xi_o(f)} = \frac{amplitude\ of\ platform\ motion\ due\ to\ wave\ at\ frequency\ f}{amplitude\ of\ wave\ component\ at\ frequency\ f}$$

$$S_{XX}(f) = [RAO(f)]^2 S_{ZZ}(f)$$

Where,

$S_{XX}(f)$ is the short term description of the vessel response

$S_{ZZ}(f)$ is the short term description of the sea state

An example of RAOs is presented in the Figure 168. Looking at heave RAO, as frequency decreases (period increases) the RAO settles to a value of 1. That means, for long-period waves (swell waves) the vessel will be in resonance with the waves and will heave (move up and down) with the waves, without any damping. Swells of wave height of 2 meters exist in the Eastern Mediterranean., in this case, the barge will heave with the waves in a 2 meters span. Looking at the roll RAO, there is a specific period where the RAO peaks; this period is the roll natural period of the vessel. If this period is avoided, roll motions will not be a problem for the vessel.

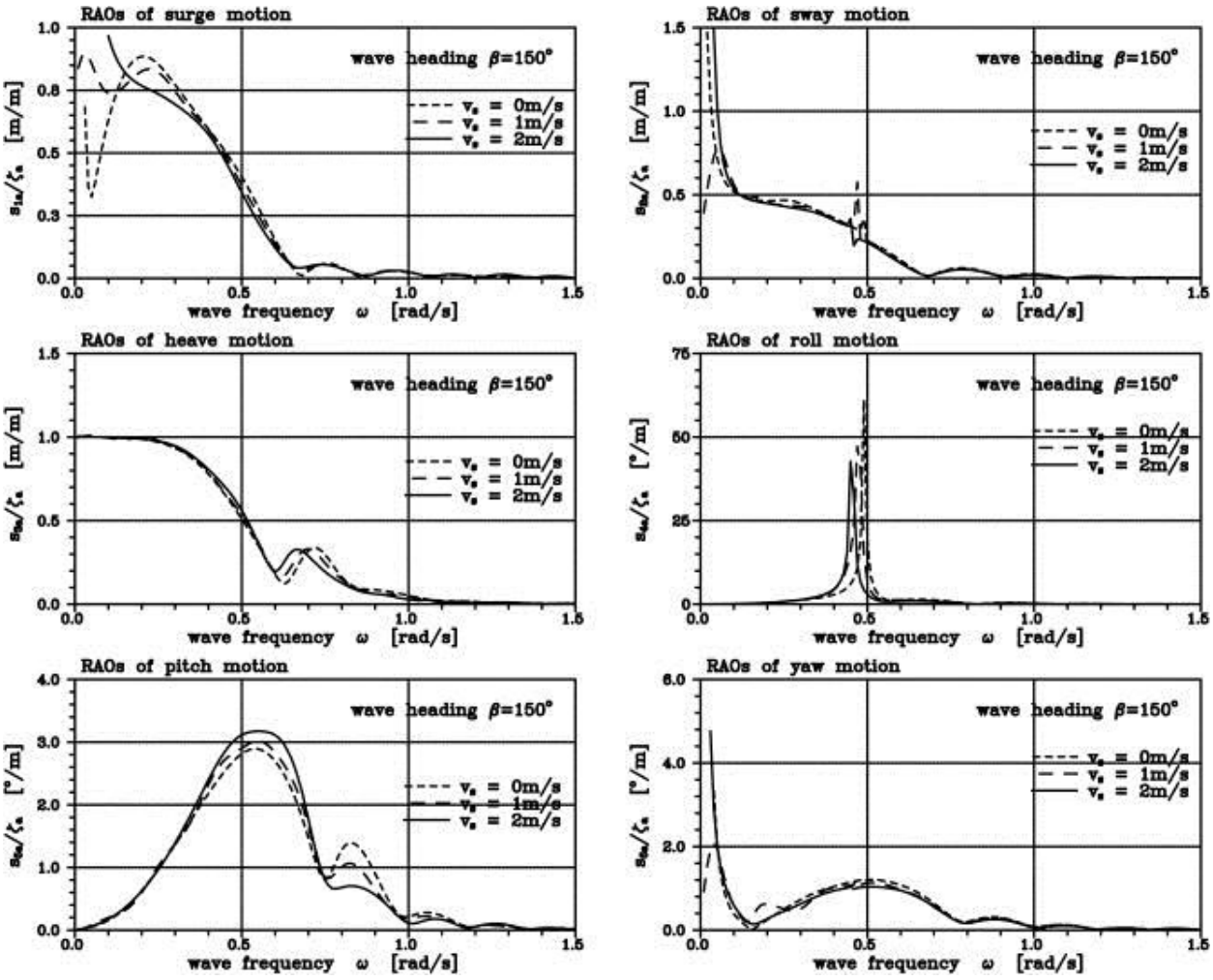

Figure 168: RAO of a vessel (example)

For an omnidirectional sea, a vessel, say FLNG vessel, can orient itself against the waves, in order to have the least response. Natural period of the pitch is considerably higher than that of the roll because the length of the ship is longer than the width. But, if there are swell waves coming from a different direction, then the vessel will start to roll, and the real problem is, when the swells coming from the side have the same natural period of vessel roll, then the roll motion will be excited and continuing on going back and forth. Roll motion in resonance in uncomfortable for operations and may cause delays.

8.3 Selection of Design Wave

The extreme contour is based on environment data. Design wave is a combination of environment data and structural response. Design wave is a point on the Hs, Tp contour that

results in the maximum response of the structure being considered. The shaded region in the figure shows the potential part of the contour to have the design wave.

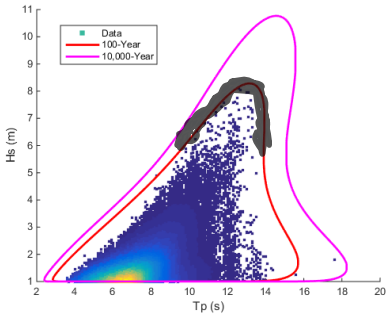

copy of Figure 159

The higher the wave is, the higher the wave loading is on the structure. Wave period is a secondary parameter but still is important in locating the design wave. The effect of period on design wave location is in fact connected to structure dynamic response. Structure dynamic response is represented in terms of response amplitude operators (RAO). The RAOs should be checked in every DOF with a number of points on the shaded area of the contour. The point resulting the maximum response is the design point. Design wave depends RAOs and RAOs are the fingerprint of vessel motion characteristics.

8.4 Effect of Uncertainties

Uncertainties in extreme estimations initiate a domino effect of build-up uncertainties. This includes uncertainties in: environment loading, vessel response, airgap height, structure applicability to a given season, or to a given location, and feasibility of operation. This chain of uncertainties creates motive for proceeding with investigations.

9 Discussion

The Eastern Mediterranean region will be one of the largest natural gas venture hubs in the world, which includes high marine activity that requires deeper investigation about metocean conditions. A metocean design basis normally includes extreme conditions of wind, waves, current, temperature and salinity. It also includes information about water levels; tidal elevations, storm surge and sea level rise. And information about splash zone, marine growth, snow and icing. However the metocean design basis of this thesis includes investigations of wave extremes only.

For structure and vessel design, wave is considered as the governing action for combined environmental loading and that is reason for focusing on wave extremes. And since wave has the largest force effects, then large uncertainties are accompanied with it. Uncertainties may

cause a structure to be either over-designed or unsafe. This tradeoff is critical in offshore environments because the operator needs to invest as much as required for achieving the pre-defined safety level, and is not willing to take the risks of either over-design (financial inefficiency) or compromising safety (vulnerability to huge losses). A critical tradeoff in a high-uncertainty environment is the reason why 90 models have been applied and uncertainties have been investigated in this thesis.

The focus on wave extremes and uncertainties make this thesis highly beneficial for structures that are mainly affected by waves, such as floating structures (e.g. semisubmersibles, SPARs, FPSOs and FLNG vessels), and structures that stand across the splash zone (e.g. jacket platforms, TLPs). However, this thesis is of limited usage to submerged structures (e.g. subsea umbilicals, risers, pipelines and flowlines), because their combined load could primarily depend on current or on system dynamics. And to structures (and applications) that are sensitive to wind speed (e.g. lifting operations). Limitations include air gap requirement calculations (for determining if a particular platform is appropriate for operation in a given location).

The Hindcast Validation chapter (Chapter 3) is performed to test the performance of hindcast comparing to measurement data. A range of comparisons have been done and all resulted that hindcast does indeed well represent the wave conditions with minor errors that can be considered acceptable. This test chapter is important because it is the proof that the author has to confirm the validation of the whole report. In addition to the reliability assessments performed by DICCA, the hindcast providers. However there are limitations in this validation chapter, such as, the chapter does not investigate the uncertainties within the measurement data itself. And that the positive test result of one location was considered automatically valid for other locations.

Seasonal analysis performed in Chapter 5 is helpful for operation planning. Short-term operations are interested in seasonal (or monthly) analysis that helps the operation planners identify the seasonal extremes and consider, in case of an operation delay, how next months would affect the feasibility and total duration of the operation. Seasonal analysis is performed in this chapter to gain understanding about the seasonal differences in the sea-state. The need of a monthly analysis should be accompanied with planning of a sensitive operation, e.g. a 21-day long operation, with heave response limit of 2 meters that is planned to start in September. For this case, a monthly analysis is required.

Directional analysis combined with swell analysis together lead to the validation of the omnidirectional assumption. It was figured out that the wind-sea is coming from one main direction, say coming from W. And swell 1 sea was coming from one main direction, which was the same direction as wind-sea. Hence both wind and swell 1 sea components are coming from one main direction. Swell 2 sea (the weaker component of swell) was coming from 2 or 3 different main directions, one of them is aligned with the wind-sea direction. Therefore, a minor part of swell 2 is left coming from different directions comparing to other wind and swell waves. These different directions of swell 2 waves are pointed out because they are believed as potential for resonant response of vessels. Swell 2 waves coming from other directions should be investigated separately, there is a possibility that their effect is very small and can be ignored, but this investigation has not been done in this thesis.

Wave extreme estimations part (Chapter 6) is a focal point of this thesis, where 90 unique statistical models are applied to significant wave height (Hs) data of Location 1, and 36 were shortlisted, the rest were discarded. The estimates from the shortlisted ones provide the whole range of possible and valid extreme estimates; a 70% confidence interval is taken as the range of extreme estimate corresponding to a given return period. The benefit of such study is that it gives a wider perspective on the possible valid extreme estimates, unlike the single-value extreme estimate, that does not reflect if the estimate is conservative or underestimating the extremes. For example, an engineer is intended to find the 100-year value of Location 1, DNV recommends few models, and one of them is ID approach with Weibull distribution. The engineer decides to use that model and got the 100-year wave extreme estimate as 11.3 meters. The engineer will not know if this number is overrating or underrating the estimate. There is no reference. But if the engineer follows this study, then will get a range of the 100-year wave extreme estimates, from 7.6 m to 9.1 m, then the engineer will realize that following the practices without some investigation might be too risky, or too expensive!

POT investigation is a crucial step to validate POT-based models. The sensitivity analysis was subjective, but it included attention to three different parts, the number of storms, the quality of the fitted distribution and the sensitivity of extreme estimation to threshold selected. With those three parts in mind, the selection process of the threshold is becoming less subjective and bounded by more “rules”. There is room for discussion and for further investigation of threshold effect on extreme estimations, but what is done in this thesis is considered to be satisfactory.

The sampling rate was included a building block of the 90 models applied because there is an interest of investigating the effect of sampling to extreme estimations. This effect is documented in Table 23. Basically if the input data is 1 hourly sampled then there is no point for further sampling it in case AM or POT approaches are used. But there may be a point in further sampling the data in case ID approach is used. This point deserves an investigation of what is the required sampling of the all-sea-state data until data independence is sufficient. This investigation is not done in this thesis. But, some hindcast data is provided in a 1-hourly, 3-hourly or even 6-hourly sampled data. The reduction factors of extreme estimations due to the sampling rates of provided data are investigated in this thesis.

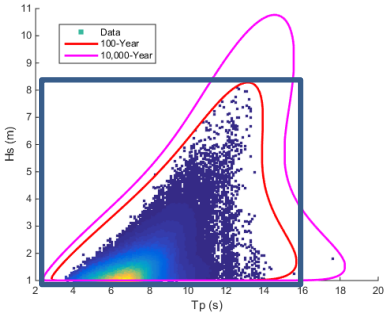

copy of Figure 159

The environmental contour depends on the distribution function selection for Hs, and on the fitting of the conditional mean and variance of Tp. It is a sensitive procedure as shown in section 8.1. Previous sections of uncertainty assessment, has helped in the selection of the proper distribution function that will result in contours close to those marginal extremes found earlier. Once the contour (best-estimate contour) is created, pairs of Hs and Tp that correspond to a given return period can be identified. The identification of pairs is an efficient approach in tackling design issues. Because in the past a structure would be designed to handle the 100-year wave height and the 100-year wave period, two marginal distributions (single-variables). Imagine the contour looks like a square (plotted in the figure as the 100-year square). This square is too conservative, because structural responses are very high for a high Hs and a corresponding high Tp. Therefore the use of contour is an efficient way of design; a structure is designed to handle the 100-year wave and the corresponding period (which is lower than the marginal 100 year period!).

10 Conclusions

The hindcast data provided by DICCA was validated with measurement data provided by IOLR. This validation made it feasible to use the hindcast data for the five locations being studied.

Given the resolution of the seasonal analysis performed (year is split into 4 seasons), the winter and autumn seasons are equally rough, with high waves up to Hs = 8 meters (during the whole

period of 37 years of hindcast data). Spring season is a moderate season, with waves up to a significant height of 4.5 meters, and summer season is a calmer season with no higher waves than Hs = 3 meters.

The sea is an omnidirectional sea; waves are mainly coming from west. A small fraction of weak swells is coming mainly from N. The main direction (omnidirectional sea) and the swell-sea direction (given because the relative direction between omnidirectional sea and swell sea is critical to ship response, e.g. vessel roll motion) are summarized in Table 34 as follows:

Table 34: Summary of Omnidirectional Sea and Swell sea directions

Location	Omnidirectional Sea	Swell	Notes
	The large majority of waves	Tiny portions of swell 2 component	
	Directions: where the waves are coming from		
Location 1	**W**	NNE, NNW	
Location 2	**NW**	NNW, NE	Highest waves Longest fetch
Location 3	**WSW**	N	
Location 4	**W**	NNW	
Location 5	**W**	swell info not available	Shallow water

The extremes of the Eastern Mediterranean sea (Location 1) are estimated using a range of models, giving a range of extreme estimates as follows (Table 35):

Table 35: Extreme estimates for the Eastern Mediterranean (Location 1)

Return Period	70% Confidence Interval for Extreme Estimations of Significant Wave Height Hs (m)			Spectral Peak Period Tp (s)
	Lower edge	Mean	Upper edge	
100 years	7.6	8.3	9.1	13.1
10,000 years	10.0	11.3	13.0	14.7

Applying long-term wave statistics result from only one distribution can be too risky (unrealistic low value) or too expensive. Applying it for a range of models gives a center of gravity for the

estimates and limits the uncertainties into defined range. This uncertainty range can be further investigated, and its impact on economy, structure steel, construction time, and etc. can be quantified.

The POT approach is too risky if the threshold level is not investigated.

The bottom-line of model selection is the fitting (visual) evaluation on a proper probability paper. By looking at the probability paper the quality of the fit can be judged immediately and the distribution behavior can be identified (either underestimating or overestimating the extremes comparing to data)

Hindcast data is provided in 1-hourly, 3-hourly or 6-hourly sampled observations. A 3 hourly sampling rate means that the provided data has one data point for every 3 hours. Some widely used hindcast data are provided in 1, 3 or 6-hourly sampling rates. This sampling rate of the hindcast file causes reduction in the extreme estimates. For a 6-hourly sampled data reduction is as follows: for annual maxima (AM) and peak-over threshold (POT) approaches, a 3% reduction is possible. For all-sea states (ID) approach, up to 14% reduction is possible.

Environmental contours for significant wave height and spectral peak period are given in Figure 169:

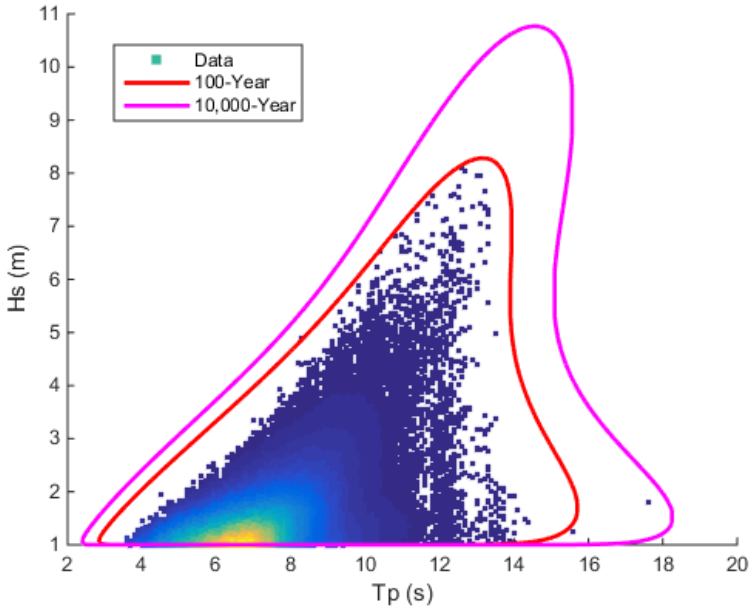

Figure 169: Environmental contours for Location 1

Extreme waves are characteristics of the environment and are described with environmental contours. Whereas design waves are characteristics of the structure and the environment, and they are described with environmental contours, wave spectrum and RAOs.

90 models are fitted, and 36 are shortlisted to give the estimates of Table 35. Two thirds of the fitted distributions are recommended by DNV, still they do not give the same result. There is no underlying true value of extremes, therefore the range of shortlisted distributions fitted provides a range of extremes, where the “true value” must lie inside.

Among the five tested distributions, Weibull, Lognormal and Gumbel have proved good quality of fitting and ability to represent extremes. Whereas GEV and Gamma are not recommended.

11 Further Work

Recommendations for further work include:

Sea State Analysis

Finer-graded directional and seasonal analyses are recommended. The performed analysis split the year into 4 seasons and the direction circle into 6 segments. The recommendation is to split the year into 12 months and the direction circle into 24 segments.

Short-term representation

Wave spectrum for operational limits and design sea states are recommended to be established.

Swell sea

Investigate the effect of swells that are coming from different directions, rather than using the omnidirectional sea.

Operation Sea-state

Using wave data for assessing the operability and feasibility of a given operation. The operability is defined as the ability to perform an operation safely according to pre-set criteria. Operability is considered when having a sea-state that is calmer than what the criteria specify. Operability is assessed by predicting the behavior of the future using data from the past. This section will also include

Risk Analysis on the impact of uncertainties

Quantifying the risk induced from uncertainty of extreme estimates. First finding the effects of uncertainty in terms of design wave, loads, applicability and feasibility of a case study operation.

Platform / Vessel Selection

Investigate for the area's sea state what are the most feasible options of vessels or platforms to be selected for both short term and long term operations

References

[1] Besio, (2016), Hindcast data files, http://www.dicca.unige.it/meteocean/hindcast.html, Il Dipartimento di Ingegneria Civile, Chimica e Ambientale (DICCA)

[2] Biton, (2016), Measurement data file, http://isramar.ocean.org.il, Israel Oceanographic & Limnological Research (IOLR)

[3] Bury and Karl, (1975), *Statistical Models In Applied Science,* London, Wiley

[4] CEM, (2006), *Coastal Engineering Manual*, United States Army – Corps of Engineers

[5] Chakrabarti, (2005), *Handbook of Offshore Engineering, volume I,* Elsevier

[6] Coles, (2001), *An Introduction to Statistical Modeling of Extreme Values,* Springer

[7] CSA International Inc., (2012), *Environmental Impact Assessment Tamar Field Development Project Offshore Israel*, Houston, Nobel Energy

[8] Davidson, A.C and Smith, (2009), *Models For Exceedance Over High Thresholds*, J.R. Statist

[9] DNV-RP-C205, (2007), *Environmental Conditions And Environmental Loads,* Høvik

[10] European Commission, (2016), *Eastern Mediterranean Natural Gas Pipeline – Pre-FEED Studies*, Innovation and Networks Executive Agency

[11] Gudmestad, (2015), *Marine Technology and Operations,* WIT Press

[12] Hasselmann, Ross, Muller and Sell, (1976), *A Parametric Wave Prediction Model,* Journal of Physical Oceanography, Vol. 6, No. 2.

[13] Haver, (2013), *Prediction of Characteristic Response for Design Purposes (preliminary version),* Statoil

[14] Haver, (2014), *Forventet antall utenfor n-års konturer (Expected Number Outside N-Year Contour),* Statoil

[15] Healy, Sanford, Dufrene, Fink, Reeves and Hopper, (2013), *Design, Installation, and Initial Performance of Ultra-High-Rate Gas Deepwater Completions – Tamar Field, Offshore Israel*, SPE, Noble Energy

[16] Holthuijsen, (2007), *Waves in Oceanic and Coastal Waters.* Cambridge University Press

[17] ISO 19902, (2007), *Petroleum And Natural Gas Industries – Fixed Steel Offshore Structures*, Switzerland

[18] Katz, Parlange and Naveau, (2002), *Statistics of extremes in hydrology,* Adv. Water Resources

[19] Kit and Kroszynski, (2014), *Marine Policy Plan for Israel: Physical Oceanography, Deep Sea and Coastal zone Overview,* Coastal and Marine Engineering Research Institute (CAMERI)

[20] Noble Energy (NBL), (2016*), Long-term outlook and U.S. Onshore Update*

[21] Nordenstrøm, (1973), *A Method To Predict Long-Term Distributions Of Waves And Wave-Induced Motions And Loads On Ships And Other Floating Structures,* Oslo

[22] Nordforsk, (1987), *The Nordic Cooperative Project, Seakeeping Performance Of Ships, Assessment Of Ship Performance In A Seaway, Trondheim, Norway, Marintek*

[23] NORSOK-N003, (2007). *Actions and action effects,* Oslo

[24] NPD, (2015), Troll Field *FACTPAGES,* Norwegian Petroleum Directorate, *http://factpages.npd.no/*

[25] Peirson, Moskowitz, (1964), *A proposed spectral form for fully developed wind-sea based on the similarity theory of A. A. Kitaigorodskii,* Journal of Geophys. Res., 69

[26] Ratner, (2016*), Natural Gas Discoveries in the Eastern Mediterranean.* Congressional Research Service (CRS)

[27] Rosen, (2001), *A Summary Of The Environmental And Hydrographic Characteristics Of The Mediterranean Coast Of Israel,* Haifa, IOLR

[28] Schenk and Robertson, (2010), *Natural Gas Potential Assessed in Eastern Mediterranean*, U.S. Department of the Interior, U.S. Geological Survey (USGS)

[29] Smith, (2001), *Measuring Risk With Extreme Value Theory,* Cambridge University Press.

[30] Stanford and Vardeman, (1994), *Statistical Methods for Physical Science,* Academic Press

[31] Tolman, (2009), *User Manual And System Documentation Of WAVEWATCH III™ version 3.14,* National Centers for Environmental Prediction, U.S. Department of Commerce

[32] Torsethaugen, (1996), *Model For A Douobly Peaked Wave Spectrum.* SINTEF report STF22 A96204

[33] Wang and Hwang, (2001), *Operational Method for Separating Wind-sea and Swell from Ocean Wave Spectra,* Journal of Atmospheric and Oceanic Technology

[34] Wang and Mehaute, (1983) *Duration Of Measurements And Long-Term Wave Statistics*. J Waterway, Port, Coastal and Ocean Engineering ASCE Vol. 190, No. 2.

[35] Winterstein, S., Ude, T.C., Cornell, Bjerager, P., Haver, S., (1993), *Environmental Parameters for Extreme Response: Inverse FORM with omission Sensitivity,* Innsbruck

[36] Wood Mackenzie, (2011), *Perspectives on Gas Exports from Israel*, energy.gov.il/Subjects/NG/Documents/עמדות/WM.pdf

Appendices

Appendices are included in the submitted USB flash disk in the following order:

A Thesis report

B Outputs

C Codes and Scripts